Conceptual Design of a Novel Small-Scale CO_2 Compressor

Based on Gas Bearing Technology

R.M. de Koning

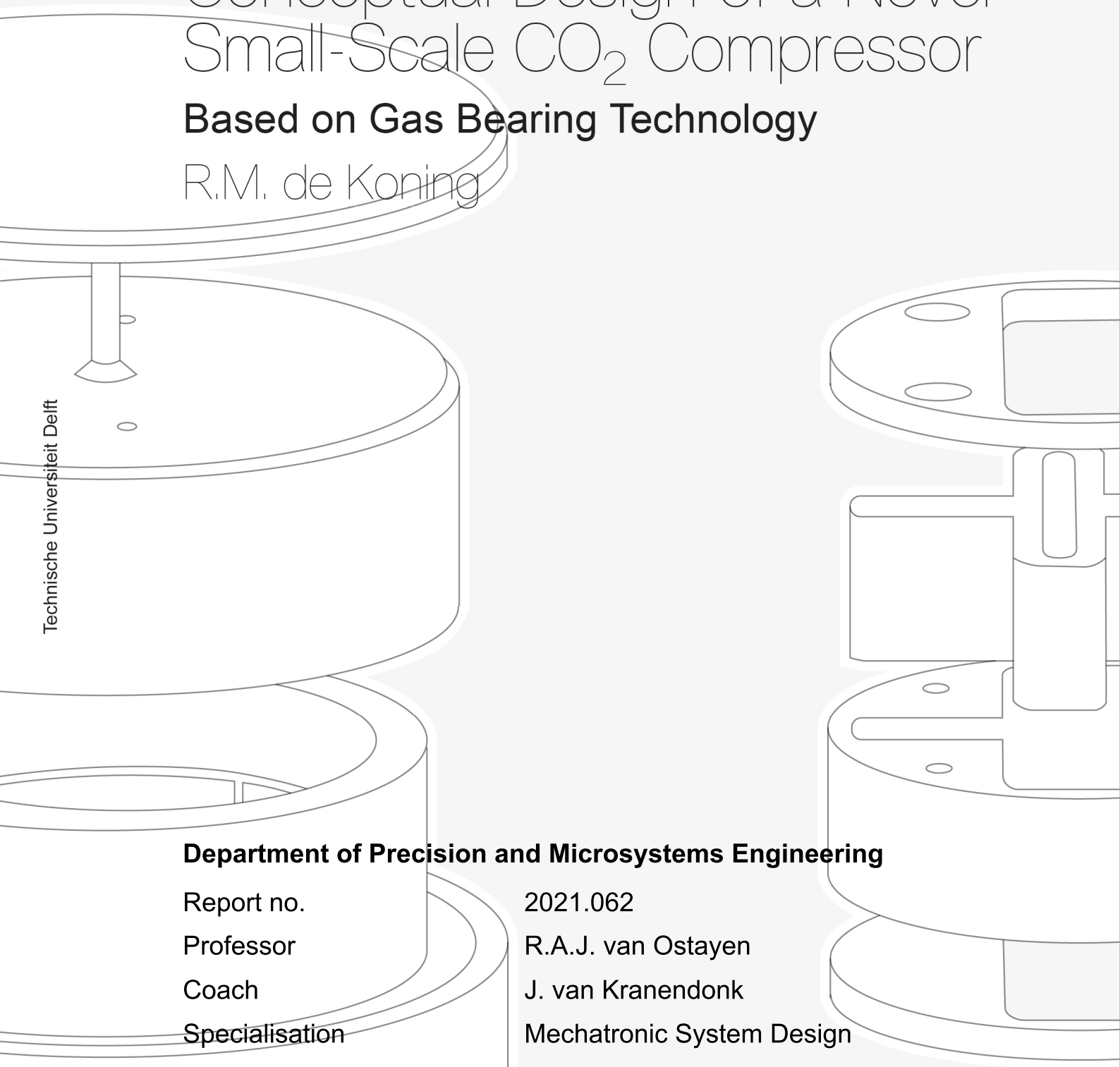

Technische Universiteit Delft

Department of Precision and Microsystems Engineering

Report no.	2021.062
Professor	R.A.J. van Ostayen
Coach	J. van Kranendonk
Specialisation	Mechatronic System Design
Type of report	Master thesis
Date	August 23rd, 2021

TU Delft

ZEF ZERO EMISSION FUELS

Conceptual Design of a Novel Small-Scale CO_2 Compressor

Based on Gas Bearing Technology

by

R.M. de Koning

to obtain the degree of Master of Science
at the Delft University of Technology,
to be defended publicly on Monday August 23, 2021 at 13:30 PM.

Student number: 4230582

Thesis committee:	Dr. ir. R.A.J. van Ostayen,	TU Delft, supervisor
	Ir. J. van Kranendonk,	TU Delft and Zero Emission Fuels, coach
	Dr. Ir. C.A. Infante Ferreira,	TU Delft
	Dr. Ir. G. Radaelli,	TU Delft

TU Delft

”On a bright sunny day it may be observed that the water dripping from the oars during rowing forms a multitude of tiny droplets that seem to float on the surface of the water. This can be quite enchanting. It has been investigated that the mechanism to explain how these drops are supported, apart from the ubiquitous surface tension, relies on the air being trapped between the fast running, flat bottomed, globules and the water surface. This experience demonstrates the feasibility of gas lubrication.”

H. Moes

Preface

This thesis about the conceptual design of a CO_2 compressor based on gas bearing technology is written to obtain the title of Master of Science in Precision and Microsystems Engineering and concludes my studies at the Delft University of Technology. I started this thesis on the advise of Ron van Ostayen with the goal to work on a broad design project and ended up with in-depth knowledge on gas bearing technology.

I would like to thank Ron for being my thesis supervisor. Most part of this thesis has been written from home due to the Covid epidemic and our two-weekly zoom calls have been more than useful. Especially your detailed knowledge about thin-films and COMSOL Multiphysics has been much appreciated. Ron also introduced me at ZEF, where the initial design goal comes from. I would like to thank Hessel Jongebreur, Ulrich Starke and Jan van Kranendonk for giving me the opportunity to be part of their sustainable mission. Jan has been a great addition to my technical insight and practical thinking and Ulrich was always there to check up on me and keep the process efficient. Here I would also like to thank the third and fourth members of my thesis committee, Carlos Infante Ferreira and Giuseppe Radaelli.

Finally, I want to say thank you to all my friends, roommates and family. I have had so many discussions with Thieme Schmidt, Juul ten Hove, Tim Swank, Rutger Naber, Marijn van Loo, Edwin van Tongeren, Rico Hooijschuur and Maurice Valentijn. It is needless to say that I couldn't have finished both my bachelor and master without my sister and parents.

Ramon de Koning
Delft, July 2021

Abstract

This thesis is created commissioned by Zero Emission Fuels with the objective to create an efficient, two-stage CO_2 compressor with a large pressure ratio and a desired lifetime of 20 years. The goal to make the system two-stage comes from a constraint in size and expenses for implementation in a methanol micro-plant. This design is aimed at long-term mass production and the current development costs are not taken into account. A large pressure ratio induces a high temperature in an adiabatic compression process. As oil deteriorates under high temperatures, a compressor is developed that operates based on gas bearing technology to obtain the desired lifetime.

The viscosity of CO_2 is a few orders of magnitude lower than oil which means that the load capacity of the bearings has to be evaluated carefully. The rotary cylinder compressor from literature is chosen as a starting point as the interfaces between all moving components are surface contacts. Almost all forces within this compressor are oscillating of nature. This means that the squeeze effect from the Reynolds equation is applicable. Where gas bearings usually operate at high frequencies, the squeeze effect already shows promising results at lower frequencies. The lay-out and dimensions of the components in the rotary cylinder compressor are adjusted and optimised to improve the load capacity.
The oil film in an oil lubricated compressor prevents leakage of compressed gas through the bearing gaps. A gas bearing doesn't have this ability and the amount of bearing gaps connected to the compression chamber and their dimensions are optimised to maintain a maximum leakage rate of ten percent of the effective mass flow of the compressor.

Both analyses are performed with the goal to keep the initial gap height and the dynamic minimum gas film thickness throughout the compression cycle as large as possible. It has been achieved to design the first stage of the desired compression process while maintaining a continuous layer of gas between all component interfaces at steady-state and therefore prevent mechanical contact and wear. The minimum film thicknesses are in the range of one to three micrometer which asks for high precision manufacturing with respect to the surface roughness, flatness, cylindricity and general tolerances of the components. This is not in line with the goal to keep the manufacturing costs low. Further research is required in the behaviour at start-up and the second compression stage which comes with higher absolute pressures. A result that should be taken away from this report is that the squeeze effect of gas bearings comes with a large load capacity at relatively low frequencies. For applications with symmetric oscillating loads that operate at high temperatures or require a long lifetime, this lubrication method should be considered.

Contents

1 Introduction

The compression of gasses to higher pressures can be performed by various types of compressors. Compressors can be split in two categories. The first ones are dynamic compressors that increase the speed of the gas by use of rotating blades to create a higher dynamic pressure. These mostly come with large volumetric flow rates. The second ones are so called positive displacement compressors that periodically contract and expand a volume to build up pressure. A common factor is that the moving components in both types are almost always hydrodynamically lubricated, in other words separated by a layer of oil. This oil film also prevents leakage of the gas that is compressed between the moving components to a large extent.

This thesis is written commissioned by Zero Emission Fuels, from now on called ZEF, and the compressor is a component of an innovative methanol micro-plant. The volumetric flow of gas that has to be compressed for this production process is a few orders or magnitude smaller than most existing compressors. This results in the design of a compressor with a low frequency or a small compression volume. The pressure has to be increased by a total factor of 80 from 0.75 bar to 60 bar. In general, gas is only compressed by approximately a factor 3 as the adiabatic nature of a compressor causes the oil film to heat up and deteriorate. When a higher pressure ratio is required, multiple compressor stages are linked together. For a total pressure ratio of 80, at least four stages with a ratio of 3 are required. The goal for ZEF is to develop a small and cheap compression system for mass production which are both not achieved by a four-stage system. With this reason, the focus has been put on the development of a two-stage compressor with a pressure ratio of just below nine.

To be able to handle the heat coming from a compression process with such a high pressure ratio, it is set out to lubricate all moving components with gas bearings. As gasses have a low viscosity, a larger surface area is required to build up pressure between two components than in an oil lubricated system. From literature a compressor is found that has only surface contacts as a line contact is not suited for this application. This rotary cylinder compressor is adjusted mechanically in multiple ways to improve the bearing load capacity and reduce the internal leakage rate to reach the desired efficiency.

1.1. Thesis Objective

In this thesis, a compressor concept will be designed and analysed on its ability to function within the goals of the methanol micro-plant of ZEF. The thesis objective is stated as follows:

"The conceptual design of an efficient two-stage compression process with a high pressure ratio based on gas bearing technology."

To measure the degree in which the compressor fulfills its functions, the following sub-questions should be answered:

1. *"Is the design able to generate sufficient load capacity to handle the loads throughout the process without making any contact between the bearing surfaces?"*

2. *"Is the design able to achieve a predetermined efficiency considering the leakage flow through gas bearings?"*

These questions will be answered throughout this report and the conclusion will reflect on both the main thesis objective as well as the sub-questions.

1.2. Outline of the Report

This report starts with a literature review in paper format in Chapter 2. The needs of the ZEF application are discussed, various compressor types are compared and the available lubrication methods are shown with focus on three pillars: hydrodynamic lubrication, dry lubricants and gas bearings. Chapter 3 introduces an existing compressor concept from literature that is intended for hydrodynamic lubrication. This concept is analysed based on its compression cycle, dynamic loads in the system and opportunities to adjust the system for gas lubrication. Chapter 4 gives a thorough analysis of the behaviour of the gas bearings and the optimum design parameters of the compressor components to obtain the best performance. Chapter 5 models the internal leakage of the compressor and the requirements to stay below a specific threshold. The conceptual design that is optimized for gas bearing application is presented in Chapter 6. Chapter 7 and 8 contain the conclusions and recommendations for further work. Additional information about several subjects that are touched upon in this report can be found in the Appendices.

2

Literature Review

This chapter presents the literature review on the subject of compressor technology focused on high pressure ratios and low mass flows. This review is presented in a paper format. It is not only a review but also a brief analysis of the required compression process itself. It is especially important as an introduction to this thesis as the initial design goal is broad and the solution space needs to be converged to formulate an innovative but realistic design approach.

The operating conditions, goals and history of compressor technology at ZEF are discussed and the challenges corresponding to that. An overview is given of the state of the art in the compressor industry in general and specifically of small-sized compressors with high pressure ratios. A simplified analysis of the thermodynamic cycle and the heat generation and transfer throughout this process is performed as this has a large influence on the available lubrication methods. Hydrodynamic and gas lubricants are discussed as well as dry lubricants and coatings. The conclusion is drawn to aim for a new rotary compressor design based on gas bearings.

Research and Design of a CO_2 Compressor for Implementation in a Methanol Micro-Plant

R.M. de Koning
High-Tech Engineering, Delft University of Technology
December 17, 2020

I. Introduction

A. Motivation

Over the last decades, multiple changes to the earth's climate have been observed. With respect to the atmosphere, each of the last three decades have been successively warmer than any preceding decades since 1850. The ocean has seen a rise in temperature as well as in global mean sea level. A correlation between these observations, the start of the industrial revolution and human influences in general is expected to be highly likely. Especially the increasing emission of greenhouse gasses like carbon dioxide (CO_2), methane and nitrous oxide into the atmosphere shows a similar pattern [1]. It is with that reason that various organizations are trying to counteract these emissions. At Zero Emission Fuels (ZEF), the goal is to create a sustainable fuel that can be produced and consumed with a zero net footprint. This complete process consists of four steps as seen in figure 1. First CO_2 and water are captured from the air. Secondly the water is split into H2 and O2 and as a parallel process, the CO_2 is compressed. In the final step, methanol is created from the compressed CO_2 and H2. The energy required for the system to run will be generated using solar panels. When the methanol is consumed, the CO_2 will return to the air and complete this circular process. This review will cover the challenges of the compression process of CO_2.

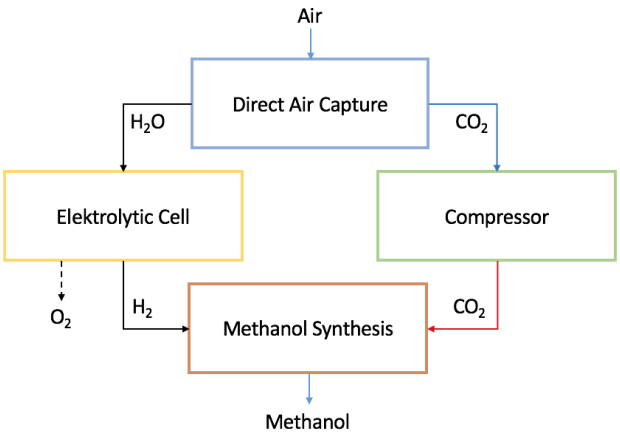

Fig. 1. Process flow diagram of the ZEF micro-plant.

B. Scope & Goal

This review is set out to create an overview of the knowledge available in compressor development. The refrigeration and air-conditioning industry as well as the similarity of compressors to combustion engines guarantee numerous studies on related subjects. It is necessary to narrow down the scope of this review to relevant information based on the properties that distinguish the compression of CO_2 from more common working fluids. The focus will be on the research that matches the requirements of the ZEF case. It is likely that not all requirements can be fulfilled using existing technology. The conclusion should be a feasible research proposal that closes a gap between the ZEF case and the current available technology.

C. Structure

This review will start with an overview of the operating conditions of the ZEF case, the corresponding challenges and the potential solutions explored at ZEF in previous projects. The compression of CO_2 in the industry will be looked at next, followed by the compressor industry in general. A dive in the thermodynamics will show what parameters influence the process. The design will be evaluated in three stages: thermal, mechanical and electrical with lubrication and wear taking a large part of the mechanical design. Finally these design considerations will be combined to find the proper compressor type for this case.

II. Problem Statement

This paragraph explains the challenges of the ZEF compressor and the knowledge gained in earlier research at ZEF. At the end of section II-A a compact overview is given by table I.

A. ZEF Operating Conditions

At ZEF the goal is to design a stand-alone methanol plant that is able to operate reliably for 20 years at high ambient temperatures e.g. in the desert. The production rate of methanol and with that the required flow rate of CO_2 is theoretically limited by the amount of energy that a solar panel is able to generate. From a practical aspect, it has been stated that the system should work with an amount of panels ranging from three to ten with a preference for the small scale. The exact value is to be determined by the compressor as the design might come with limitations or as this could potentially match an off-the-shelf compressor. As the complete system is being developed at time of writing, all system values are working estimates. A study on the order of magnitude of the system

yields an approximate 300 watt power source per solar panel of which 10 percent is available for the compressor. Three solar panels therefore give freedom to consume 90 watt. The corresponding CO_2 mass and volume flow at inlet conditions could respectively reach a maximum of 2.86e-5 kg per second or 69 liter per hour which is well below the specifications of most commercial compressors as will follow in section III-B. Next to this, this flow comes from the direct air capture which delivers a pressure below atmospheric pressure at 0.75 bar. The efficiency of the methanol synthesis depends on the discharge pressure of the compressor. The optimization of this pressure is out of the scope of this review and the requirement for the compressor is set to be 60 bar. As compressors are usually not bound by the absolute pressure but by the applied pressure ratio, this would yield a ratio of 80 for a single-stage setup. From a financial perspective it would be preferred to keep the number of compressor stages to a minimum. More stages increase the material and production costs and the size of the total plant. As a pressure ratio of 80 in a single-stage would be an unrealistic goal, the focus will be on a two-stage setup with a pressure ratio of just below 9. Most calculations in this research will be based on this. Where refrigeration and air-conditioning compressors operate in a closed-loop system, this system will be open-loop. The inflow will be continuously new CO_2 captured from the air. Even though most water content will be filtered out before compression, a zero percent humidity can't be guaranteed. CO_2 dissolved in water forms carbonic acid and the effect of potential corrosion should be investigated and taken into account at the material selection of the compressor. The outflow of the compressor will be used to produce methanol. That means that any lubrication inside the system that flows along with the CO_2 to the next process step will be lost. Lubrication plays an important role in life expectancy and therefore poses a challenge. All these factors are often intertwined and add up to a rather complex system.

B. ZEF History

Prior to this study, several CO_2 compression setups have been explored at ZEF. A three- as well as a four-stage reciprocating piston compressor was designed and built. These systems were developed with the goal to compress CO_2 combined with liquid water. Sufficient operating time wasn't reached to draw a conclusion on the formation of carbonic acid and the consequences of potential corrosion. As mentioned, a wet lubricated system with an open-loop flow demands a continuous flow of lubrication. The potential of using an oil-free PTFE seal was investigated and tested. A PTFE O-ring started leaking at 7 bar. A combination of an NBR O-ring that puts preload on a PTFE-graphite seal was leak tight until 55 bar in a static test. This combination is commercially available, for higher pressure applications as well [2]. Signs of wear were noticed but the test was not conclusive about the cause. As a cost-effective method, the refrigeration market has been explored. The compressors used in this application are designed for a relatively low flow rate compared to the compressor market but are still oversized for ZEF, especially when it comes to a multi-stage system where higher stages usually decrease in size. A Purswave 1.9 cc rolling piston type refrigerator compressor, one of the smallest to be found with an estimated minimum flow rate of 180 liters per hour assuming an 80 percent volumetric efficiency, has been ordered and tested see figure 2a-c. A maximum pressure of 40 bar was reached with the inlet side connected to the atmosphere. An observation that has been made, was the high power consumption of the motor. The power input was more than tenfold the amount you would expect from an adiabatic compression calculation. The transmission has not been designed for such a high load on the piston and therefore requires a torque from the motor outside its operating window. This resulted in overheating and eventually caused failure of the rotor see figure 2d. The compressor specifications are clearly not meeting the process requirements, but there might be long-term potential in adjusting some of the specifications of such a compressor.

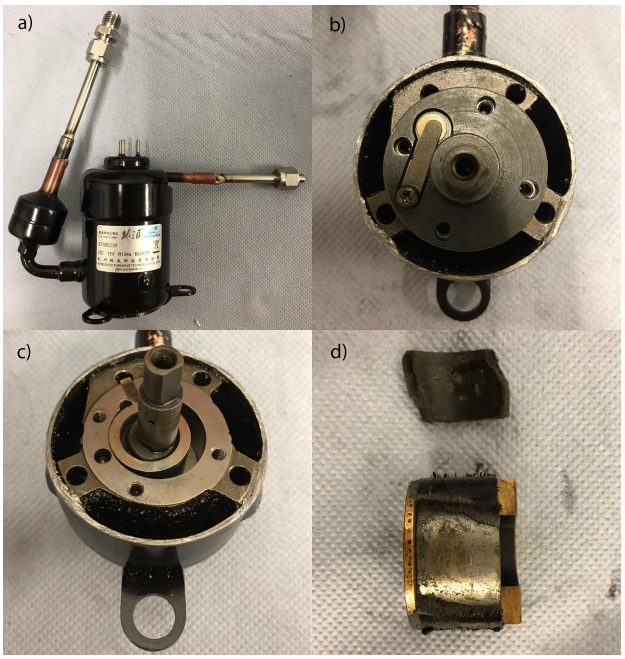

Fig. 2. a) Purswave 1.9 cc rolling piston compressor. b) Compressor internals including discharge reed valve. c) Compressor internals including crankshaft, rolling piston and vane. d) Rotor failure due to overheating.

TABLE I
OVERVIEW OF THE OPERATING CONDITIONS AND CHALLENGES OF THE ZEF COMPRESSOR SYSTEM

Power	$P_{suction}$	$P_{discharge}$	Pressure ratio	Mass Flow rate	Volume Flow rate	Type	Lifetime
90 W	0.75 bar	60 bar	80	2.86e-5 kg/s	69 l/h, 1.91e-5 m^3/s	Open-loop	20 years

III. State of the Art

A. Commercial history of CO_2 compression

The application of CO_2 as a working fluid in compressors has been in and out of fashion during the last two centuries. From 1850 till the early 1900s compressors used CO_2, NH_3 and SO_2 for refrigeration on cargo ships and for comfort-cooling. Since the last two fluids have toxic properties, the CFC fluids where introduced around 1930 as a safer solution. As the market evolved into that direction, CO_2 dropped from an 80 percent market share to being completely phased out by 1980 [2]. At the end of the 20th century climate change started to draw attention and with the establishment of the Montreal Protocol in 1987 and the Kyoto Protocol in 1997 foot was set in a new direction. Use of fluids with a high global warming potential (GWP) or ozone depletion potential (ODP) were suppressed or banned. Industries had to start looking for alternatives. The most commonly used alternative with a relatively high GWP of 1430 but a zero ODP quickly became R134a. Research continued towards different alternatives and between 1994 and 2002 the number of papers on CO_2 as a primary refrigerant increased from 7 to 47 percent at the IIR-Gustav Lorentzen conference on natural working fluids [3]. Currently there are only about nine fluids with a GWP below ten and an ODP of zero. Two of these are synthetic and called HFO's with R1234yf being the most widely adopted. Six out of seven natural fluids are either toxic and/or highly flammable [4]. With large companies like coca-cola and car manufactures like Daimler putting their resources in this movement, a lot of progress has been made. The industries are now divided in their choice of working fluid based on the application with CO_2 being a natural fluid and slightly better for the environment on one side and R1234yf operating at conditions more suited to the original machines but synthetic and mildly flammable on the other side. Daimler and Volkswagen sold their first cars equipped with a CO_2 compressor in 2017 [5], but there is a long way to go in technological development before CO_2 compressors are the standard. For the ZEF application it is encouraging to see to ongoing research into this topic. The market doesn't provide commercial compressors that meet the specifications mentioned in paragraph II-A as the refrigeration process usually requires higher flow rates, lower pressure ratios, operating between 25 and 90 bar, and shorter lifetime. For the short-term, knowledge about, among other things, high pressure containment, CO_2 properties and lubrication can be of good use.

B. Compressor types

As commercial compressors specifically designed for CO_2 are not matching the demands of the ZEF process, a broader approach can be taken. Compressor are available in a large number of types of which the most well-known ones are to be found in car engines and airplanes. All of these types are designed with different design parameters in mind suited for their application and these can be used to make a first sorting. Figure 3 shows approximate range of refrigeration capacities

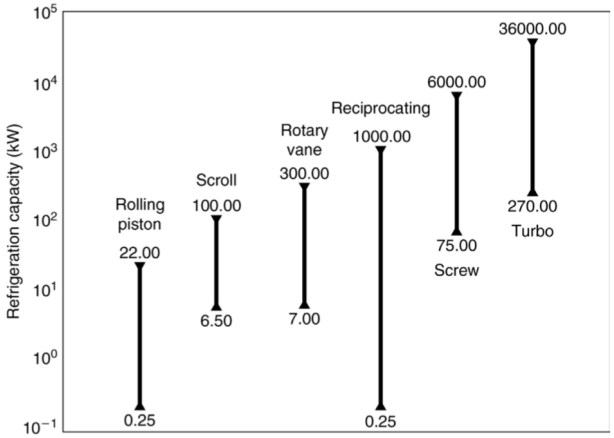

Fig. 3. Approximate range of capacity covered by various compressor types [6].

covered by various types of compressors [6]. The refrigeration capacity is not relevant for this research but it gives a good estimate of the relative power consumption range of these compressor types. This overview is not sufficient to base a conceptual choice on but it represents an important direction. Within the rotary compressor family, a broader distinction can be made [6], [7]. Screw and lobe compressors are used for high flow rates, rotary vane and scroll compressors for intermediate rates and are known to be more fragile when used in high pressure applications. The rolling piston compressor is used in smaller setups which was also found in paragraph II-B. This compressor type uses a piston that 'rolls' eccentrically in a cylinder in which the suction and discharge chambers are separated by a vane with a spring as shown in figure 4a

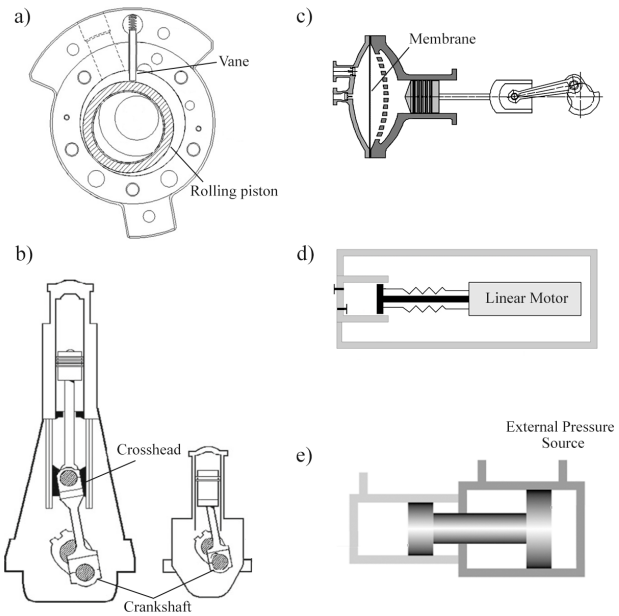

Fig. 4. Schematic overview of compressor types with potential for use in the ZEF micro-plant.

[8]. Reciprocating compressors are all equipped with a piston moving up and down through a cylinder. The differences can be found more specifically in the driving force and the interaction with the working fluid. Compressors with a crankshaft are common. A crosshead can be added for improved guiding and wear reduction, see figure 4b [9]. This is inherent in a linear compressor type which is driven by a linear motor and therefore minimizes lateral forces on the piston, figure 4d [10]. Linear compressors are often found in smaller scale applications. Diaphragm compressors completely separate the working fluid from the driving piston by a flexible membrane, which prevents contamination and therefore could for example make an oil separation process unnecessary, figure 4c [11]. Design of a flexible membrane with an airtight seal for a long life-time is a challenge. A pressure intensifier is an alternative reciprocating concept which is not able to operate by itself but needs an external pressure source, figure 4e [12]. This is interesting since this source could have lubricating properties, enhance cooling and will create a linear driving force as well. As figure 3 is such a rough overview, table II shows the mass flow rates and pressure ratios that correspond to papers that will be discussed in this review. These are ranked from top to bottom based on increasing mass flow rate. The second compressor comes close to the operating conditions from ZEF with a small mass flow and a high pressure ratio.

TABLE II
OVERVIEW OF MASS FLOW RATES AND PRESSURE RATIOS OF COMPRESSORS FROM LITERATURE

Paper	Type	Fluid	PR (-)	Mass flow (kg/s)
[44]	Linear	Refrigerant	1.1 - 1.27	1.2 - 4.6e-4
[47]	Linear	Refrigerant	8.97	9.6e-4
[46]	Linear	Nitrogen	1.5 - 3.5	0.12 - 1.39e-3
[46]	Crankshaft	Nitrogen	1.4 - 3.8	0.25 - 1.51e-3
[49]	Linear	R134a	2.5	2.6e-3
[50]	Rolling Piston	R290	Unknown	9.5e-3
[45]	Crosshead	Hydrogen	4.5	2.5e-2

With these concepts selected and their distinctive features touched upon, it is useful to revisit the challenges the ZEF system poses mentioned in paragragh II-A more extensively. It will become clear that most of these have mutual influence. This creates insight to determine which concept is the best fit.

IV. THERMODYNAMIC PROCESS

The theoretical power consumption of a compressor is determined by two values. Firstly, the work done per compression cycle and secondly, the amount of cycles executed per second, the frequency. Both are part of a complex process and influenced by the design of the compressor. The design of a compressor can only be optimized when these relations are taken into account.

A compressor is often assumed to be an adiabatic process. This means that during the cycle no heat is exchanged with the environment. The high operating frequency of a compressor barely allows time for heat exchange. When exactly enough heat is exchanged to the environment to operate at constant temperature, the process is called isothermal. The cycles for the first and second stage of the adiabatic compression of CO_2 with a swept volume of 1.9 cc and 5 percent clearance volume are shown in figure 5 and the work done can be found by the area inside the cycles. The same process for isothermal operation is shown with dashed lines. These graphs and the efficiency path shown in equations 2 and 3 are constructed using the formulas written by Ueno, Bye and Hunter [13]. A parameter can be defined to indicate the state at which the process operates, the polytropic index, n, which always takes the value 1 for an isothermal process and, for CO_2 at 70 degrees Celsius, a value of 1.289 for an adiabatic process. An adiabatic process has a higher discharge temperature and usually needs cooling after compression or in case of multi-stage compression, in between stages. The necessity of cooling will be discussed in section V-B. Independent of the process, the sum of the work done and heat exchanged to and/or from the system between inflow and cooled outflow should be equal to the enthalpy difference, see equation 1.

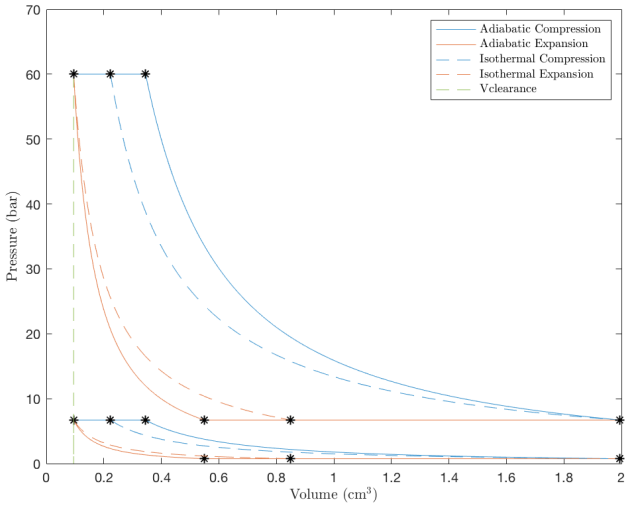

Fig. 5. Volume-Pressure diagram of the first and second stage of adiabatic and isothermal compression cycles of CO_2 with a swept volume of 1.9 cc and a 5 percent clearance volume.

$$dh = \frac{\dot{W}_{compressor} + \dot{Q}_{compressor} + \dot{Q}_{intercooling}}{\dot{m}} \quad (1)$$

An infinite amount of processes exist next to an isothermal and adiabatic process as shown in figure 6 where the x-axis gives the polytropic index from 1 to 1.4. These processes will have different intermediate enthalpy states, but will add up to the same total. The compressor operates adiabatic where the $\dot{Q}_{compressor}$ line crosses zero. To the left from this point, heat is exchanged from the sytem to the environment while to the right heat is added. However hard to achieve, isothermal operation is usually preferred, given its lower total power consumption and lower discharge temperature.

The polytropic index is an example where the thermodynamic process influences the operating conditions

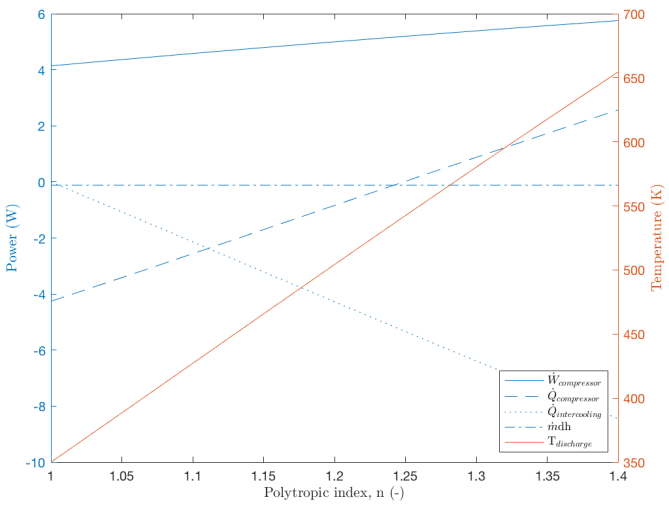

Fig. 6. Effect of polytropic index on power consumption, cooling capacity and discharge temperature of a compressor with a pressure ratio of 9 and a mass flow of 2.86e-5 kg/s.

of the compressor. Table III shows the dependencies between a set of important parameters and the resulting operating conditions for an increase in parameter value with a constant mass flow. In ZEF's case the compressor has to be able to increase the pressure from 0.75 bar to 60 bar which makes the total pressure ratio a constant. Both the clearance ratio and the swept volume can be adapted to optimise the requirements for among other things lubrication and sealing, heat exchange and motor transmission. The number of stages is open but a minimum is preferred from a financial perspective as mentioned before. An increase would come with a constant total power but creates the opportunity to cool the gas more often in between stages.

This table is analysed from an ideal perspective which creates a good overview of the process and a starting point for the design. However, an ideal assumption is not complete enough for a full design. The inflow won't be constant. A lower suction pressure will result in an increased pressure ratio with a corresponding higher power consumption and discharge temperature rise. The opposite might occur as well. The discharge pressure is part of an equilibrium process between the consumed high pressure CO_2 by methanol synthesis and the flow from the compressor. The flow from the compressor is bound by the input from the direct air capture. The compressor is a link that needs to adjust its frequency to the right conditions. The direct air capture and methanol synthesis should be aligned. Cooling won't be constant either. It depends on exchange area, residence time and temperature gradient which all change during the cycle. In practice an overlap of multiple PV-curves with different polytropic indices will exist. The clearance ratio influences power consumption by irreversibilities in the process. The mass in the clearance volume goes through a full cycle, being first compressed and straight after expanded inside the cylinder, with the ratio between the discharged volume and the total amount of compressed volume called the volumetric efficiency. Since no process operates at 100 percent efficiency, energy will be lost and a power increase will be the result. A maximum clearance ratio is set to be able to reach the required discharge pressure. Leakage is influenced by the pressure ratio and the size of the compressor (stage), which are both a function of the amount of stages selected. These are all factors that need to be taken into account.

TABLE III
CHANGE IN TOTAL POWER, WORK PER CYCLE, FREQUENCY AND DISCHARGE TEMPERATURE FOR THE INCREASE OF FIVE KEY PARAMETERS IN PROCESS DESIGN WHILE MAINTAINING A CONSTANT MASS FLOW.

Parameter	Power	Work	Frequency	Temperature
Polytropic index	Up	Up	Down	Up
Pressure ratio	Up	Up	Up	Up
Clearance ratio	Constant	Down	Up	Constant
Swept volume	Constant	Up	Down	Constant
Number of stages	Constant	Down	Down	Down

V. DESIGN

The thermodynamic process pursues the purpose of a compressor, increasing the pressure. These calculations do not include practical feasibility. A compressor needs proper mechanical design to reach these values and most likely compromises have to be made between costs, efficiency and the goals.

The performance of a compressor is generally measured by its efficiency. In a multi-component system, efficiency is a broad concept. A three step overview can be made of a compressor's efficiency path.

$$\dot{W}_{system} >_{(C)} \dot{W}_{shaft} >_{(B)} \dot{W}_{actual} >_{(A)} \dot{W}_{Theoretical} \quad (2)$$

$$\eta_{system} = \eta_{C,elec} * \eta_{B,mech} * \eta_{A,thermal} \quad (3)$$

The thermodynamic process has been discussed in depth in paragraph IV. For a constant mass flow rate, it was shown that the theoretical power depends on the operation conditions under which the process is carried out, with heat exchange as one of the main factors.

A. Thermal Design

The temperature in the compressor depends on the heat generated, which is a function of the pressure ratio and friction, and the heat added or removed from the system by heat exchange. The pressure ratio per stage decreases when more stages are added. When it's assumed that the gas temperature can be cooled back in between stages to its initial temperature, the adiabatic discharge temperature of each stage will be as shown in table IV. The effect on the discharge temperature reduces rapidly for four stages or more. As the goal is to minimize the number of stages, heat transfer calculations are based on a two-stage system.

TABLE IV
ADIABATIC DISCHARGE TEMPERATURE FOR DIFFERENT AMOUNTS OF COMPRESSOR STAGES WITH A TOTAL PRESSURE RATIO OF 80 ASSUMING A CONSTANT 350 KELVIN INLET TEMPERATURE.

Number of stages	1	2	3	4
PR (-)	80	8.94	4.31	2.99
T (K)	838	542	468	435

A small compressor size comes with a relatively high heat exchange rate with the environment compared to the industry. This is due to scaling as the surface-area-to-volume ratio increases for smaller objects. For a constant mass flow rate, a compressors mass per stroke and with that the swept volume decreases inversely proportional to its frequency. When the frequency is increased by a factor 4 as shown in figure 7, the swept volume is decreased by a factor of 4. The corresponding surface area will only decrease by a factor $\sqrt[3]{4^2}$ and with that the area-to-volume ratio will increase by a factor $\sqrt[3]{4}$ which is equal to a value of 1.59. The mass and swept volume are related to the heat production and the surface area to the heat sink and therefore a higher ratio raises the heat exchange capacity. This can be seen in figure 7 as well since the temperature curves are initially steeper for higher frequencies and smaller volumes. These curves are constructed using a lumped capacity model. This is valid since the gas inside the compressor is turbulent and under high temperature and pressure conditions and will therefore have a uniform temperature. A lumped model can be used in early stages of design. More accuracy can be achieved by differential and hybrid models [14].

$$T = e^{-\frac{U}{\rho * c} * \frac{A}{V_s} * t} * (T_0 - T_e) + T_e \tag{4}$$

All curves show a decreasing heat exchange capacity. The mass in the cylinder is constant but the compression process makes that the volume and surface area are dynamic values. A sinusoidal decreasing surface area is assumed as this is common for reciprocating piston compressors, neglecting speed differences due to pressure changes. A compression stroke at 1 hertz takes 0.5 seconds as the other 0.5 seconds are spent during the expansion stroke. Next to that the heat production rises throughout the stroke as this is coupled with the pressure ratio. Heat production due to friction and valve dynamics are left out. A peak can be seen in all temperature curves around 70 percent of the stroke which is the moment the pressure reaches the discharge pressure and the valve opens assuming the first stage of a two-stage compressor with a total pressure ratio of 80. From here on the temperature stops rising due to pressure increase and cooling takes over.

The decrease of the swept volume is the result of increasing the frequency which comes with another effect. As the flow rate is constant, the residence time of the smaller volume inside the compressor decreases inversely proportional to the frequency as well. Naturally the gas temperature throughout the stroke depends on the initial and ambient temperatures. Equation 4 shows that the exponent in the process is influenced by the surface area equally as the residence time [15]. For higher frequencies, the residence time decreases more than the area increases relative to the swept volume. It can be seen that this effect is significant. For this process, the discharge temperature at 1 hertz would be approximately 50 and 100 degrees lower than at 4 and 16 hertz, respectively. Based on figure 6 a lower frequency and bigger swept volume would therefore increase the thermodynamic efficiency of the process.

Huff and Radenmacher (2013) analysed the effect of internal heat transfer on a CO_2 compressor's performance [16]. They calculated the instantaneous heat transfer coefficient in a piston compressor using the transient velocity field in the piston based on the frequency and varied the wall temperature between 0 and 120 degrees Celsius. Their results showed an effect of less than 1 percent on the isentropic and volumetric efficiency. Applying their mass flow rate and frequency on the model used to construct figure 7 and varying the ambient temperature in the same range, only shows a temperature change of 1.1 degrees. The heat exchange compared to the heat production is negligible. It was also observed that the effect of running at lower frequencies is significantly reduced with a difference of only 6 degrees at 1 hertz. This proves that bigger compressors usually behave adiabatically as is often assumed and that it might be possible to use this advantage in the ZEF compressor.

More options to improve the heat exchange capacity can be explored. The shape of the compressor could theoretically be adjusted but from a practical perspective a cylindrical shape is used. The only variable in the equation that has not been discussed is the heat transfer coefficient. For a compressor this variable consists of multiple layers. In this model three layers are taken into account: convection from the compressed gas to the cylinder wall, conduction through the wall and convection to the environment, see equation 5.

$$U = (\frac{1}{h_{c,i}} + \frac{L}{kA} + \frac{1}{h_{c,o}})^{-1} \tag{5}$$

The first two values are significantly larger than the last one due to turbulent, high pressure conditions inside the cylinder and a thin wall thickness, L. The material of the wall could be changed to improve the conduction but a this moment steel is acceptable. Increasing the total heat transfer coefficient is therefore mainly dependent on the convection from the wall to the environment, $h_{c,o}$. Free convective air comes with values between 3 and 25 W/m^{2}K [15]. The temperature curves in figure 7 are based on a value of 150 W/m^{2}K to simulate a desired effect. An improved flow around the wall, the use of water, oil or other fluids with a high heat transfer coefficient and the use of fins for additional surface area are feasible solutions. Application of these solutions might be better suitable for some of the compressor types discussed in paragraph III-B and could be a motivation to further develop that specific type.

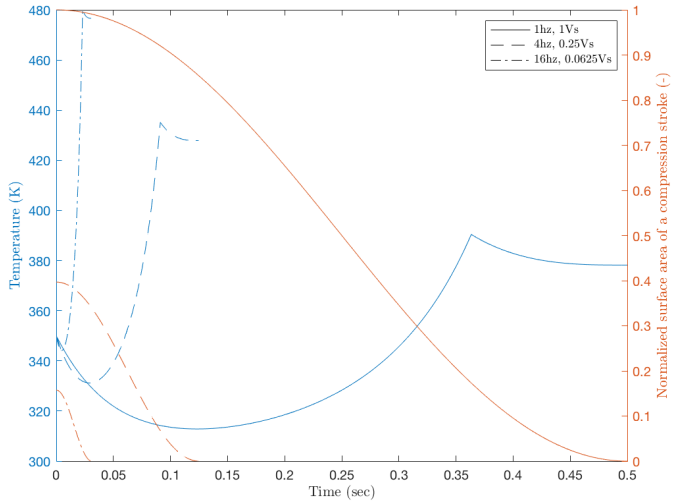

Fig. 7. Progression of temperature and normalized surface area of a compression stroke with different frequencies and swept volumes of the first stage of a two-stage compressor with a total pressure ratio of 80.

B. Mechanical Design

A compressor is a mechanical system that consists of multiple components that move with respect to each other. Moving components usually come with friction and wear and specifically for a compressor leakage may influence the total performance. From a mechanical point of view it is desired to keep all these factors to a minimum.

Friction results in a direct increase in power to reach the discharge pressure. Wear shortens the lifetime of the system. A direct relation between the two is not obvious and depends on the system characteristics. Wear can be defined by Archard's wear equation [17], see equation 6, and is expressed as a wear volume with C the wear coefficient, H the hardness of the contact surface, W the normal load and L the sliding distance. $\frac{C}{H}$ is often expressed as the wear rate k in mm^3/Nm. The sliding distance is defined by the desired lifetime of the system in seconds, the distance per stroke, x_{stroke} and the frequency, f.

$$V = \frac{C}{H} * W * L = k * W * (336e6 * 2 * x_{stroke} * f) \quad (6)$$

Acceptable wear for a compressor depends on the induced leakage and drop in efficiency caused by it. The clearance between piston and cylinder is usually in the range of ten micrometers. A 1.9 cc compressor with an 80 percent volumetric efficiency is able to process the mass flow required by ZEF at a frequency of 16 hertz. For the given lifetime, this would result in approximately 3.3 billion cycles and a sliding distance of 83 million meters. It is convenient to express the load as a contact pressure to include the geometric dependency, the wear volume will then change in a wear depth. For a contact pressure that is based on the average gas pressure of the compressor, a wear rate between 10^{-9} and 10^{-12} mm^3/Nm is needed to keep the wear depth equal to the initial clearance. The range is caused by the assumptions made on the contact area, a 1.9 cc cylinder with a stroke-to-bore ratio of 1 and a piston height of 10 mm is used, which has a minimum value with an average pressure distribution around the piston and a maximum when a hertz contact is applied. Especially in lubricated contacts, the reality will be somewhere in the middle [18]. Regarding the wear coefficient, the following is stated by Jin and Fisher [19]:

> "The key to computational wear prediction is the wear factor or wear coefficient. A simple pin-on-plate machine, which is usually used, may not replicate the lubrication conditions which can be important for some bearing surfaces such as metal-on-metal combinations. Such a problem can be partially overcome by using different wear factors/coefficients, determined from full simulator studies by matching the predicted wear with the experimental measurements. . . . A comprehensive consideration of lubrication in computational wear modelling in metal-on-metal bearing is still lacking. Direct wear prediction without experimental input of wear coefficients would be very difficult, if not impossible".

As written it is hard to quantify the exact wear rate. Wear can be categorized in abrasive, adhesive, fatigue, thermal and corrosive wear and the severity is largely affected by the dominant wear mechanism [20]. This can be expressed in a wear mode diagram which shows the wear rate in correlation with the wear mechanisms. It should be noted that for each material combination, lubrication type and operating window such a diagram will look differently, see figure 8 [21], [22].

As the lifetime of 20 years has such a serious influence on the wear depth, it is key to reduce the other factors. These are related to the choice of compressor type and the type of lubrication. For this project, it is sufficient to get an overview of the potential ranges that can be achieved with different

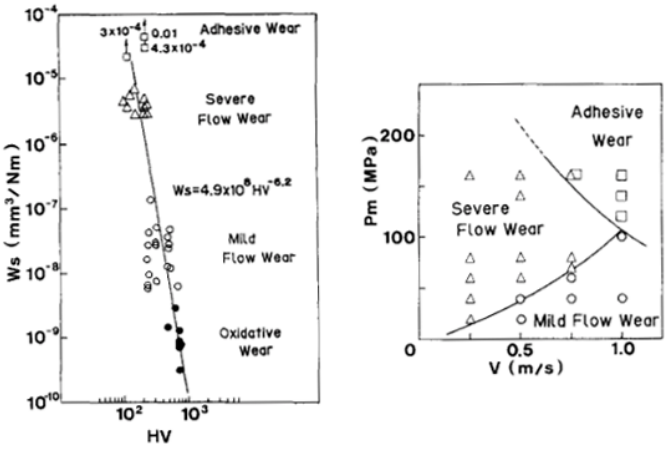

Fig. 8. Left: Relationship between the specific wear rate W_s and the hardness H_v for lubricated sliding of carbon steel. Right: Wear mode diagram in lubricated sliding of carbon steel at 133 H_v. [22]

types of lubrication. A brief overview of the characteristics that come with a few important lubrication methods will be shown next.

1) Hydrodynamic lubrication: The most common way to reduce friction and wear in compressors and engines is the use of lubrication oil. Oil functions as a coolant for the compressor components and motor at the same time. The operating conditions and the choice of oil are closely related with the tribological performance and come together in a Stribeck curve as shown in figure 9. The horizontal axis shows the ratio between the fluid film thickness and the surface roughness, λ. Below a value of one, the surface roughness is larger than the fluid film. Here the friction force is based on coulomb friction only and depends on the coefficient of friction between the two surfaces and the normal force, equation 7. Above a value of three, the fluid is in the hydrodynamic regime and friction is mainly based on the dynamic viscosity of the fluid, the contact area, the film thickness and the relative velocity, equation 8. In the middle of these regimes mixed lubrication can be found, where surfaces asperities touch but load is also partially carried by the fluid. This is the point were significant wear starts to occur [23].

$$F_{f,coulomb} = f_{fri} F_n \tag{7}$$

$$F_{f,viscous} = \frac{\mu_v A}{h_o} v \tag{8}$$

The horizontal axis can also be expressed by the duty parameter which depends on the fluid velocity, the dynamic viscosity of the fluid and the load. A smaller duty parameter comes with a lower λ and thinner fluid film [24]. The operating frequency has already been discussed in section V-A in relation to discharge temperature with a preference for the low side. From a lubrication perspective, the frequency is directly related to the fluid velocity between the piston and cylinder. The viscosity seems like a free value to choose to the circumstances, but is dependent of the temperature, pressure and shear rate [25]. A high oil temperature leads to a drop in viscosity, where a high pressure on the oil film increases the viscosity. The temperature of the oil is not equal to the gas temperature and requires an elaborate thermal model to be determined. Friction by itself enhances heat generation for example. The viscosity and with that the oil temperature should be kept in a certain range to avoid wear of the piston and cylinder, but also to maintain the thermal stability of the oil itself. Oil is known to degrade through oxidation reactions and thermal decomposition which break the fluid down and form heavy insoluble products such as sludge [26]. Below 60 degrees Celsius the reactions are comparatively slow, but the life of an oil is reduced by 50 percent for every 15 degrees Celsius temperature rise above 60 degrees, according to the Arrhenius equation for chemical reaction rates [27]. On top of that, solubility of CO_2 in oil is significantly larger than of most inert gasses which also decreases the viscosity. Beerbower

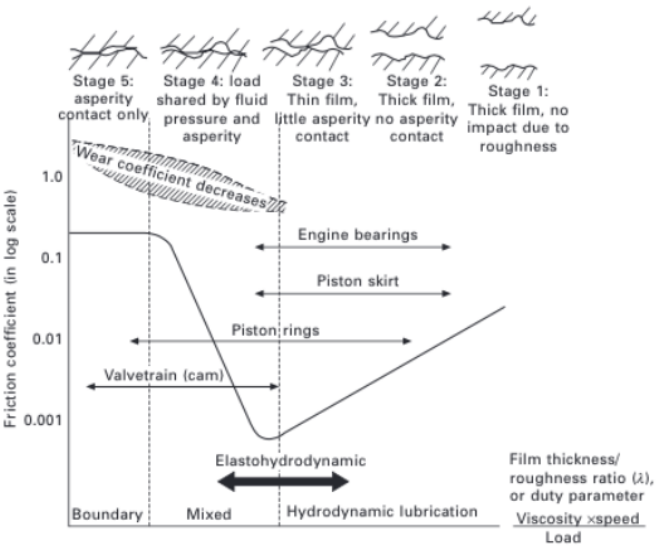

Fig. 9. The Stribeck diagram with lubrication regimes, contact illustrations and engine tribological components [23].

and Greene [28] conducted experiments by dissolving CO_2 in mineral oil at 27 bar and 27 degrees Celsius which led to a viscosity ratio of 0.31. A higher gas pressure increases the solubility even more but a higher gas temperature on the other hand seems to reduce the solubility of CO_2 slightly. Altogether, reaching a higher viscosity to compensate for a lower frequency might be challenging. The pressure of the compressed gas is the main factor for the loads on the oil film. A maximum pressure of 60 bar is high for a compressible gas, but hydraulic systems are usually able to reach multiple factors beyond this value. Lastly, it should also be noted that all these factors are dynamic throughout each cycle. With a high relative velocity at mid-stroke and a zero velocity at the TDC and BDC. The gas temperature behaves as shown in figure 7 and the normal load is a combination of the sinusoidal piston velocity and the pressure rise throughout the stroke. Machines with heavy stationary loads can be limited by the wear during start-ups [25]. After significant operating time, wear can occur due to oil contamination and flowing particles that grind the surface. The lowest wear rates are usually caused by oxidative wear only [29]. An overview of typical ranges of friction coefficients and wear rates is given in table V.

TABLE V
TYPICAL COEFFICIENTS OF FRICTION AND WEAR RATES IN MM^3/NM FOR DIFFERENT LUBRICATION REGIMES IN METAL-METAL CONTACT.

Regime	Coefficient of friction	Wear rate
Dry	0.6-0.8 [19]	$10^{-3} - 10^{-7}$ [29]
Boundary/mixed	0.08-0.12 [23]	$10^{-7} - 10^{-9}$ [19], [29]
Hydrodynamic	0.005-0.0005 [23], [29]	$< 10^{-9}$ [29]

It is most likely that the system should almost continuously operate in the hydrodynamic regime for a maintenance free system. Keeping the oil temperatures low for lifetime purposes of the compressor components as well as the oil might be

more important than for efficiency as discussed previously. An optimum has to be found between the frequency and resulting temperature, viscosity and relative velocity. The last path in the equation that can be altered is the load. The pressure on the oil film can be reduced by an increase in contact area. So far most assumptions have been made with a crankshaft mechanism in mind. Since only the load normal to the oil film has to be taken into account, a more fundamental design choice like linear actuation might be a step towards full film lubrication.

2) Dry Lubricants: An alternative approach that can be taken is the use of solid, dry lubricants. This could be an attractive option due to their simplicity, cleanliness, low expense, quiet operation, low maintenance, low outgassing and high temperature capability [30]. This last point in particular is a major advantage over oil. A few materials are well-known for their low friction properties as a solid material. Graphite, molybdenum disulfide (MoS_2) and PTFE will be discussed but do not give a complete overview [31]. The wear resistance is often on the low side and/or depends on the conditions. It is common practice to apply dry lubricants as coatings or as composites and filler materials. All these variables influence the properties of these materials and a compact overview of the main advantages and limitations will be given.

Graphite is known to wear away as fine dust under vacuum conditions, but sees a sharp reduction in its wear rate by contact with some condensible vapors at low pressures [32]. It is with this reason that graphite it often applied in water lubricated systems. CO_2 unfortunately does not induce this effect [33], but sufficient vapor pressure can under certain conditions be as low as the partial pressure of water in ambient air. As the compressor is filled with filtered CO_2 captured from the air, it is at this moment uncertain what the fraction of water vapour will be. Graphite has a good resistance against high temperatures. It experiences a drop in lubricating property for a window just above room temperature which can be counteracted by certain additives [34]. The wear rate of a dry sliding bronze-graphite composite was measured in the order of 10^{-5} mm^3/Nm which decreased by a factor 10 under water lubrication [35]. Values in the range of 10^{-6} are generally seen for experiments with graphite and graphite composites sliding on metal surfaces [36].

Molybdenum disulfide, opposed to graphite, has a low wear rate in the range of 10^{-6} mm^3/Nm in medium and high vacuum and experiences an increase when measured in atmospheric air [37]. Tests with dry nitrogen show a decrease by a factor 10 compared to air which is promising for dry CO_2 [38]. MoS_2 has a wide temperature operating range. On heating in air oxidation becomes appreciable above 370 degrees Celsius and rapid above 560 degrees [39]. In nitrogen and hydrogen atmospheres lubrication is usually better.

Pure PTFE has one of the lowest coefficients of friction, but comes with an extremely high wear rate. Adding fillers of different materials and mass fractions can improve the wear rate significantly with small effect on the friction coefficient and has been studied thoroughly. Pure PTFE shows wear rates between 10^{-3} and 10^{-4} mm^3/Nm. Fillers of among others bronze, glass, graphite and MoS_2 can reduce this to get close to values of 10^{-7} [40], [41]. The filler materials also influence the temperature resistance of the composite. Inorganic fillers tend to wear faster at increasing temperatures than organic fillers which are relatively stable up to 150 degrees Celsius and increase rapidly after [42].

3) Gas seals: As filling the piston-cylinder clearance with oil is a solution, so is filling it with a gas. This is useful to deal with higher temperatures and reduce contamination, friction, wear and maintenance. For a passive gas application, the term clearance seal is often used. In theory it is possible to generate internal pressure due to the relative velocity of components similar to oil. However, the viscosity of gasses is generally lower which would ask for a higher relative velocity or lower normal loads. The latter is often accomplished by combining radial springs with a linear actuation [43], [44]. As no contact occurs at all, friction is only generated due to viscous forces and wear is negligible. A large number of studies have been conducted on the leakage of clearance seals. This is often modelled as a steady flow through an annulus, a couette-poiseuille flow, driven by the pressure difference across the piston [44], [45]. For oil seals a rough assumption is that 10 percent of the oil mass flow rate is dissolved CO_2 [46] and is often assumed negligible. Dry lubricants in new condition show even lower values. For clearance seals the results vary widely due to differences in geometry and operating conditions. An appropriate cylinder-piston clearance range for a moving coil linear compressor with a maximum power input of 100 watt is set to be between 8 to 12 micrometers [43]. With appropriate in this case defined as the compromise between sufficient clearance to avoid contact and wear but not too much to prevent excessive leakage losses. The in-cylinder change in mass and pressure during a cycle shows a significant downtrend for different clearances between 3 and 5 micrometers for high pressure hydrogen applications [45]. Liang et al. (2014) found a seal leakage power loss of maximum four percent of the total motor output power [46]. It is generally stated that, with proper design, it is possible to create acceptable leakage rates. This proper design will come with high machining tolerances and with that high production costs.

An active application is called an aerostatic seal. In this case the internal pressure is fed to the system from an external source which adds lateral stiffness. An example of a linear compressor with aerostatic seal is shown in figure 10. One of the major advantages is that the lubricant, in this case high pressure CO_2, will be a continuous flow of clean gas which solves issues with contamination, heating and wear of the lubricant itself. Santos et al. (2019) show the volumetric and isentropic losses of a linear piston compressor due to its aerostatic seal [47]. Both undergo a reduction of 2.5 and 4 percent respectively when the radial clearance is varied from 2.5 to 10 micrometers. It is worth mentioning that the

total power loss due to friction is only between 0.2 and 0.4 percent of the total power. This research was carried out with a discharge pressure and with that aerostatic pressure of 10.3 bar. The load carrying capacity and stiffness of the gas film depends on the flow rate and pressure of this film and will most likely influence the efficiency significantly. Another remark is that when the aerostatic pressure relays on the discharge pressure, the start-up sequence may still be prone to friction and wear.

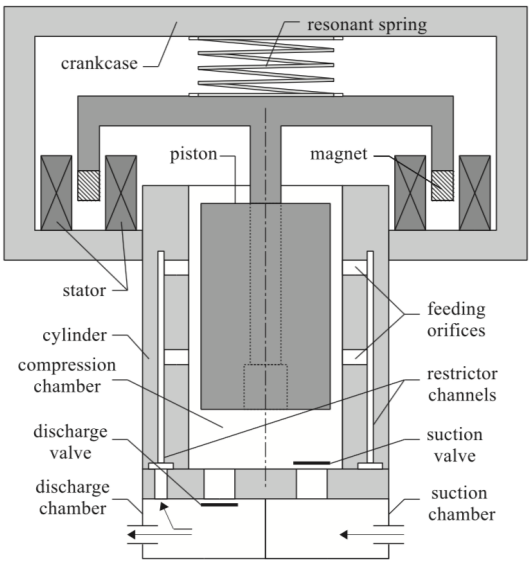

Fig. 10. Schematic showing the main moving parts of a linear compressor with aerostatic seal [47].

As mentioned it is beneficial to continuously renew the lubricant. The ZEF process starts with the capture of air and filtering of CO_2. When the CO_2 is extracted a mixture of gasses and water stay readily available next to CO_2. A gas needs to be compressed before being used as a lubricant. As this comes with a new compression process, this would be inefficient. Water is another option but comes with a lower viscosity and boiling point than oil for passive lubrication. Pressurizing water is easier than gas but still not desired as a side process. Adding water will also stimulate corrosion especially in contact with CO_2.

Lubrication, friction and wear of the sliding components of a compressor have been discussed in depth. The valves of a compressor belong to the mechanical design as well and come with leakage and ask for a slight over-pressure to open. This consequently decreases the efficiency and increases the power consumption. Valves also come with a lifetime that has to reach the 20 year requirement. Several concepts for valves exist and can be optimized. For this research only the number of valves in the different compressor types will be taken into account.

C. Electrical Design

Compressors are usually driven by electric motors. Most common is a rotary motor with a stator and a rotor. AC motors can be plugged directly to the grid and the input frequency dictates the rotational speed. Compared to a synchronous motor, the induction motor is slightly less efficient but self-starting and cheaper and therefore often seen in the industry. For applications with renewable energy sources, which usually generate DC power, it might be attractive to use a DC motor to avoid the necessity of an inverter. It is highly likely that a DC-DC converter is still necessary to regulate the input voltage. For lifetime and efficiency purposes a brushless DC motor with a permanent magnet rotor is a suitable option. Next to rotary motors, linear reciprocating motors are used in small compressors equipped with a spring. They are tuned to operate at their resonance frequency. In general linear compressors operate with a higher efficiency than reciprocating compressors [46], [48]. A quick drop in efficiency in linear compressors has been noticed in experiments at off-resonance performance. A 5 percent change of the drive frequency away from the resonance requires 11 percent extra electrical power [49]. The resonance frequency depends on the moving mass, the spring stiffness and the gas stiffness shown in equation 9.

$$k_{gas} = \frac{(P_{discharge} - P_{suction}) * A_p}{x_p} \tag{9}$$

Where a rotary motor usually comes with a geometrically determined stroke length, x_p, a linear motor has the option to vary this length dynamically. As the mass flow and suction pressure may vary at ZEF, the compressor needs to be controlled continuously to maintain a high efficiency. A rotating motor is often combined with a crankshaft mechanism that creates a transmission that is not part of a linear motor. A linear motor that is able to reach the required force might be very large. For both systems counts that the lifetime of the motor might actually be the limiting factor for the overall compressor but will not be taken into account for this review. For ZEF a factor that might be of influence is that rotary motors are much more common and probably off-the-shelf available with the required specifications, where the chance will be higher that a linear motor needs to be custom-made and therefore more expensive.

VI. Summary

The main thermal, mechanical and electrical characteristics as referred to in equation 3 have been discussed. From a thermal perspective it is difficult to keep a two-stage compressor within a normal temperature window. A three- or four-stage compressor would reduce the temperatures significantly but would increase the design and production costs. Mechanically, lubrication is the key to a high efficiency and sufficient lifetime. Hydrodynamic lubrication is most likely limited by the lifetime of the oil itself, especially with the temperatures of a two-stage compressor. Dry lubricants show high wear rates. Clearance and aerostatic seals are

promising when the lubricant is continuously renewed. Implementation in one of the compressor types is the biggest challenge here. A linear motor is more efficient electrically and has the benefit of exerting low lateral forces on the seals. Rotary motors are more common, easier to tune and the DC type requires less converter steps.

Looking back at figure 4, the question rises which compressor type fits the combination of these properties best. Rotary motors with crankshaft mechanisms, figure 4b and 4c, come with the highest lateral forces on the piston-cylinder interface. One remark that has been left out so far is that a crankshaft mechanism comes with extra rotating contact surfaces between the crankshaft and the connecting rod, and the connecting rod and the piston, which are locations where clearance or aerostatic bearings are hard to implement. Linear motors, figure 4d, are not preferred due to control development in a compressor with high mass flow fluctuations. A pressure intensifier, figure 4e, could work with a separate oil pump to feed the intensifier. The inlet side of the intensifier would be cooled by this oil and the actuation would be linear. The system would come with six valves as the oil pump has two and the intensifier four. The size and costs would probably increase due to the extra oil circuit. The rolling piston compressor, figure 4a, is ideal as it has a direct connection, no added moving components, between the rotary motor and the piston. It also comes with only one discharge valve and no suction valve. It is a challenge to implement clearance and aerostatic seals with minimal leakage. If necessary this could be done by altering the mechanical concept slightly. Similar compressors like a revolving vane compressor might be useful to evaluate [51].

To conclude, for ZEF two solutions seem feasible. It is possible to run an oil-lubricated compressor system with a decent lifetime when the number of stages is increased to three or four. For a more precise lifetime estimation, a more elaborate thermal and wear analysis is required. This would open up space to use more off-the-shelf components which might need alterations in terms of size. The second solution is more experimental and involves the implementation of clearance and aerostatic seals in an existing compressor type. A minimum amount of relative moving components is preferred. A linear compressor would be the first choice followed by a rolling piston compressor.

VII. Thesis Proposal

As a continuation on this literature review, a DC, rolling piston type, rotary compressor will be designed based on aerostatic and aerodynamic bearings making use of compressed CO_2. For contact surfaces with small or zero loads, dry lubricants might be applied or added to the air bearing.

References

[1] IPCC, 2014: Climate Change 2014: Synthesis Report. Contribution of Working Groups I, II and III to the Fifth Assessment Report of the Intergovernmental Panel on Climate Change [Core Writing Team, R.K. Pachauri and L.A. Meyer (eds.)]. IPCC, Geneva, Switzerland, 47 pp.

[2] Eriks BV, "Eriflon Zuigerafdichting", 2015. Available:https://eriks.nl/dam/nl/downloads-eriks-nl/productdatasheets/afdichtings–&-rubbertechniek/Afdichtingstechniek/hydrauliek-en-pneumatiek-afdichtingen/zuigerafdichtingen/RX®-Eriflon-Zuigerafdichting-0410.pdf. [Accessed 30 March 2020].

[3] Kim M-H, Pettersen J, Bullard CW. Fundamental process and system design issues in CO2 vapor compression systems. Prog Energy Combust Sci 2004;30:119–74.

[4] "Refrigerants Product Data Summary", Linde-gas.com. [Online]. Available: https://www.linde-gas.com/en/images/Refrigerants-Product-Data-Summary_tcm17-108590.pdf. [Accessed: 21- Feb- 2020].

[5] "Daimler takes delivery of CO2 compressors - Cooling Post", Cooling Post, 2017. [Online]. Available: https://www.coolingpost.com/world-news/daimler-takes-delivery-of-co2-compressors/. [Accessed: 21- Feb- 2020].

[6] G.F. Hundy, Refrigeration, Air Conditioning and Heat Pumps, 5th ed. Elsevier Science & Technology, 2016, p. 60.

[7] R. Brown, Compressors, selection and sizing, 3rd ed. Gulf, 2005, p. 3.

[8] J. Yang et al., "A sensitivity study of size parameters in a twin-type rolling piston compressor", International Journal of Refrigeration, vol. 36, no. 3, pp. 786-794, 2013.

[9] T. Jao and A. Verhelst, "Marine Engine Oils", Encyclopedia of Tribology, pp. 2164, 2013.

[10] "Hofer Diafragm Compressors", Www-eng.lbl.gov. [Online]. Available: http://www-eng.lbl.gov/ shuman/NEXT/GAS_SYS/diaphragmcompressor10-02_hofer.pdf. [Accessed: 31- Mar- 2020].

[11] C. Bradshaw, E. Groll and S. Garimella, "A comprehensive model of a miniature-scale linear compressor for electronics cooling", International Journal of Refrigeration, vol. 34, no. 1, pp. 63-73, 2011.

[12] "Hydraulic intensifiers - Pressure intensifier — Hänchen", Herbert Hänchen GmbH & Co. KG. [Online]. Available: https://www.haenchen-hydraulic.com/pressure-transformer/pressure-intensifier.html. [Accessed: 31- Mar- 2020].

[13] K. Ueno, R. Bye and K. Hunter, "Compressor Efficiency Definitions", 2003.

[14] M. Oliveira, M. Diniz and C. Deschamps, "Thermal modelling and analysis of an oil-free linear compressor", IOP Conference Series: Materials Science and Engineering, vol. 90, 2015.

[15] A. Mills, Basic heat and mass transfer, 2nd ed. 2013, p. 50.

[16] H. Huff, R. Radenmacher, "CO2 Compressor-Expander Analysis", 2003.

[17] J. Archard, "Contact and Rubbing of Flat Surfaces", Journal of Applied Physics, vol. 24, no. 8, pp. 981-988, 1953.

[18] D. Brewe, "Slider Bearings", in Modern Tribology Handbook, B. Bhushan, Ed. CRC Press, 2001, pp. 996-1003.

[19] Z. Jin and J. Fisher, "Tribology in joint replacement", Joint Replacement Technology, pp. 31-61, 2014.

[20] K. Kato, K. Adachi, "Wear Mechanisms", in Modern Tribology Handbook, B. Bhushan, Ed. CRC Press, 2001, pp. 273-299.

[21] T. Akagaki and K. Kato, "Wear mode diagram in lubricated sliding friction of carbon steel", Wear, vol. 129, no. 2, pp. 303-317, 1989.

[22] T. Akagaki and K. Kato, "Effects of hardness on the wear mode diagram in lubricated sliding friction of carbon steels", Wear, vol. 141, no. 1, pp. 1-15, 1990.

[23] Q. Xin, Diesel engine system design, 1st ed. Cambridge: Woodhead Publishing Limited, 2011, pp. 651-664.

[24] M. Kalin, I. Velkavrh and J. Vižintin, "The Stribeck curve and lubrication design for non-fully wetted surfaces", Wear, vol. 267, no. 5-8, p. 1237, 2009.

[25] D. Sander, H. Allmaier and H. Priebsch, "Friction and Wear in Automotive Journal Bearings Operating in Today's Severe Conditions", Advances in Tribology, pp. 144-167, 2016.

[26] Ö. Karacan, M. V. Kök and U. Karaaslan. "Dependence of Thermal Stability of an Engine Lubricating Oil on Usage Period", Journal of Thermal Analysis and Calorimetry 55, no. 1, 1999.

[27] L. Severa, M. Havlíček and V. Kumbár, "Temperature dependent kinematic viscosity of different types of engine oils", Acta Universitatis Agriculturae et Silviculturae Mendelianae Brunensis, vol. 57, no. 4, pp. 95-102, 2009.

[28] A. Beerbower & D. F. Greene, "The Behavior of Lubricating Oils In Inert Gas Atmospheres", ASLE TRANSACTIONS, 4:1, 87-96, 1961.

[29] K. Kato, "Friction and wear of passive metals and coatings", Tribocorrosion of Passive Metals and Coatings (pp. 90–93). Woodhead Publishing (2011).

[30] D. Burris and W. Sawyer, "A low friction and ultra low wear rate PEEK/PTFE composite", Wear, vol. 261, no. 3-4, pp. 410-418, 2006.

[31] Graphite, Molybdenum Disulphide and/or P.T.F.E.?", Industrial Lubrication and Tribology, vol. 15, no. 11, pp. 25-26, 1963.

[32] R. Savage and D. Schaefer, "Vapor Lubrication of Graphite Sliding Contacts", Journal of Applied Physics, vol. 27, no. 2, pp. 136-138, 1956.

[33] H. Wang, "Graphite Solid Lubrication Materials", Encyclopedia of Tribology, pp. 1550-1555, 2013.

[34] H. Sliney, "High temperature solid lubricants: when and where to use them", Design Eng. Conf, Philadelphia, United States, 1973.

[35] J. Jia, J. Chen, H. Zhou, J. Wang and H. Zhou, "Friction and wear properties of bronze–graphite composite under water lubrication", Tribology International, vol. 37, no. 5, pp. 423-429, 2004.

[36] P. Blau and R. Martin, "Friction and wear of carbon-graphite materials against metal and ceramic counterfaces", Tribology International, vol. 27, no. 6, pp. 413-422, 1994.

[37] S. Kim, C. Ahn and T. Kim, "Tribological characteristics of magnetron sputtered MoS2 films in various atmospheric conditions", KSME International Journal, vol. 16, no. 9, pp. 1065-1071, 2002.

[38] S. Domínguez-Meister, T. Rojas, M. Brizuela and J. Sánchez-López, "Solid lubricant behavior of MoS2 and WSe2-based nanocomposite coatings", Science and Technology of Advanced Materials, vol. 18, no. 1, pp. 122-133, 2017.

[39] J.P.G. Farrm, "Molybdenum disulfide in Lubrication. A review", Wear, vol. 35, no. 1, pp. 1-22, 1975.

[40] J. Khedkar, I. Negulescu and E. Meletis, "Sliding wear behavior of PTFE composites", Wear, vol. 252, no. 5-6, pp. 361-369, 2002.

[41] T. Blanchet and F. Kennedy, "Sliding wear mechanism of polytetrafluoroethylene (PTFE) and PTFE composites", Wear, vol. 153, no. 1, pp. 229-243, 1992.

[42] D.C. Evans, J.K. Lancaster, "The Wear of Polymers", Treatise on Materials Science & Technology, vol. 13, pp. 85-139, 1979.

[43] H. Dang, "Development of high performance moving-coil linear compressors for space Stirling-type pulse tube cryocoolers", Cryogenics, vol. 68, pp. 1-18, 2015.

[44] C. Bradshaw, E. Groll and S. Garimella, "A comprehensive model of a miniature-scale linear compressor for electronics cooling", International Journal of Refrigeration, vol. 34, no. 1, pp. 63-73, 2011.

[45] Y. Deng, N. Miao, D. Wu, Y. Liu, X. Zhai and J. Tong, "A new high-pressure clearance seal with flexible laddered piston assembly in oil-free miniature compressor for potential hydrogen applications and investigation on its dynamic sealing efficiency", International Journal of Hydrogen Energy, vol. 44, no. 45, pp. 24856-24866, 2019.

[46] K. Liang, R. Stone, W. Hancock, M. Dadd and P. Bailey, "Comparison between a crank-drive reciprocating compressor and a novel oil-free linear compressor", International Journal of Refrigeration, vol. 45, pp. 25-34, 2014.

[47] C. Santos, T. Dutra and C. Deschamps, "Scrutinizing the sources of inefficiencies in the piston-cylinder clearance of an oil-free linear compressor", International Journal of Refrigeration, vol. 104, pp. 513-520, 2019.

[48] B. Ku, J. Park, Y. Hwang, and J. Lee, "Performance Evaluation of the Energy Efficiency of Crank-Driven Compressor and Linear Compressor for a Household Refrigerator", Proceedings of International Compressor Engineering Conference, Purdue, 1218, pp. 1-16, 2010.

[49] K. Liang, R. Stone, M. Dadd and P. Bailey, "A novel linear electromagnetic-drive oil-free refrigeration compressor using R134a", International Journal of Refrigeration, vol. 40, pp. 450-459, 2014.

[50] J. Wu and A. Chen, "A new structure and theoretical analysis on leakage and performance of an oil-free R290 rolling piston compressor", International Journal of Refrigeration, vol. 49, pp. 110-118, 2015.

[51] K. Tan, K. Ooi, "A novel revolving vane compressor with a fixed-vane", International Journal of Refrigeration, vol. 34, pp.1980-1988, 2011.

3

Mechanical Analysis

This chapter elaborates on the literature review and presents a concept that needs to be modified for gas bearing implementation. This concept is analysed on its compression process and corresponding mechanical loads as a preparation for the bearing design.

3.1. Concept Analysis

Currently available compressor types, usually based on liquid (mostly oil) or dry lubricants, are not able to reach ZEF's desired lifetime, especially for high pressure ratios and with that high temperature environments. The performance under these conditions can be improved when gas bearings are applied. The design of the surface interfaces between components for this application asks for a specific approach. All bearings are designed to carry loads. In compressors these bearings are commonly also used to seal the high pressure compartment from leakage. Liquid and dry lubricants actively prevent this by respectively creating a fluid layer in the bearing gap or completely closing the gap. Both of these properties are missing in gas bearings, which is why the leakage rate has to be evaluated carefully.

Both the load capacity as well as the leakage rate are a function of the bearing gap height and film thickness, h and the relative velocity V of the moving components. The working principle differs when we consider a sliding or a rotating bearing, but in all cases a dynamic pressure $P_b(x,y)$ will build up in the gap which will be discussed in Chapter 4. The integral of this pressure over the surface area A_1, which is the gap length L times the gap width w, yields the load capacity given in equation 3.1.

$$F_b = \int P_b(x,y)\, dA_1 = \int_0^w \int_0^L P_b(x,y)\, dxdy \tag{3.1}$$

A first estimate of the leakage rate can be made by looking at a fully-developed combined Couette-Poiseuille flow, see Figure 3.1 [1]. The flow rate is the integral of the fluid velocity u over the area A_2 which is the gap width times the gap height h, see equation 3.2. The fluid velocity consists of two terms: the Couette and Poiseuille terms shown in equation 3.3. The first one is driven by the relative velocity of the moving components and depends on the gap height. The second term is driven by the pressure difference $P_{in} - P_{out}$ and depends on the dynamic fluid viscosity μ, the gap length over which the pressure drops and the gap height as well. Throughout a compression cycle these terms will alternately cooperate and oppose each other. A detailed leakage analysis is discussed in Chapter 5.

$$Q = \int u\, dA_2 = \int_{-h/2}^{h/2} u\, w dz \tag{3.2}$$

$$u = u_1 + u_2 = \underbrace{\frac{V}{2}\left(1 + \frac{2z}{h}\right)}_{\text{Couette}} + \underbrace{\frac{1}{2\mu}\frac{P_{in} - P_{out}}{L}\left(\frac{h^2}{4} - z^2\right)}_{\text{Poiseuille}} \tag{3.3}$$

The surface areas A_1 and A_2 and the ratio between length, width and height are important parameters and are preferably scaled freely.

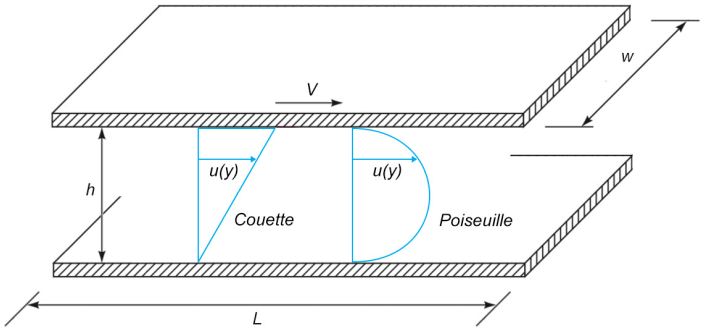

Figure 3.1: Couette and Poiseuille flow in the gap between two parallel plates.

The main function of a compressor is periodically enlarging and reducing a closed volume. It is not necessary to start designing from scratch as that function won't change. It is useful to evaluate the existing rolling piston type geometries and analyse the feasibility to implement gas bearings. Figure 3.2 gives an overview of several rolling piston type rotary compressors that are found in literature.

All compressors shown in Figure 3.2 have a piston that changes the volume in part of the cylinder due to the eccentric placement of the piston. That volume is closed at all ends. One end is created by the interface between the piston and cylinder walls, which results in a line contact in three-dimensional space. The second one is realised by a sliding vane that makes a connection between the piston and cylinder. In Figures 3.2a-3.2d, the vane makes a line contact between the vane and either the piston or cylinder wall. This contact type can't be changed as the angle of contact changes dynamically throughout the motion. The concepts in Figures 3.2e and 3.2f replace this line contact by a surface contact by integrating the vane in both the piston and cylinder. These surface contacts are relevant as their lengths appear in equations 3.1 and 3.3 as the variable L. This value approaches zero for a line contact which has a large impact on the leakage rate and ability to build up dynamic pressure. Another problem of the same nature that remains with an integrated vane comes from the width and height of the vane. These have small, finite dimensions that appear in the same way in equations 3.2 and 3.3 as the variables L and w. Preferably the width of the vane should be enlarged and the height reduced. This evaluation should be done for each contact pair.

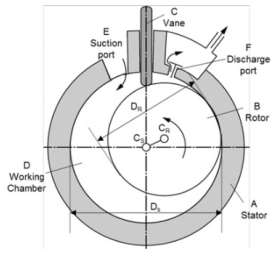

(a) Rolling piston compressor [2]

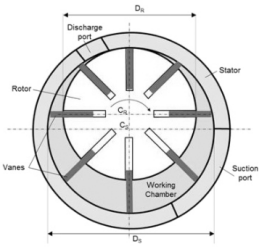

(b) Sliding vane compressor [3]

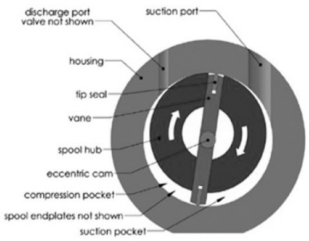

(c) Rotary spool compressor [4]

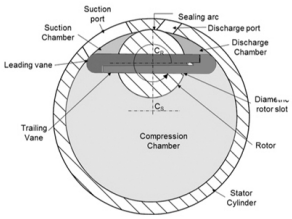

(d) Coupled vane compressor [5]

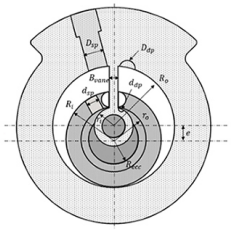

(e) Revolving vane compressor [6]

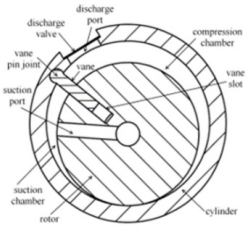

(f) Swing vane compressor [7]

Figure 3.2: Overview of several rolling piston type compressors found in literature.

Another rotary compressor that is based on the eccentricity with respect to the cylinder is the rotary cylinder compressor (RCC) in Figure 3.3. This design comes completely without a vane and also eliminates the line contact between the piston and cylinder wall.

In this case, the shaft is fixed in an eccentric position with respect to the cylinder. The shaft consists of a shaft-axis that fits inside the piston and a shaft rotary bearing, see Figure 3.4. The eccentric motion is created by the shaft rotary bearing that is forced to rotate around a different centre than the cylinder. This constraint is explained in detail in paragraph 3.2. The piston is thereby forced by the casing to rotate in an oval path with respect to the shaft centre. To be able to do this, the piston will reciprocate around the shaft and inside the cylinder. The result is that the volume between the piston and casing enlarges on one side and reduces on the other side during the rotation. This creates two compression chambers that operate out of phase.

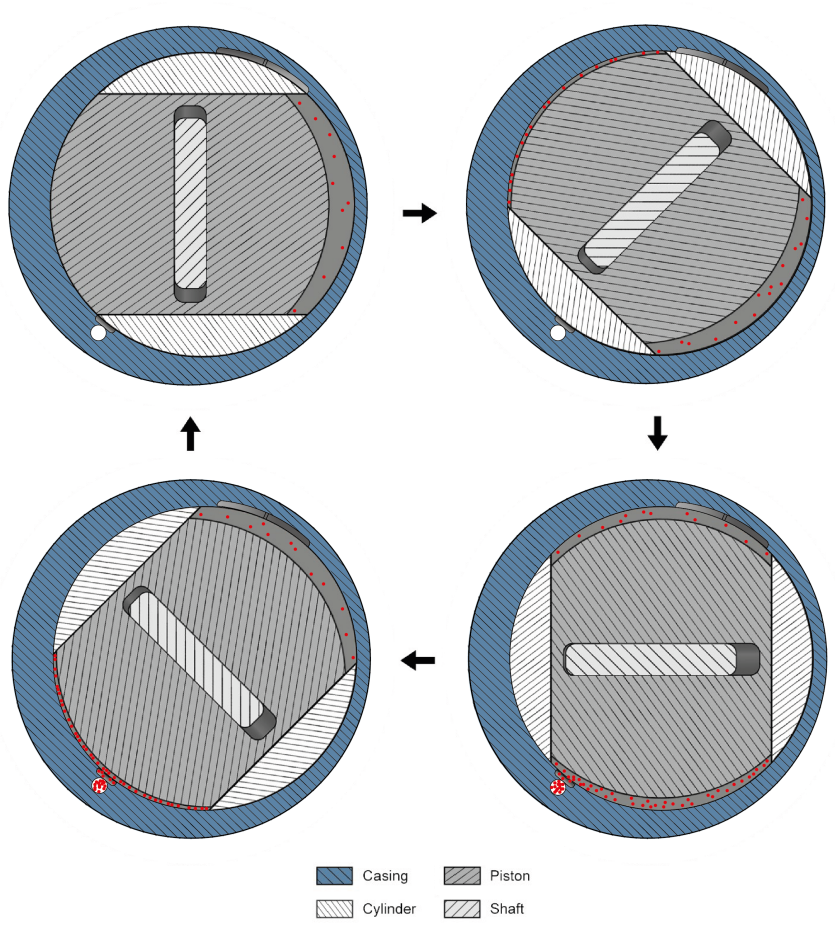

Figure 3.3: Top cross-sectional views of the working principle of a rotary cylinder compressor.

The gas enters and exits the compression chambers via slots in the casing. In the top-left view, the compression chamber just exhausted all its high pressure gas in the exhaust slot which is then closed by the cylinder wall. In the top-right figure the cylinder wall moves past the suction slot which enables the compression chamber to fill with low pressure gas. A detailed explanation about this can found in paragraph 5.1.

This concept comes with only surface contacts, which is an improvement with respect to all concepts in Figure 3.2 as the value of L is significantly larger. Adjustments have to be made to this design to optimise the performance of the gas bearings and seals. An overview of the rotary cylinder compressor as given by Hu et al. can be found in Appendix A.1 .

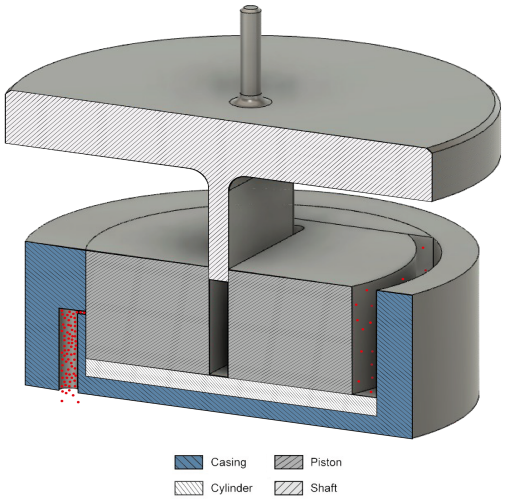

Figure 3.4: 3D view of the rotary cylinder compressor with raised shaft to show the internal components.

3.2. Shaft Design

It is a required that the shaft should be constraint to move in x- and y-direction while still being able to rotate freely. This function is performed by a rotary bearing that will take the loads in x- and y-direction of the gas pressure that are transferred from the piston to the shaft. The chamber of the bearing in the casing is placed eccentrically with respect to the chamber of the cylinder. The load capacity of a gas bearing is influenced by the surface area of the bearing which has a linear relationship with the radius and height of the bearing. Figure 3.5 shows the front and side cross-sectional view of an assembly with a shaft equipped with a large rotary bearing.

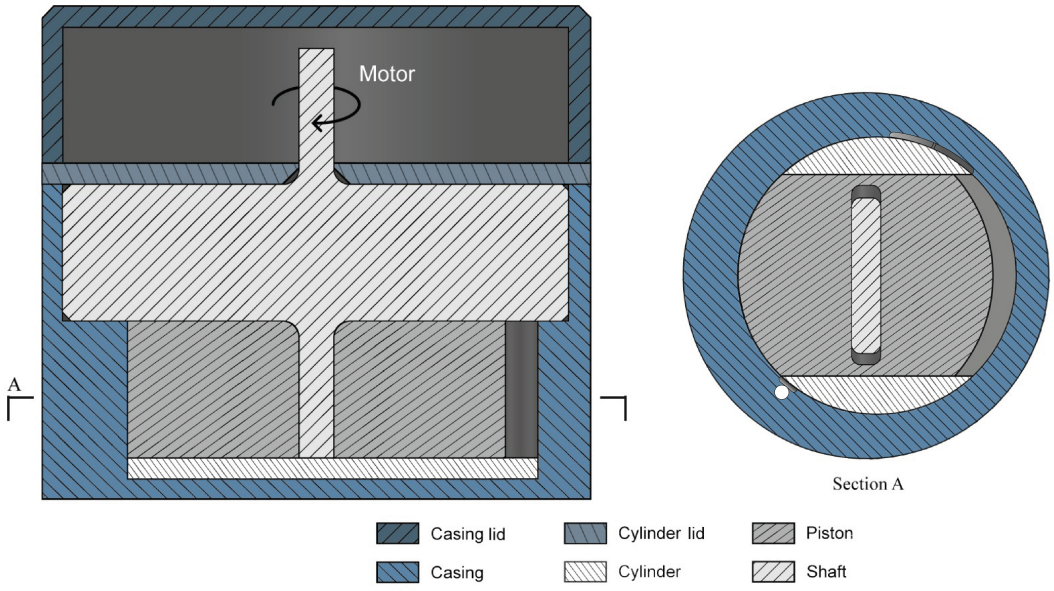

Figure 3.5: Front and top cross-sectional view of a shaft-actuated compressor with shaft rotary bearing.

The bearing of the shaft is only added on the top side. In this way a moment is introduced in the bearing next to the transverse load. This can be prevented in multiple ways:

- A second rotary bearing surface can be added below the piston. Each bearing will take care of half of the transverse load which means that the top bearing can be halved. The part of the shaft inside the piston is now connected on both ends which also reduces bending of this component

by roughly a factor of ten. However, one of the rotary bearings has to either fit through the piston or be constructed out of two separate parts. This is undesired as the gap between the cylinder sleeve and the shaft bearing asks for high precision. An illustration of this concept can be found in Appendix A.2.

- The compression chamber could be duplicated and added on top of the shaft rotary bearing. As the gas pressure now pushes on both sides of the shaft rotary bearing, the moments will cancel each other. The volume flow rate of this compressor is set as a requirement which means that when the compression chamber is doubled, the size of each chamber should be halved. This means that both the piston and cylinder have to be produced twice, which would increase the production costs. This concept is also visible in Appendix A.2.

- Putting the rotary bearing in line with the actual gas pressure would make that no moment is introduced at all. It is possible to 'fold' the bearing around the compression chamber, separated by the cylinder sleeve. A precise slot where the folded bearing can rotate in, would complicate the production process. Therefore the casing will be split in two parts and a separate cylinder sleeve is introduced in Figure 3.6. The top left figure shows the design that is actuated via shaft. In the top right figure the cylinder and shaft switch from position and the motor is attached to the cylinder. This particular design solution is discussed in depth in section 3.5.

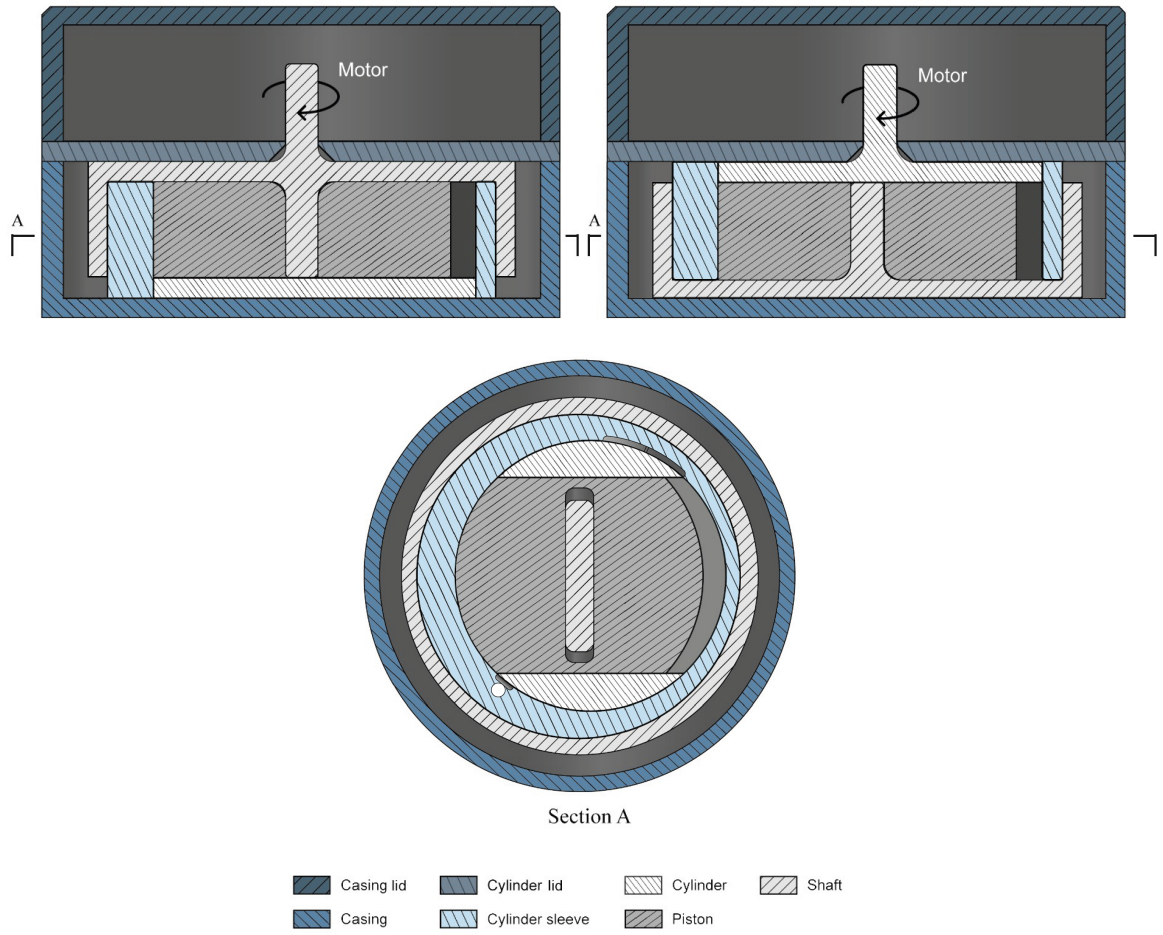

Figure 3.6: Front and top cross-sectional views of a shaft-actuated (left) and cylinder-actuated (right) compressor with 'folded' shaft rotary bearing to prevent the introduction of a moment and with a separate cylinder sleeve component.

3.3. Compression Cycle

The swept volume per second of the compressor is determined by the frontal area of the piston, A, twice the eccentricity of the compressor, e, which yields the stroke and twice the rotational frequency, f as there are two compression chambers, see equation 3.4. The swept volume per second is directly related to the volumetric flow rate which has a constant requirement. The instantaneous volume of one compression chamber depends on the angle of rotation, θ between 0 and 2π radians, given in equation 3.5. The initial position at 0 radians is shown as the right compression chamber in the top left of Figure 3.3 which is the starting position in Figure 3.7a which shows the course of the volume and pressure throughout a full adiabatic compression cycle. The volume starts at its maximum value which means that the suction stroke has just been completed. From here the volume will decrease to a minimum value, the clearance volume, here assumed five percent of the compression chamber volume. During this stroke the pressure increases to a maximum value and remains at that value to the end of the compression stroke at π radians while simultaneously high pressure is exhausted. The compressed air in the clearance volume will then expand until we reach the suction pressure and keeps this pressure until the end of the stroke at 2π radians. Over- and underpressures due to the valves are not considered.

$$\dot{V}_{swept} = 4Aef \tag{3.4}$$

$$V_{swept} = Ae(1 - cos(\theta)) \tag{3.5}$$

$$Power = T\omega = P_{cc}Aesin(\theta)2\pi f \tag{3.6}$$

The power consumed by the system, neglecting friction, can be calculated using the torque and the rotational frequency, see equation 3.6 and Figure 3.7b. The required torque is a function of the pressure and the moment arm, where the moment arm itself comes from the eccentricity of the compressor and changes with the angle of rotation. During the compression stroke, the moment arm is positive which asks for power input. The moment arm becomes negative when passing π radians. This means that the pressure effectively pushes the compressor and the power becomes negative. These figures present the process within one compression chamber. As the RCC has two compression chambers that oppose each other and are π radians out of phase, the negative power of the opposing chamber can be subtracted from the positive power, reducing the instantaneous power. This is also true for the effective torque on the components and bearings.

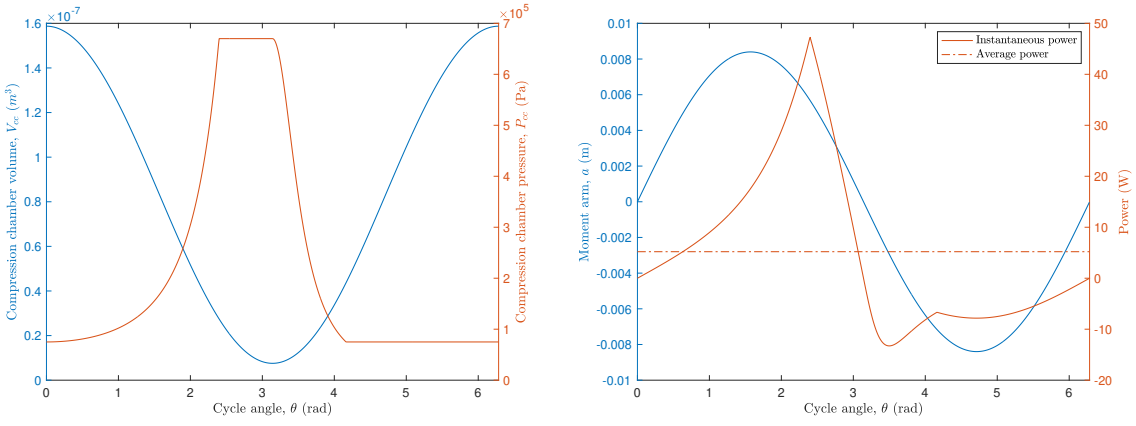

(a) (b)

Figure 3.7: Overview of the course of the volume and pressure in the compression chamber and the moment arm and power of a single compression chamber during a full cycle.

3.4. Flow Analysis

A high pressure ratio of 8.9 combined with a 5 percent clearance volume yields a 76 percent volumetric efficiency, η_v. This value has been set as a design requirement. Within the design process, the volumetric efficiency can be compensated for by either the compression chamber volume or the rotational frequency to be able to reach the target flow rates. The percentage of mass that leaks towards the low pressure compartment and the pressure of the gas when it leaks add to the amount of lost power. This amount should be kept below 10 percent, defined as a percentage η_l of the required mass flow rate $\dot{m}_{in}$. Both losses originate in multiple places throughout the compressor and will be analysed in Chapter 5 and 6.

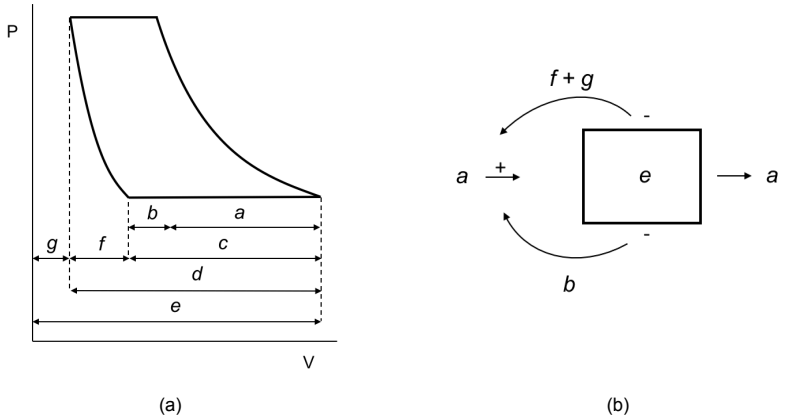

Figure 3.8: (a) Breakdown of the volumes inside the compression chamber during a cycle. (b) The inflow, internal flows and outflow of the system.

It was stated that the mass flow rate of the compressor is an external requirement as this is coupled to the production rate of methanol. This means that the compressor should be designed to that operating point. Figure 3.8a gives a breakdown of the mass flow rate in the compression chamber. The total volume of the compression chamber is defined by the required mass flow, the leakage rate and the percentage of clearance volume. The inflow, internal flows and outflow of the system are drawn in Figure 3.8b. It visible that losses circulate from the compression chamber back to the inlet. As the CO_2 is initially captured from the air, it is essential that the gas is contained within the system. The system should therefore be hermetically closed so that losses end up and remain in the low pressure compartment. Leakage is therefore defined as high pressure gas that expands to the low pressure compartment without doing any work.

$$a: \quad \dot{m}_{in} \qquad\qquad e: \quad \frac{\dot{m}_{in}(2-\eta_L)}{\eta_v}(1+cl)$$

$$b: \quad \dot{m}_{in}(1-\eta_L) \qquad\qquad f: \quad \frac{\dot{m}_{in}(2-\eta_L)}{\eta_v}(1-\eta_v)$$

$$c: \quad \dot{m}_{in}(2-\eta_L) \qquad\qquad g: \quad \frac{\dot{m}_{in}(2-\eta_L)}{\eta_v}cl$$

$$d: \quad \frac{\dot{m}_{in}(2-\eta_L)}{\eta_v}$$

As explained by the equations in section 3.1, the leakage rates between the air bearings are closely related to the dimensions of the components. Table 3.1 gives an overview of the values of the design mass and volume flow rates shown in Figure 3.8b. The mass flow is constant for all stages of a compressor. The volumetric flow decreases from the first stage to the second as can been seen in the second and third row. The last column of the table shows the volume of the compression chamber considering 50 rotations per second and two compression chambers. The values of d are added to this table as these should correspond with $\dot{V}_{swept}$ in equation 3.4 and will be used frequently throughout the mechanical design process.

	a	e	b	$f+g$	d		V_{cc}
$\dot{m}$	2.86e-5	4.35e-5	0.29e-5	1.20e-5	4.14e-5	m	4.35e-7
$\dot{v}_{stage1}$	2.53e-5	3.83e-5	0.25e-5	1.05e-5	3.65e-5	v_{stage1}	3.83e-7
$\dot{v}_{stage2}$	2.82e-6	4.28e-6	0.28e-6	1.18e-6	4.08e-6	v_{stage2}	4.29e-8

Table 3.1: Overview of the design flow rates in both compressor stages in kg/s and m^3/s and corresponding compression chamber sizes in kg and m^3.

3.5. Actuation

Figure 3.3 shows a cross-sectional view of the compressor. The gas pressure pushes on the piston which consequently pushes on the shaft via the piston-shaft bearing. In the original 3D design, the shaft extends out of the piston and is connected to the rotor of the electric motor. All the work done to compress the gas in the compression chamber comes from the torque of the motor through this shaft, which will consequently also pass through the piston-shaft bearing. Theoretically, the system consists of three moving components which could all be the primary connection to the actuator. As the piston rotates and reciprocates simultaneously, the practical implementation of such an actuator would make the system overly complex. The shaft and cylinder are both feasible options as their centres are not moving as shown already in Figure 3.6.

Figures 3.9 and 3.10 show the propagation of forces and torques through the system for respectively a shaft-actuated and cylinder-actuated system. The compression chamber pressure is taken into account as well as the following terms related to the moving components: the rotational inertia of all the components and the mass and centrifugal force of the piston. Gas bearings are well-known for their low coefficients of friction which are often way below a value of 0.01. As this already reduces the friction loads to less that one percent of the gas pressure loads, these will be neglected for all bearings that see other loads. For gas bearings it is not accurate to visualize the forces through point loads, but rather by distributed loads. However, to compare both actuation methods this overview does point out the differences clearly.

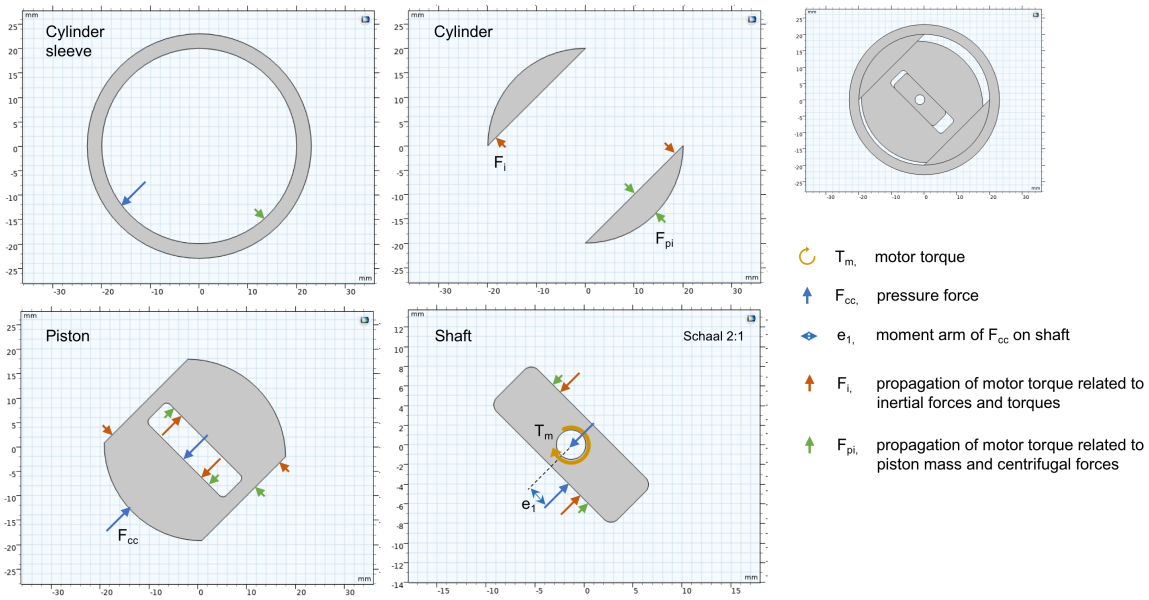

Figure 3.9: Schematic overview of the forces on the bearing surface of a shaft-actuated system.

When the motor is connected to the centre of the shaft in Figure 3.9, the torque that is created by the pressure force only adds to the bearing between the piston and the shaft. The torque produced by the blue arrows on the shaft is directly counteracted by the yellow torque, T_m, from the motor. The other

components only handle the three remaining terms. When the cylinder is actuated, the pressure torque on the shaft will propagate, via the yellow arrows F_m, through the piston-shaft bearing to the piston and then via the piston-cylinder bearing to the cylinder and motor. This creates that the pressure torque is cancelled within the piston-shaft bearing. The pressure force will still be handled by the piston-shaft bearing surface.

The magnitude of the inertial loads carried by the bearing surfaces depends on the actuation method as well. The inertia of each component stays the same, but the load on a specific bearing is a summation of the inertial terms that depends on the motor location. In a shaft-actuated system, the shaft will see all the inertial terms except for the shaft inertia on top of the pressure torque. While in a cylinder-actuated system, it will only see the shaft inertia. The opposite situation occurs at the piston-cylinder bearing.

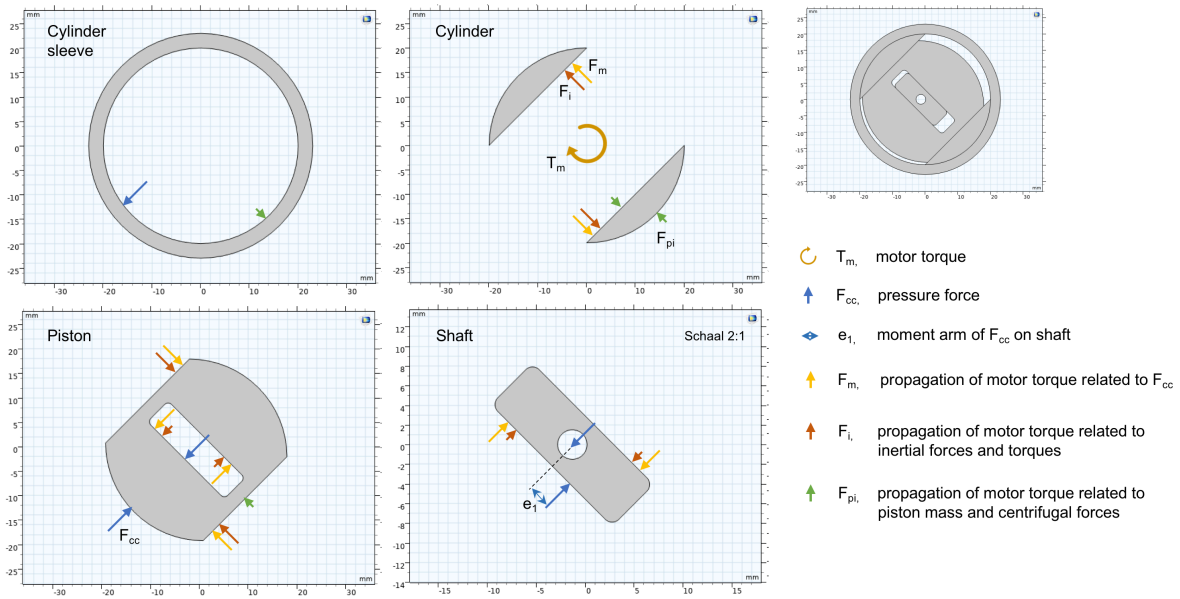

Figure 3.10: Schematic overview of the forces on the bearing surface of a cylinder-actuated system.

This yields the following design question: which actuation method yields the best load distribution over the bearing surfaces to enhance gas lubrication? The answer depends on the geometry, the sizes of the components and the behaviour of the thin-film in between. A thorough analysis will be made in Chapter 4 which shows which actuation method will be superior based on the bearing performance. The overviews in these figures will be used within that chapter to define and calculate the exact loads on each surface throughout a compression cycle.

Motor behaviour

The work done by a torque as shown in Figure 3.7b has to be delivered by the motor, which can be approached in two ways. A DC motor splits its supply voltage, V_s, in an induced voltage in the windings, E, and a voltage to overcome the motor resistance, $R_m I_a$, see equation 3.7.

$$V_s = E + R_m I_a \tag{3.7}$$

The induced voltage is directly coupled to the rotational speed of the motor and the current to the torque of the motor. When the supply voltage is kept constant, the rotational speed will drop to increase the torque. The supply voltage can be actively controlled to keep the rotational speed constant while the torque changes with the load. In this case, the rotational inertia of the system becomes irrelevant and the motor torque will be exactly equal and opposite to the loads on the system. However when the speed is free to change, part of the compression chamber torque will be used to change the rotational speed of all the components which basically averages the motor torque over the cycle. The eccentricity

of the piston creates two more torque terms. The first one is a result of the linear inertia, the mass, of the piston and the second one is caused by the centrifugal force that appears when the piston doesn't rotate around its centre of mass. This can be expressed as differential equation 3.8.

$$T_{cc}(\theta) + T_{motor}(\dot{\theta}) + T_{inertia}(\ddot{\theta}) + T_{mass-p}(\theta, \dot{\theta}, \ddot{\theta}) + T_{cf-p}(\theta, \dot{\theta}) = 0 \tag{3.8}$$

For an uncontrolled system, a small moment of inertia will have little impact on the instantaneous torque on the bearing. The components and motor will adjust their speed and torque rapidly and the third term in the equation can be neglected. The high load periods will have a slightly longer duration due to the slower rotational speed. A system with a large moment of inertia will process most of the compression chamber torque to adjust the speed of the components. This speed adjustment will be small and the change in motor torque with it. This will result in an almost constant motor torque with a small ripple.

The fourth term in the equation, the torque related to the mass of the piston, changes sign periodically and causes a ripple in the rotational speed. When both the rotational speed and eccentricity are large, this term might be larger than the compression chamber torque. The torque due to the centrifugal force is equal to the piston mass term except for the additional term that depends on the angular acceleration. This is explained in the complete differential equation in Appendix A.3. It must be noted that the definition of small and large are relative with respect to the size of the compression chamber torque.

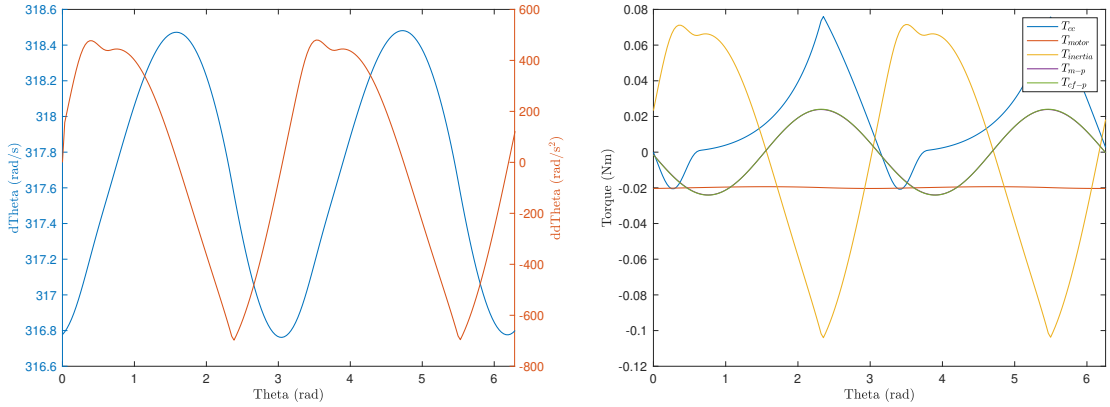

(a) Fluctuation of the rotational speed.

(b) Division of compression chamber, inertia and motor torques.

Figure 3.11: Rotational speed and torque distribution throughout a cycle when a large rotational inertia is taken into account.

Figure 3.11b shows the five terms, summed from two opposing compression chambers, of the differential equation over time for a system where the summed moment of inertia of all components has been modelled as a steel cylinder with radius 0.025 m and height 0.03 m and the piston mass is 0.119 kg at 25 percent of the total mass. For these parameters it can be concluded that the extra term in the mass torque with respect to the centrifugal torque can be neglected. The deviation of the rotational speed is only 0.5 percent of the average speed. As expected this creates a motor torque that is almost constant throughout the cycle operating between -0.0203 and -0.0194 Nm. From a design perspective of the motor, a small operating window can be used to obtain a high motor efficiency. Depending on a shaft- or cylinder-actuated system and whether the supply voltage is controlled or not, a different combination of these torques will yield a different load on each of the gas bearings.

4

Gas Bearing Design

In this chapter, the compressor design is analysed on the performance of the gas bearings using a thin-film flow model. First only the forces are applied where after the torques are added based on different actuation methods. This is done for all surfaces and a final set of parameters is presented for optimal bearing performance of the overall system.

The rotary cylinder compressor consists of four main components that interact via bearing surfaces that can be categorized in five sections. The in-plane bearings are not shown in Figure 4.1 and include all interfaces between moving components in the xy-plane.

1. Piston-shaft bearings
2. Piston-cylinder bearings
3. Cylinder-cylinder sleeve bearings
4. Shaft-cylinder sleeve bearings
5. In-plane bearings

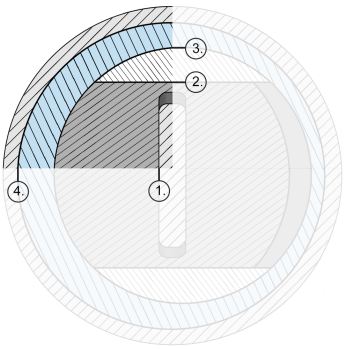

Figure 4.1: Bearing surfaces.

It is set out to lubricate all these surfaces by the implementation of gas bearings. For gasses, the density is a function of the pressure where it can be assumed constant for liquids like oil. In general it can still be assumed that both the density and the viscosity are a few orders of magnitude lower for gasses like CO_2 than for liquids. It is therefore important to analyse the load capacity of all bearing surfaces carefully. This can be done using a thin-film flow model that is based on the Reynolds equation, see equation 4.1 [8].

$$\frac{\partial}{\partial x}\left[\frac{\rho h^3}{\eta}\frac{\partial p}{\partial x}\right]+\frac{\partial}{\partial y}\left[\frac{\rho h^3}{\eta}\frac{\partial p}{\partial y}\right]=6\left\{\frac{\partial}{\partial x}\left[\rho h\frac{(U_1+U_2)}{2}\right]+\frac{\partial}{\partial y}\left[\rho h\frac{(V_1+V_2)}{2}\right]+\frac{\partial}{\partial t}(\rho h)\right\} \tag{4.1}$$

The two terms on the left side of the equation are the pressure terms that yield the pressure distribution of the fluid film. On the right side three terms can be found. The first and second term are based on the velocities of the boundaries in both x- and y-direction. Both these terms can be split up into two new terms: a wedge and a stretch term. The wedge term comes from the partial derivative of the film thickness, h, and represents the tilting of the boundary. The stretch term comes from the partial derivative of the average velocity which indicates an increase or decrease of the velocity over one boundary. This term is often neglected as the boundaries are usually solid materials. The third term

on the right side of the equation comes from the z-direction of the system and is called the squeeze term and consist of two parts as well. When one boundary moves with a different speed in z-direction than the opposing boundary, the film thickness will change with time. When the medium in the system is incompressible the density will not change over time. For gas lubrication however this term can't be neglected.

$$p_A = \frac{RT_0}{M_n}\rho \tag{4.2}$$

It is often assumed that thin-film flows are isothermal and an ideal gas. This makes that the absolute pressure is related to the density by a constant factor, shown in equation 4.2 with T_0 the constant temperature, M_n the molar mass of the gas and R the universal gas constant. Substituting this relation in equation 4.1 eliminates the density. This equation is used by COMSOL Multiphyics to solve thin-film gas flows and is known as the modified Reynolds equation.

The bearing surfaces as listed above will all be analysed based on the corresponding loads they need to cope with. The film pressure induced by the squeeze term is only a stable solution when the loads oscillate around zero, in other words when the surfaces sequentially approach and move away from one another. For the wedge terms two different velocity profiles have to be considered: a rotary profile, with a constant velocity in one direction, and reciprocating, with a sinusoidal velocity profile. The stretch terms are not considered as the bearing surfaces are constructed out of steel.

A careful decision must be made as to which terms are relevant. An overview of the load cases that are analysed will be given at the beginning of each section. Multiple cases will come up for discussion to make the proper design choice. An optimisation process is required to obtain a minimum force and torque on a bearing with a large surface area. Often, these three parameters are coupled through the geometry. The bearing analysis will show that even though these parameters are often linearly interdependent, the film thickness changes non-linearly due to bearing side leakage. Next to that, the frequency might not relate to one of these three parameters directly but is part of equation 3.4 and has a significant influence on the film behaviour.

4.1. Piston-Shaft Bearing

The piston-shaft bearing is directly coping with the pressure of the compression chamber gas that pushes on the piston. The compression chamber volume changes in a sinusoidal way and the corresponding pressure profile is visible in Figure 3.7a. As a second chamber is located opposing the first chamber and operates half a cycle out of phase, the piston will only handle the sum of both sides. From the shaft point of view, this also means that the load will alternate sides and the squeeze term will be applicable. Next to that the piston and shaft have a sliding velocity relative to one another. This velocity is sinusoidal and given by the derivative of the moment arm of the compression chamber pressure to the shaft seen in Figure 3.7b. This velocity is only of use when a wedge is created between the surfaces. This wedge occurs when a moment is passed on via the bearing. The resulting pressure on the piston-shaft bearing is not simply the gas pressure on the piston head divided by the surface area ratio. A pressure distribution occurs that is centered around a specific point and decays towards the edges.

The following loads may occur on the piston-shaft bearing and combinations of these will be discussed in this section:

Forces

1. Compression chamber force, F_{cc}

Torques

1. Compression chamber torque, T_{cc}
2. Motor torque, T_{motor}
3. Rotational inertia torque, $T_{inertia}$
4. Piston mass torque, T_{m-p}
5. Piston centrifugal torque, T_{cf-p}

Force Transfer

A model is created that couples two thin-film flow simulations, one for each side of the shaft. A total film thickness is defined as twice the nominal film thickness, h_{nom}, and is dynamically divided over both models, just like the piston will move closer to the side of the shaft that has a higher compression chamber pressure. The absolute film pressure and film thickness on both sides is calculated using the modified Reynolds equation. Only the force as a result of the compression chamber pressure, the piston height, P_h and piston width, P_w are given as an input, see equation 4.3. The model balances this with the film pressure by adjusting the film thickness accordingly which is largely influenced by the approach velocity, which is the velocity at which the piston surface approaches the shaft surface. The inertia of the components and torque of the motor are not taken into account.

$$F_{cc} = P_{cc} P_h P_w \tag{4.3}$$

Initially the dimensions of the components will be chosen by geometric constraints. The piston dimensions shouldn't be below 3 mm to enhance the production process. The eccentricity shouldn't be less than 2 mm to avoid that the clearance volume will be affected significantly by the production tolerances. n the design of Figure 3.6, the piston represents a quarter of the diameter of the cylinder. The minimum diameter is given by twice the eccentricity and an estimated 7 mm for the piston and shaft wall thicknesses. The minimum piston width is than determined by equation 4.4. The width of the piston also constraints the width of the shaft.

$$2e + 7 \leq \frac{4P_w}{\pi} \tag{4.4}$$

This relation makes the minimum eccentricity of 2 mm leading as it yields a minimum piston width of 8.7 mm. It is possible to alter the frequency via the piston height. The smallest piston height of 3 mm would yield the lowest net load on the bearing. As will be explained later in this chapter, a square piston will now be assumed. The corresponding frequency can be determined by combining equation 3.4 and the value of $\dot{v}_{stage1} - d$ in Table 3.1. Figures 4.2a and 4.2b show the resulting load capacity and bearing film thickness for a system that operates at 60 Hz with piston dimensions of 8.7x8.7 mm. The bearing surface dimensions are taken equal which is an overestimation for a small compressor as the piston wall thickness and eccentricity can't be neglected.

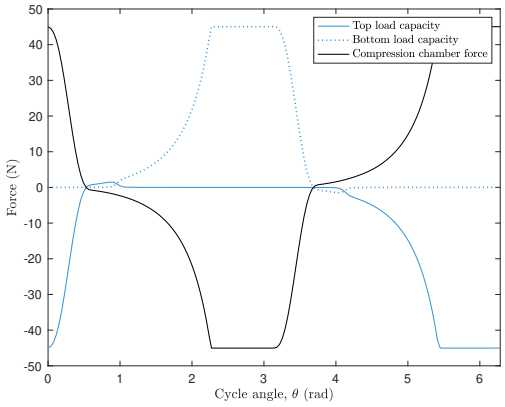

(a) Compression chamber force and bearing load capacity.

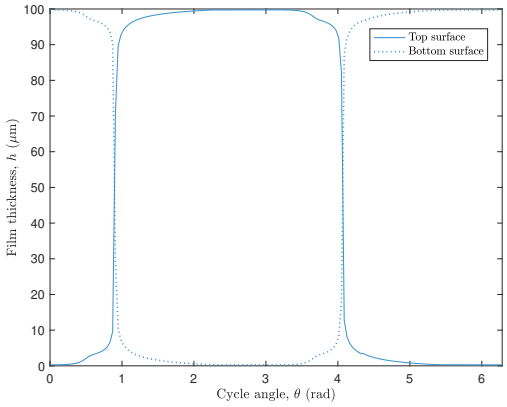

(b) Dynamic bearing film thickness.

Figure 4.2: Dynamics of the piston-shaft squeeze bearing undergoing only the force of a single compression cycle of both compression chambers at 60 Hz with e=2 mm, P_w=8.7 mm and P_h=8.7 mm.

All results will show the second full cycle of the simulation. The results of the first cycle experience deviations from the steady-state due to the initial conditions. More details about the effects of the initial conditions like the start-up film thickness can be found in Appendix A.4.

The minimum film thickness obtained is 0.24 micrometer and occurs at the end of the high pressure exhaust phase. This is expected as the maximum force is applied here with the longest duration. At

a constant force the film thickness decreases over time due to side leakage of the bearing. The solid lines will show the top bearing surface and the dotted lines the bottom bearing surface for all graphs considering the piston-shaft bearing. It is interesting to see that the dominant bearing surface switches from the top to the bottom side each cycle as seen in Figure 4.3. This doesn't happen simultaneously with the compression chamber force switching sides. This delay is caused by the existence of a negative load capacity on the top bearing surface as the piston and shaft try to separate. Around 4.1 radians in Figure 4.2a, it is visible that the negative load capacity can not longer hold the top piston surface close to the shaft while the compression chamber force increases. When the piston area is increased to 30x30 mm, both the force on and the area of the bearing increase equally, which yields a poor improvement of the film thickness to only 0.27 μm.

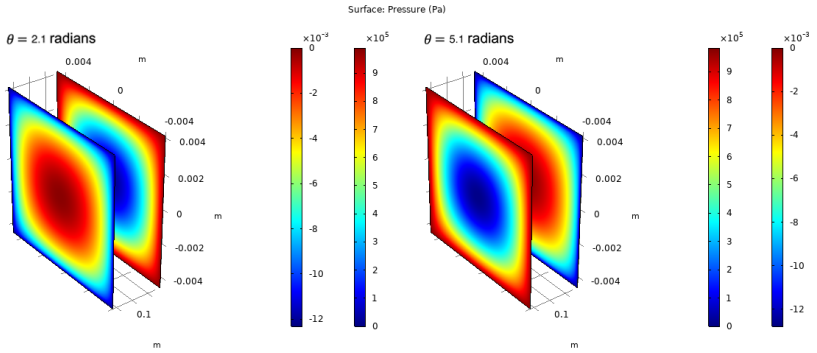

Figure 4.3: Pressure distribution of the piston-shaft top and bottom surface at two instances within the compression cycle of Figure 4.2.

Surface Area Ratio

The piston is slightly wider than the shaft which yields a surface area ratio below one. This also means that the average gas pressure between the piston and shaft should be larger than the gas pressure in the compression chamber which comes with such an undesired thin gas film. It is not simply possible to increase this ratio as the width of the shaft is limited by the width of the piston. Increasing the width of the piston as well would defy the purpose. Enlarging the whole system would eventually approach a ratio of one as applied in the figure above.

Figure 4.4b, which shows a simplified model of the compressor components from Figure 3.6, sacrifices part of the cylinder-piston bearing surface area to increase the shaft width relative to Figure 4.4a. This might be a good trade-off when the loads on the piston-cylinder bearing are lower than on the piston-shaft bearing. When the piston width is not constraint to a quarter of the cylinder diameter, it becomes possible to change the compression chamber dimensions freely. The width can be decreased without

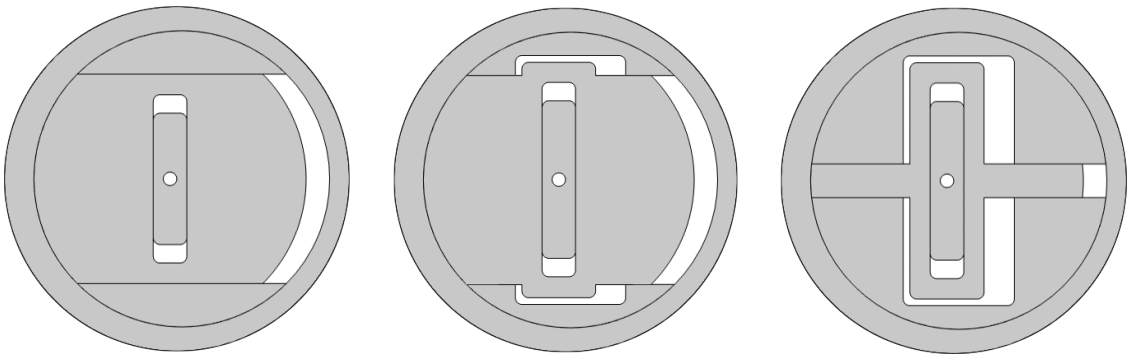

(a) (b) (c)

Figure 4.4: Geometric adjustments to improve the surface area ratio between the piston and the shaft.

giving in on the shaft width as shown in Figure 4.4c. This results in a large improvement of the surface area ratio and with that the film pressure of the piston-shaft bearing. Increasing the shaft area with respect to the piston area can also be done in the out-of-plane direction, not shown in these figures. The following sections will analyse the improvement that can be made using this adjusted design.

Optimisation

The piston width is not coupled to the diameter and bearing surface area anymore and equation 4.4 doesn't have to be satisfied. Therefore the piston width can be decreased to a minimum of 3 mm as imposed by the production process which reduces the pressure force. The bearing surface area is now coupled to the shaft width, S_w, instead of the piston width.

$$A_{ps} = P_h S_w = S_h S_w \tag{4.5}$$

To find the optimum set of design parameters, the sensitivity of each parameter with respect to the film thickness will be analysed. An overview of the domain of each parameter is given below. The piston height is coupled to the piston width to avoid a slender structure in the loaded direction. The maximum piston width and eccentricity are coupled to maintain a piston-cylinder bearing width larger than zero, explained later by equation 4.10. The maximum eccentricity could also be limited by the piston-shaft bearing width, explained in equation 4.6. The maximum values that could potentially appear are 47.0 mm for the piston width and 10.2 mm for the eccentricity when the other parameter takes its minimum value. The frequency should naturally stay above a value of zero and an estimated 500 rotations per second is used as the upper limit for the electric motor.

$$\begin{aligned}
P_h: &\quad [3\ mm \quad 10P_w\ mm] \\
P_w: &\quad [3\ mm \quad \sqrt{D^2-(4e+9)^2}\ mm > \\
e: &\quad [2\ mm \quad \frac{\sqrt{D^2-P_w^2}-9}{4}\ or\ \frac{D-S_w-16}{2}\ mm > \\
f: &\quad < 0\ Hz \quad 500\ Hz]
\end{aligned}$$

Figure 4.5a shows the change of the film thickness for a cycle with varying bearing surface dimensions that are not equal to the piston dimensions and Figure 4.5b shows the same for varying rotational speeds. Three different cases are discussed in Figure 4.5a. A minimum rotational speed has been chosen in such a way that the surface dimensions can be increased while down scaling the eccentricity to a minimum value of 2 mm for the largest surface dimensions following equation 3.4. This is done to have a clear comparison as the eccentricity doesn't influence the bearing as long as there is not torque applied.

The first two graphs show the film thickness for a piston area of 3x3 mm and a bearing surface of 30x3 mm which means a tenfold amplification. This results in a minimum film thickness of 1.4 micrometer. When in the third and fourth graphs the width of the bearing surface is increased by another factor of two, the minimum film thickness will increase to 2.1 micrometer. When instead the height of the bearing surface is increased by a factor of two, the minimum film thickness in graphs five and six will increase to 2.7 micrometer. It must be noted that for this simulation the piston head height has been increased equally at constant rotational speed to avoid creating a surface area amplification in two dimensions. This means that the compression chamber force on the bearing grows with the surface area of the bearing. The effectiveness of the bearing however increases faster than the surface area due to a decrease in side leakage caused by the short distance to the edge in that direction. It would therefore be beneficial to keep the bearing surface shape as square as possible. The initial assumption that the smallest compression chamber force yields the best result is only valid for a large, square bearing surface. It is beneficial to increase the piston area in height which yields a non-square piston that is larger in the direction that has not been amplified as in Figure 4.4c. This effect decays when a larger distance to the edge is reached. The relation between compression chamber force and surface area also causes the wider bearing to switch later from the top to the bottom bearing surface.

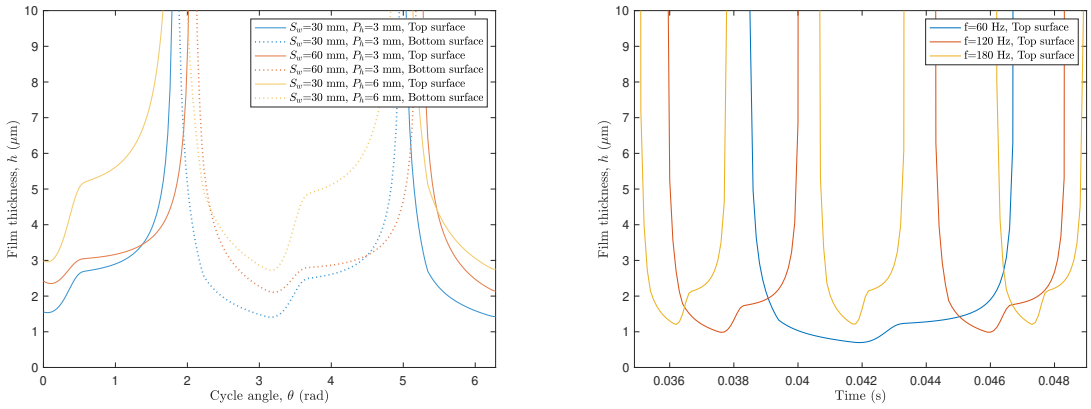

(a) 253 Hz with different bearing surface dimensions.

(b) S_w=30 mm and P_h=3 mm at different frequencies.

Figure 4.5: Sensitivity of the bearing surface dimensions and frequency on the film thickness with e=2 mm and P_w=3 mm.

Figure 4.5b compares the effect of different frequencies on the film thickness at constant surface dimensions of 30x3 mm. Only the top side of the bearing is shown for clarity. An increase in rotational speed shows a smaller decrease in film thickness due to the larger approach velocity and the shorter duration of the force. An overview of all minimum film thicknesses can be found in Table 4.1.

Surface dimensions	h	f	h
S_w=30 mm, P_h=3 mm	1.4 μm	60 Hz	0.7 μm
S_w=60 mm, P_h=3 mm	2.1 μm	120 Hz	1.0 μm
S_w=30 mm, P_h=6 mm	2.7 μm	180 Hz	1.2 μm

Table 4.1: Overview of minimum film thicknesses for several piston-shaft bearing configurations with e=2 mm and P_w=3 mm.

A larger shaft width increases the performance of the gas film. In practise, this width is limited by the maximum desired diameter of the compressor. Equation 4.6 relates the eccentricity and shaft width, which is equal to the bearing width, to the diameter of the cylinder. The additional 16 mm is a summation of wall thicknesses and spaces between the components. For a 2 mm eccentricity and maximum cylinder diameter of 50 mm, this equation yields a maximum shaft width of 30mm.

$$D_c = S_w + 2e + 16 \tag{4.6}$$

An increase in both piston height and rotational speed yields a minimum eccentricity of 2 mm. When this minimum has been reached, a trade-off between these two parameters has to be made. Figure 4.6 shows a linear increase in the piston height and with that bearing surface height from 3 to 60 mm. As the piston height is constraint to ten times the piston width, from 30 mm on the piston width increases as well. The corresponding frequencies for these combinations of piston heights and widths following equation 3.4 are shown on the right y-axis.

These combinations of piston heights, widths and frequencies are used to calculate the minimum film thickness in Figure 4.7. As already mentioned, the relative size of the bearing surface height to width is important. Especially when the height is much smaller than the width, the bearing functionality will increase significantly due to the decrease in side leakage. This effect is larger than the reduced functionality related to the drop in frequency. When the bearing surface height becomes larger than the width, the performance gain will slow down as the largest leakage path is now the width. In this model, this is by coincidence also the point where the piston width should start growing with the piston height to stay within is domain. The piston width adds pressure force without any positive influence on the bearing area and a rapid drop in the minimum film thickness can be observed.

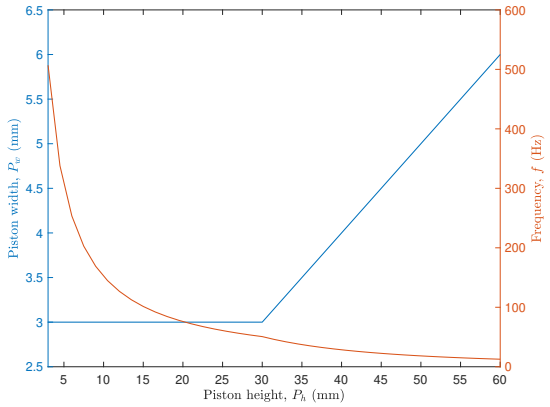

Figure 4.6: Scaling of the piston width and frequency with the piston height to satisfy its domain and the volumetric flow rate with e=2.

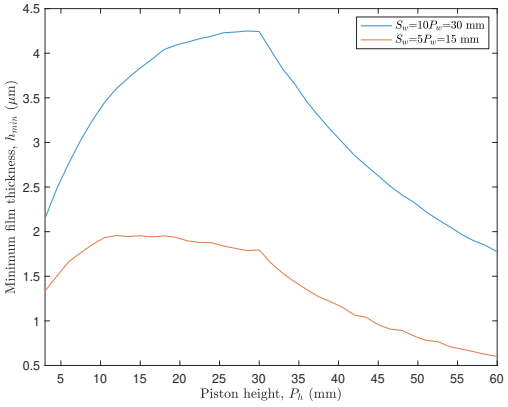

Figure 4.7: Effect of the piston heights and corresponding widths and frequencies from Figure 4.6 with e=2 mm on the minimum film thickness for two different bearing widths.

The conclusion that a non-square piston with a square bearing surface increases the performance holds true when the influence of the frequency is taken into account. The thickest film is obtained at maximum piston height reachable without increasing the piston width. The film thickness will change when the constraint on the diameter and with that maximum bearing width changes as can be seen in the figure but the behaviour of the system will be similar.

An overview of the results for the adjusted design in a force-only model is as follows:

- The piston width only increases the pressure force and should be minimized.
- An increase in piston height with equal increase of the bearing surface height increases the film thickness at constant frequency.
- An increase in frequency with constant piston dimensions increases the film thickness.
- A larger surface area ratio comes with a better bearing performance which is limited by the maximum desired diameter of the cylinder.
- An increase in piston height is dominant over a decrease in frequency when the surface shape changes towards a square and the piston height stays within its domain for a minimum piston width.

Within the given constraints, the optimal design for the piston-shaft bearing to cope with the compression chamber force is given in Table 4.2.

e	P_w	P_h	S_w	S_h	f	h_{min}
2 mm	3 mm	30 mm	30 mm	30 mm	50.4 Hz	4.3 μm

Table 4.2: Overview of the optimal design parameters for the piston-shaft bearing to cope with the compression chamber force.

Torque Transfer

When a torque is exerted on the film, a wedge will occur as a smaller film thickness and higher approach velocity on one side will shift the centre of the pressure sideways. The dynamic torques in the system have been analysed using Figure 3.11. Combinations of these, result in four distinct load cases for the piston-shaft bearing surface, all shown in Figure 4.8. The simplest case, T_0, is cylinder-actuated and with a constant rotational speed. This means that no compression chamber torque and no inertial terms are experienced by the piston-shaft bearing. This has already been discussed as this yields force transfer only. The second solution, T_1, is still cylinder-actuated but now with inertial terms and

results in the shaft inertia pushing on the bearing surface. The shaft inertia is taken as 45 percent of the total inertia applied in equation 3.8 with the cylinder taking 30 percent and the piston the remaining 25 percent. T_2 consists of the compression chamber torque and mass and centrifugal terms from the piston as this case is shaft-actuated with a constant rotational speed. Finally the rotational inertia's of the piston and cylinder are added to T_2 which yields T_3.

From a design perspective of the bearing, it should be analysed which case yields the best bearing behaviour. For the piston-shaft bearing, this result might be obvious. The outcome of these scenarios have to be combined with the results of the same scenarios on the other bearing surfaces in the next sections of this report to get a complete design overview.

$$T_0 = 0 \quad \text{(Cylinder-actuated, constant RPM)}$$
$$T_1 = T_{inertia-shaft} \quad \text{(Cylinder-actuated)}$$
$$T_2 = T_{cc} + T_{mass-p} + T_{cf-p} \quad \text{(Shaft-actuated, constant RPM)}$$
$$T_3 = T_{cc} + T_{mass-p} + T_{cf-p} + T_{inertia-piston} + T_{inertia-cylinder} \quad \text{(Shaft-actuated)}$$

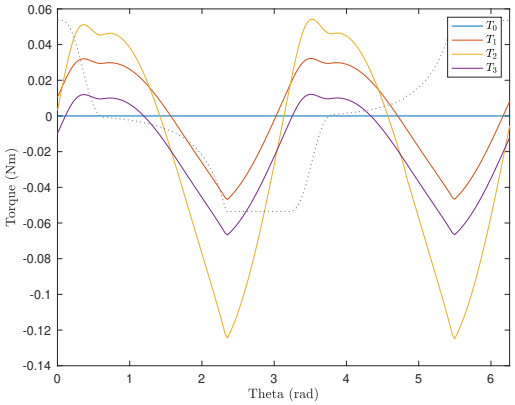

Figure 4.8: Piston-shaft bearing torque load cases for different actuation methods with f=64 Hz.

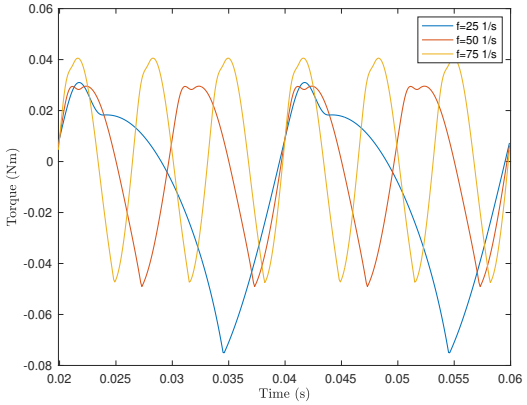

Figure 4.9: Change in shape and magnitude of the bearing torque loads for different frequencies and corresponding piston areas.

The magnitude and shape of these torques are influenced by several parameters from Table 4.2. The question arises whether this optimum still holds when an additional torque needs to transferred through the bearing on top of the compression chamber force. All cases are in practise a combination of the compression chamber torque and the torque related to the piston mass and centrifugal force. The rotational inertia and motor torque are a direct result of these. Therefore an optimum can be found when looked at a combination of these first three terms as in equation 4.7. The mass and centrifugal torques are merged to one term as they are equal.

$$T = T_{cc} + T_{mass-p} + T_{cf-p} = P_{cc}P_hP_wesin(\theta) + 2m_p(2\pi)^2f^2e^2sin(\theta)cos(\theta) \tag{4.7}$$

The piston mass, m_p, is a function of the piston width and height. This makes that both terms can be rewritten using equation 3.4 into equation 4.8 in which all other parameters are merged into two constants, C_1 and C_2.

$$T \propto \frac{C_1}{f} + C_2ef \tag{4.8}$$

This makes it easy to see that the eccentricity should be minimized just like in the force-only model. The frequency has an optimum value. A low frequency and large piston width or height will drive the first term up and the second term down, while the opposite ratio will result in a small first term and a large second term. Figure 4.9 shows the dominance of the pressure term at low frequencies and the clear sinusoid appearing at higher frequencies. At the intermediate frequency, the amplitude is significantly smaller. A minimum amplitude is found at a frequency of 64 rotations per second. This means that the

frequency now has an optimum value considering the torque instead of only the goal to maximize it as seen in the previous paragraph.

For a squeeze bearing the amplitude of the torque is not the only factor. The symmetry around the zero torque line and the phase of the torque with respect to the force on the bearing have a large impact on the resulting film thickness. This is solved using the thin-film model in COMSOL Multiphysics similar to the force transfer cases. The minimum film thicknesses for all four load cases are shows in Figure 4.10 for the same combination of piston heights, widths and frequencies as the force-only model in Figure 4.6. The x-axis starts at a piston height of 24 mm corresponding to a frequency of 64 Hz which gave the smallest torque amplitude. The force-only model resulted in the thickest film at a piston height of 30 mm. This makes that the optimum for the combination of the two is expected to lay in between. The plot is extended to 45 mm as this will be useful for comparison with the piston-cylinder bearing.

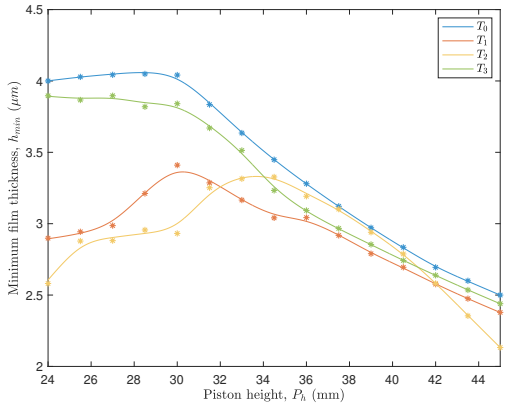

Figure 4.10: Minimum film thicknesses versus piston heights and corresponding widths and frequencies from Figure 4.6 for different torque load cases with e=2 mm.

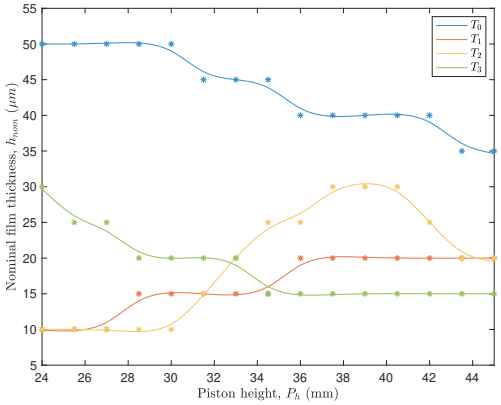

Figure 4.11: Nominal film thickness belonging to the optimum minimum film thickness for different piston heights and corresponding widths and frequencies from Figure 4.6 and e=2 mm.

Figure 4.11 introduces the nominal film thickness, h_{nom}, which is defined as the film thickness when the shaft is positioned in the centre between both piston surfaces. The minimum film thickness results of all analyses so far determine the maximum surface roughness required to avoid the surfaces of making physical contact. This nominal film thickness is directly linked to the production tolerances of the hole in the piston and the shaft that has to fit inside. As these films have no sealing function for the compressor, this value can be optimized for manufacturing. For a gas film that is only loaded with a force and zero torque, a larger nominal film thickness is better as there is effectively more mass of gas between the two surfaces to build up pressure. At some point, the gap becomes so wide that all extra mass escapes before pressure is build up and the inertia of the system will have a negative impact. All analyses for the force-only model have been executed with a nominal film thickness of 50 μm.

Each combination of piston height, width and frequency is analysed for multiple nominal film thicknesses in discrete steps of 5 μm. In practise, this creates a 3D solution space. Figure 4.11 shows for each piston height, the nominal film thicknesses that correspond to the largest minimum film thicknesses of Figure 4.10. It has been decided to make the minimum film thickness the priority as the minimum film thickness avoids the actual surface contact, while the nominal film thickness is only a manufacturing requirement. The objective could theoretically be altered to find the largest nominal film thicknesses while keeping keeping the minimum film thickness above a specific threshold.

As expected, no torque yields the thickest film in Figure 4.10 with its optimum still around a value of 30 mm for the piston height. The film is slightly thinner than obtained from the force-only model. Even though no torque is applied, in this model the bearing is able to create a wedge. That is caused by the sliding velocity of the piston surface relative to the shaft. Two parallel sliding surfaces won't build up pressure, but move the existing pressure in the direction of the sliding velocity which creates a small

torque. The surfaces will therefore tilt slightly to obtain a zero net torque. This result is therefore more realistic than the result from the force-only model. Straight after 30 mm the film thickness decays again due to the increase in piston width. The other load cases show two different shapes. T_1 and T_2 start with a thinner film, find an optimum between a piston height of 30 and 34 mm and thereafter fall in line with T_0. T_3 starts with a thicker film and stays continuously close to T_0.

T_2 initially has the lowest optimum of the three which matches with its high torque in Figure 4.8. T_1 and T_3 show film results that are not in line with the torque values found. T_3 maintains a much thicker film than T_1 below a piston width of 30 mm and T_1 is more similar to T_2. The largest impact on the film is made when a torque is applied while the pressure force is switching from the top to the bottom surface and has a small value. The phase of the force with respect to the torque is dotted in the background of Figure 4.8. A minimum film thickness can be expected between 1 and 2 radians and again between 4 and 5 radians as the pressure switches from the top to the bottom surface but still needs to handle the torque which can be seen in Figure 4.12. The effect of the torque becomes smaller when the nominal film thickness is thinner. This can be explained by the difference in maximum pressure on both surfaces. It can be observed in Figure 4.13 that the pressure distribution is almost equal for both nominal film thicknesses at locations where the torque load coincides with the high pressure between the surfaces, while the difference is large due to the wedge shape at lower pressures. This phenomenon could be investigated in later work.

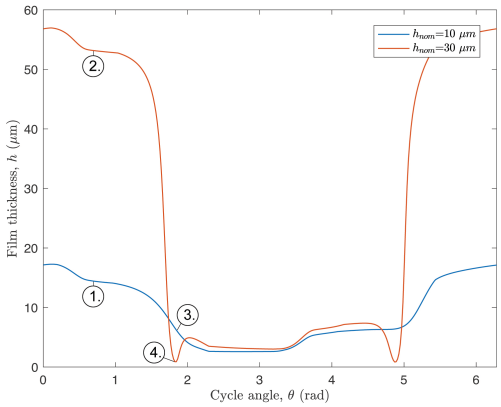

Figure 4.12: Minimum film thicknesses for T_3 with P_h=39 mm and e=2 mm for two different nominal film thicknesses with equal loads.

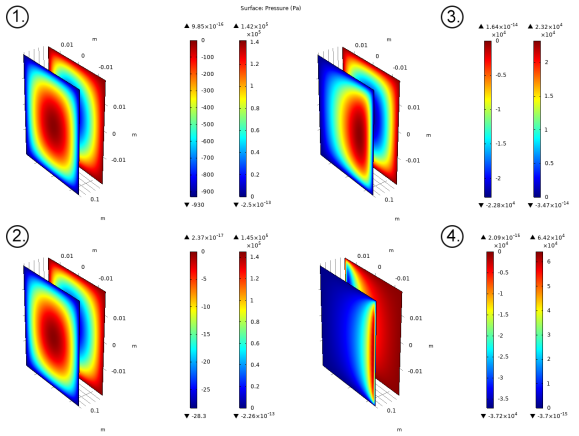

Figure 4.13: Pressure distribution plot at two locations for each nominal film thickness in Figure 4.12.

As the piston height increases and the frequency decreases with it, the torque cases of Figure 4.8 scale in the direction of the pressure term. This makes that they become less symmetric and also change sign at a different point in time. This development together with the effect of the nominal film thickness on the torque, explain why the nominal film thickness in Figure 4.11 moves up and down as the piston height increases. The curves are expected to be smooth when the step size of the nominal film thickness calculations is taken smaller. For this report, it would ask for more computational power and the main principle is demonstrated.

An overview of the results for the adjusted design in a full model including forces and torques is as follows:

- The effect of the force-only model on the minimum film thickness becomes dominant in the full model when the piston width starts to increase above its minimum value of 3 mm.
- The torque amplitude and shape depend on the frequency.
- The minimum film thickness depends not only on the torque amplitude but also on the phase of the torque load to the phase of the force.

- A decrease in nominal film thickness can correct for the influence of the torque on the minimum film thickness.
- The best minimum film thickness doesn't necessarily coincide with its highest nominal film thickness and a trade-off should be made based on the manufacturability.

4.2. Piston-Cylinder Bearing

The force as a result of the compression chamber pressure is oriented parallel to the piston-cylinder bearing surfaces. The alternating nature of this force was the stabilizing factor of the piston-shaft bearing film. It should be analysed whether a same squeeze effect can be generated by the loads on the piston-cylinder bearing or whether the sliding velocity of the piston with respect to the cylinder can fulfill this function. The following loads may occur on the piston-cylinder bearing and combinations of these will be discussed in this section:

Forces

1. Piston mass force, F_{mass-p}
2. Piston centrifugal force, F_{cf-p}

Torques

1. Compression chamber torque, T_{cc}
2. Motor torque, T_{motor}
3. Rotational inertia torque, $T_{inertia}$
4. Piston mass torque, T_{mass-p}
5. Piston centrifugal torque, T_{cf-p}

The piston mass and centrifugal torques that have been discussed, come with corresponding forces that are parallel to the piston-shaft bearing and therefore orthogonal to the piston-cylinder bearing, drawn as the green arrows in Figures 3.9 and 3.10. While the compression chamber force was only a function of the angle and the bearing surface area, these forces depend on more design parameters of the compressor, see equation 4.9. The first part of the mass term is related to the angular acceleration of the compressor. Figure 4.14 shows this term isolated for the parameters obtained from the piston-shaft bearing. For now, it can be concluded that this value is negligible which yields a total force that is equal to twice the centrifugal force. Especially when the inertia of the components changes significantly, this should be re-evaluated. This equation can be rewritten as a constant, C_3, containing all the parameters that are not part of equation 3.4 times the frequency. It is logical that the mass and centrifugal forces are related to the frequency of the compressor.

$$F_{pc} = \underbrace{m_p \ddot{\theta} e \cos\theta - m_p (2pi)^2 f^2 e \sin\theta}_{F_{\text{mass}-p}} \underbrace{- m_p (2pi)^2 f^2 \,\text{esin}\,\theta}_{F_{cf-p}} \propto C_3 f \tag{4.9}$$

The full area of the piston-cylinder bearing depends on multiple parameters as well, see equation 4.10. On top of that, the adjusted design has an area that is split in two components which shrinks and grows periodically. Growing draws low pressure gas in the bearing, therefore this can't be seen as a full area of high pressure. A moment is also introduced due to the uneven areas which causes tilting of the bearing which has a negative effect on the film. The worst case scenario is created when the minimum available surface area at any point in the compression cycle is used and slides back and forth from the center of the full length towards the edge with the motion of the piston. The full bearing length is shown in Figure 4.15 as the sum of the orange and blue lines. Only the blue lines, the worst case, remain when an additional two times the eccentricity is subtracted from equation 4.10

$$A_{PC-full} = P_h * C_w = P_h * (\sqrt{D_c^2 - P_w^2} - (2e + 9) - 2e) \tag{4.10}$$

The distribution of the compression chamber torque, the inertial terms and the motor torque doesn't change compared to Figure 3.11b. The loads on the piston-cylinder bearing surface have a similar structure. The shaft- and cylinder-actuated loads are swapped as the piston-cylinder bearing experiences loads when the cylinder is actuated which is the opposite for the piston-shaft bearing. This means that T_0 is now T_2 and T_1 is T_3. Additionally, the inertia of the shaft and cylinder are swapped

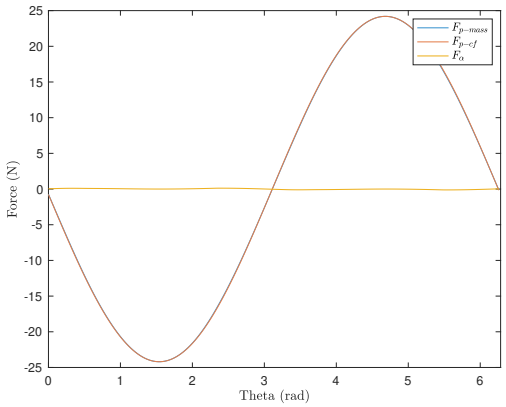

Figure 4.14: Forces on the piston-cylinder bearing due to the piston mass and centrifugal forces.

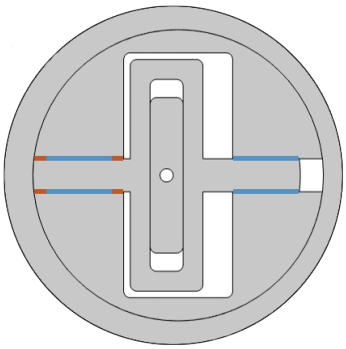

Figure 4.15: Worst case modelled piston-cylinder bearing area at most off-centre position.

between T_1 and T_3.

$$T_0 = T_{cc} + T_{mass-p} + T_{cf-p} \quad \text{(Cylinder-actuated, constant RPM)}$$
$$T_1 = T_{cc} + T_{mass-p} + T_{cf-p} + T_{inertia-piston} + T_{inertia-shaft} \quad \text{(Cylinder-actuated)}$$
$$T_2 = 0 \quad \text{(Shaft-actuated, constant RPM)}$$
$$T_3 = T_{inertia-cylinder} \quad \text{(Shaft-actuated)}$$

The equations for the piston-cylinder force, area and torque show that the geometric parameters are even more intertwined than in the piston-shaft bearing analysis. The eccentricity still has a negative influence on the torque and added to that is a negative coupling to the bearing surface area. This yields the same minimum result of 2 mm at all times. The piston width has a similar but weaker negative coupling to the bearing surface area. When the width is increased for a decrease in frequency, it even decreases the force. The same is true for the piston height, except for the fact that the piston height has a positive effect on the bearing surface area. The frequency is linear proportional to the force on the bearing which makes a lower frequency preferred. However, the pressure term of the torque is inversely proportional to the frequency which points toward an optimum value.

This concludes that the same input can be given to the thin-film model as for the piston-shaft model shown in Figure 4.6. The piston height is linearly increased with an increase of the piston width from 30 mm onward to satisfy the domain, the frequency decreases accordingly. For this bearing, the nominal film thickness is set to 2.9 μm as this bearing also has a sealing function against internal leakage explained in Chapter 5. Figure 4.16 shows the minimum film thickness for the combined force and torque loads on the piston-cylinder bearing.

The results are quite straightforward. The minimum film thickness for load case T_2 rises due to the decrease in frequency and with that bearing force and growth of the bearing surface while there is no applied torque. All other three load cases have each there own optimum, which is related to the size, shape and phase of the torque. The nominal film thickness is equal for all cases which makes that this optimum can't be altered. An overview of the optimum of each load cases can be found in Table 4.3.

	e	P_w	P_h	f	h_{nom}	h_{min}
T_0	2 mm	3.6 mm	36 mm	35.2 Hz	2.9 μm	1.7 μm
T_1	2 mm	4.05 mm	40.5 mm	27.8 Hz	2.9 μm	1.9 μm
T_2	2 mm	6 mm	60 mm	12.7 Hz	2.9 μm	2.5 μm
T_3	2 mm	4.5 mm	45 mm	22.5 Hz	2.9 μm	2.1 μm

Table 4.3: Overview of the optimal design parameters for the piston-cylinder bearing to cope with the compression chamber force and different torque load cases.

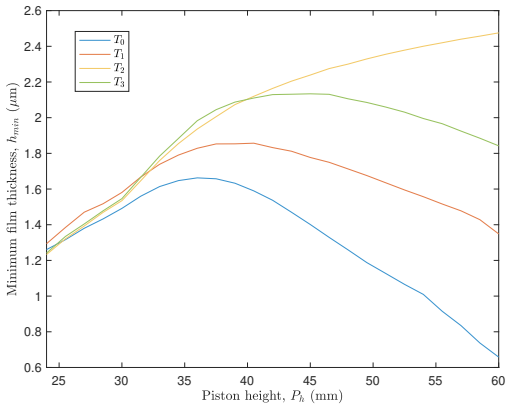

Figure 4.16: Minimum film thickness versus piston heights and corresponding widths and frequencies from Figure 4.6 with e=2 mm.

Optimal Actuation Method

A conclusion on the preferred actuation method can be drawn from these results in combination with those of the piston-shaft bearing. Since both bearing surfaces have a different geometry, it might be easier to produce a tighter tolerance or smoother surface roughness on one bearing surface than the other. When looked at the absolute values, the following conclusions can be drawn:

- At the piston-shaft bearing, the optima for all load cases are found at values for the piston height of 34 mm and lower which means at relatively high frequencies.
- At the piston-cylinder bearing, the optima for all load cases are found at values for the piston height of 36 mm and higher which means at relatively low frequencies.
- The absolute minimum film thickness of the piston-shaft bearing is for each set of parameters at least equal to approximately 2.5 times thicker than the piston-cylinder bearing. This pleads for an optimum at a larger piston height and lower frequency to shift this in favor of the piston-cylinder bearing.
- The nominal film thickness of the piston-shaft bearing has three high points: T_0 over the whole range, T_2 at P_h=39 mm and T_3 at P_h=24 mm. Considering the previous point, T_0 and T_2 are viable options.
- T_0 yields the worst minimum film thickness of all load cases for the piston-cylinder bearing where T_2 has the best result.
- When, from a manufacturing point of view, the nominal film thickness proves more important, then T_0 would the proper solution.
- For the rest of this report, it is assumed that the system is shaft-actuated with a speed controller like load case T_2 with the set of parameters as given in Table 4.4.

	e	P_w	P_h	f	$PS-h_{nom}$	$PS-h_{min}$	$PS-h_{nom}$	$PS-h_{min}$
T_2	2 mm	3.9 mm	39 mm	30 Hz	30 μm	2.9 μm	2.9 μm	2.1 μm

Table 4.4: Overview of the design parameters for both the piston-shaft and piston-cylinder bearing to cope with the force and torque loads.

4.3. Cylinder-Cylinder Sleeve Bearing

The force transferred from the piston to the cylinder in paragraph 4.2 is passed on from the cylinder to the cylinder sleeve which is rigidly attached to the world. In Chapter 5, the situation is analysed where the geometry is adjusted slightly. The outer surface of the cylinder could be extended which closes off the compression chamber. The gas pressure inside the compresssion chamber will then also push the cylinder against the cylinder sleeve, As a rotary bearing is applied, no torques have to be taken into account. The following loads may therefore occur on the cylinder-cylinder sleeve bearing and combinations of these will be discussed in this section:

Forces

1. Piston mass force
2. Piston centrifugal force
3. Compression chamber force

For this analysis, the parameters from Table 4.4 are used. The cylinder-cylinder sleeve bearing rotates in clockwise direction with given frequency. In contrast to the sliding bearings seen before, this speed doesn't oscillate throughout each cycle and can be seen as a plain journal bearing with a few remarks. The load is still oscillatory and a squeeze term is still applicable. The piston opening disrupts the full journal bearing on both sides, see Figure 4.17b. The nominal bearing gap height is taken as 2.9 micrometer as this bearing also functions as a seal similar to the piston-cylinder bearing.

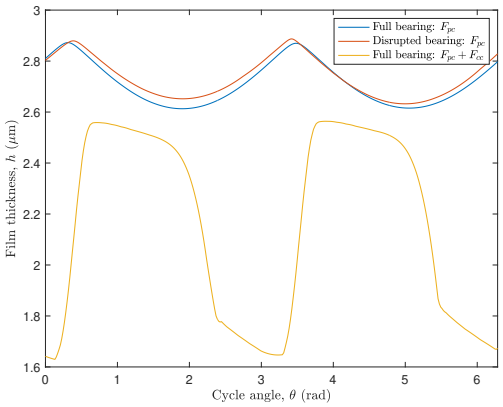

(a) Comparison of the film thickness during a compression cycle of a full, disrupted and closed-off geometry.

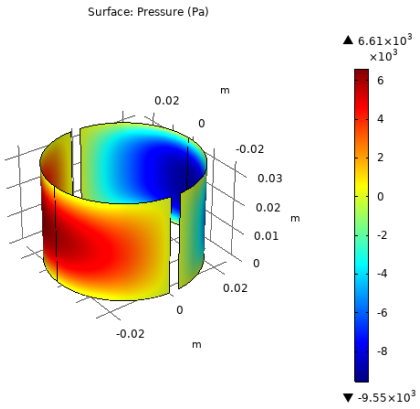

(b) Pressure distribution plot belonging to the disrupted bearing.

Figure 4.17: Simulation of the film thickness of the cylinder-cylinder sleeve bearing according to Table 4.4 and h_{nom}=2.9 μm.

The system is first modelled as a full plain bearing that only experiences the mass and centrifugal forces from the piston which is the case for a cylinder with a disruption for the piston. This is then compared with the actual model including the disruption in Figure 4.17a. It is clear that there is almost no difference between the two results. This can be explained by the fact that the disruption is less than five percent of the bearing area and the loads coming from the piston are perpendicular to these points. In this simulation the pressure at the piston boundaries is kept constant at inlet pressure while in reality it will increase with the pressure in the compression chamber which has a positive effect.

When the cylinder is closed, the third graph of Figure 4.17a is obtained. This creates a much thinner gas film each moment throughout the cycle. This could be a desired design choice when it is beneficial with regard to the internal leakage in Chapter 5.

The disrupted bearing configuration and the closed cylinder configuration yield respectively a minimum film thickness of 2.7 and 1.7 micrometer. These values are in the range but even on the low side compared to the piston-shaft and piston-cylinder bearings. This bearing is not included in the complete optimization process of paragraphs 4.1 and 4.2 as the manufacturability of a cylinder is much simpler

than the surface shapes analysed for the other bearings. If it is deemed necessary to improve these results, this would most likely result in a smaller piston width and lower frequency to reduce the force on the bearing without changing the surface area.

4.4. Shaft-Cylinder Sleeve bearing

The shaft-cylinder sleeve bearing is a full journal bearing and can be analysed in the same way as the previous paragraph. The compression chamber force is transferred from the piston via the shaft to the cylinder sleeve and is the only load. The diameter of the bearing is 65 mm which is equal to the cylinder diameter plus the thickness of the cylinder sleeve. Similar to the piston-shaft bearing, the nominal film thickness, the space between the surfaces in centred position, is free to choose as the internal leakage is not influenced by this bearing. Figure 4.18a shows that the thickest film occurs when a nominal film thickness of 10 μm is applied. The minimum film thickness takes a value of 3.4 μm as visible in the full cycle shown in Figure 4.18b.

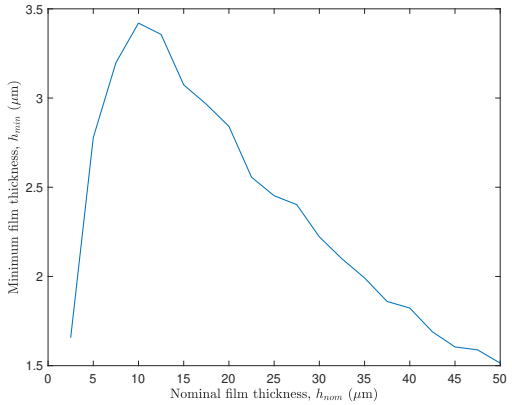

(a) Effect of different nominal film thicknesses on the minimum film thickness.

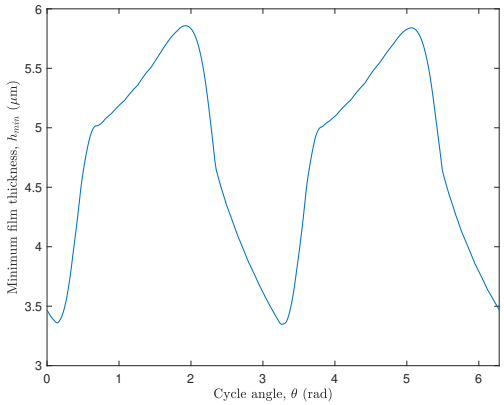

(b) The course of the film thickness during a full compression cycle with h_{nom}=10 μm.

Figure 4.18: Simulation of the film thickness of the shaft-cylinder sleeve bearing according to Table 4.4 with D_s=65 mm.

4.5. In-plane Bearings

The final category of bearings is oriented parallel to all the loads coming from the compression process. The gravitational force of the components hasn't been analysed yet. When the compressor is in upright position like Figure 3.6, this force will be exerted on these bearings. As gravity is always pulling in the same direction, this category will operate without a squeeze effect. By itself, there is also no wedge shape which means that the relative velocity of the components won't build up pressure. It is possible to add surface textures, grooves and ridges, to artificially create a wedge principle. Each bearing surface has a different relative velocity, reciprocating or rotating, and different a load. This asks for a detailed analysis which is not covered in this report.

Another solution is to flip the compressor on its side. In this way, the in-plane bearings will see no load at all and won't need a gas film to prevent excessive friction and wear. The gravitational force is now added as a constant force to all bearings analysed in paragraphs 4.1 through 4.4. It can be assumed that all moving components won't exceed a mass of 0.5 kg which results in a force of five newton, equivalent to approximately five percent of the compression forces. The effect on the squeeze bearings will be small.

5

Internal Leakage

In this chapter, the design is analysed on the amount of high pressures gas that escapes from the compression chamber and exhaust port towards the low pressure compartments via the bearing gaps. The forces associated with these pressure differences should add to a balanced design. A model is presented by which several designs are compared. This results in a maximum required gap to keep the efficiency above the desired threshold.

5.1. Component Lay-out

The compressor comes with an hermetically closed casing which makes that no CO_2 mass is lost at any time. In this case the expansion of high pressure gas in the bearing gaps towards the low pressure compartments is defined as internal leakage, which has a negative effect on the volumetric efficiency and the power consumption. Due to this internal leakage, several components within the compressor will experience a pressure above the inlet pressure. This may come in two ways: as a complete compartment that builds up a pressure, or as a force related to the pressure drop in the gap between the components.

In a design like Figure 3.6, these forces can separate some components and create mechanical contact on the in-plane surfaces of other components. The shaft may for example be pushed against the cylinder lid, creating a larger leakage path from the high pressure compression chamber to the opposing low pressure compression chamber and increasing friction and wear of the contacting surfaces. It is possible to vary the lay-out of the components while respecting the functionality of the bearings from Chapter 4.

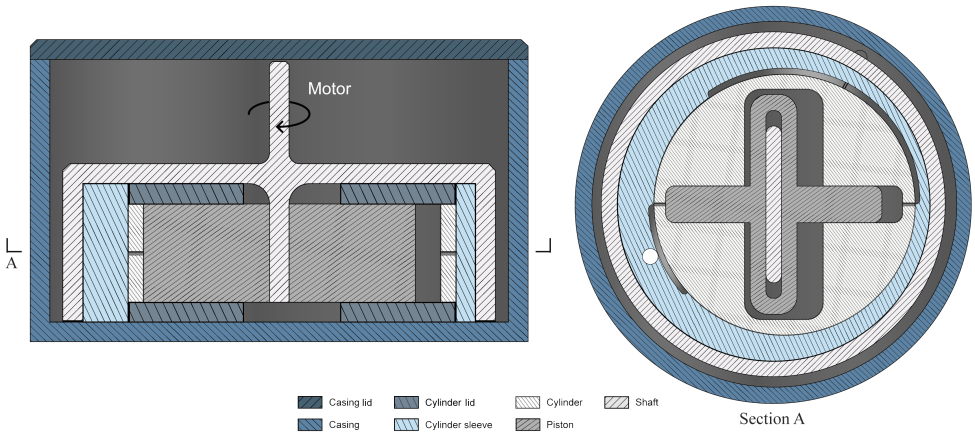

Figure 5.1: Front and top cross-sectional views of a shaft-actuated compressor with a cylinder that fully encloses the compression chamber including suction and exhaust ports.

It should be taken into account that both moon-shaped parts of the cylinder have to be connected to maintain the squeeze effect of the piston-cylinder and cylinder-cylinder sleeve bearings. It is necessary that the compression chamber is either enclosed by multiple components that are all rigidly connected to the casing or by one single component. In the first category, the casing floor and casing lid can be used, but extensions of the cylinder sleeve can fulfill this function as well. The second category creates an enclosure by the shaft or the cylinder. An advantage of the cylinder enclosure is that it yields a fully symmetric lay-out which automatically balances the forces due the pressure drops. This is caused by the fact that no other components other than the piston are captured within the cylinder. For other lay-outs, some leakage paths have to be made intentionally shorter to balance these forces. This is prone to unbalance as in practise a dynamic system like this won't behave exactly as modelled and next to that, it adds undesired internal leakage. The cylinder enclosure is also the only solution that in addition to the top and bottom surface can also enclose the radial direction of the compression chamber. Figure 5.1 shows the best of nine different configurations that can be found with an overview of the pros and cons in Appendix A.6. A distinction is made between a shaft-actuated and cylinder actuated system as not all configurations can be implemented in both cases. No difference is made between the original and adjusted design.

Suction and Exhaust Ports

The gas flow towards and from the compressor is a critical part of the system. The choice has been made to create the actual inlet of the compressor through the casing lid but the inlet to the compression chamber via the floor. This means that new gas will be sucked through the motor which exhibits a cooling effect. As the compression chamber is rotating inside the cylinder sleeve, a transition has to be made from a stationary to a moving component. A tiny hole inside the cylinder connects to a slot in the cylinder sleeve wall. Gas flows from the compression chamber to the exhaust slot between 2.4 and π radians in Figure 3.7a and from the suction slot to the compression chamber between 4.1 and 2π radians. The discharge pipe from the exhaust slot out of the compressor goes through the cylinder sleeve and casing floor. The supply towards the suction slot is another slot inside the cylinder sleeve wall as this flow doesn't have to be contained.

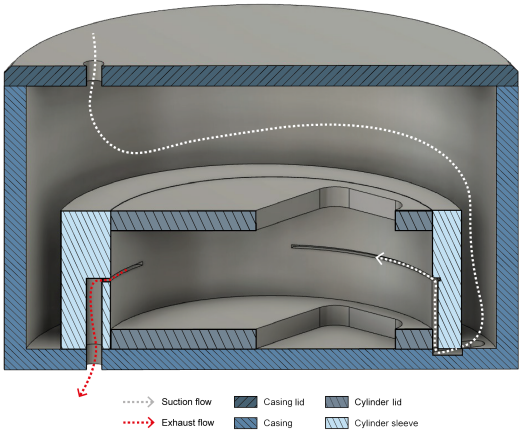

Figure 5.2: Gas flow via the suction and exhaust slots and floor connections

Especially the size of the holes and the exhaust slot are a main cause of internal leakage as will be discussed in the next paragraph. Both these holes and slots have to be able to transport a sufficient gas flow to process the volume stated in Table 3.1. Each hole and slot has to be able to transport the complete compressed compression chamber volume within 12 percent of the compressor's revolution time, which is equal to the length of the slot over the circumference of the cylinder. The width of the slot is equal to the diameter of the hole, which is together with the length of the slot the only parameter that influences the leakage rate. The depth of the slot can therefore be chosen freely in such a way that almost the entire pressure drop is caused by the hole in the cylinder. The low viscosity of the gas and relatively high fluid velocity create a turbulent flow. When a pressure drop of 0.1 bar is assumed,

the Darcy-Weisbach equation [1] leads to a hole diameter of just over 0.5 mm and a slot depth of 1.0 mm.

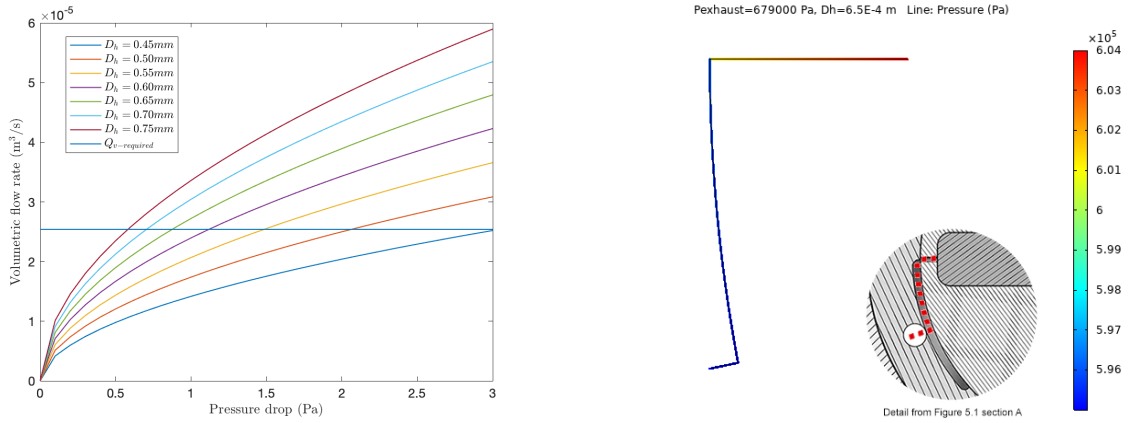

(a) Volumetric flow rate for several hole diameters and pressure drops.

(b) Overview of the pressure drop in the volumetric flow model.

Figure 5.3: Analysis of the volumetric flow rate through the exhaust hole and slot using COMSOL Multiphysics.

To validate the results, a more detailed simulation is done using COMSOL. Figure 5.3b shows a model of the exhaust hole and slot that ends in the exhaust tube through the cylinder sleeve. A detail of were the model is located in the compressor is shown in the bottom right corner. The system is modelled using the Churchill friction model. The surface roughness for the hole is set to 1.5 micrometer (drawn tubing) and 46 micrometer (commercial steel) for the other components. The flow is assumed to be turbulent with Reynolds numbers between 4000 and 14000. It can be seen that the pressure drop mostly takes place over the exhaust hole and the first bend. Both bends are modelled with a loss coefficient, k, with a value of 1. The fluid velocity in the first bend however is larger than in the second bend due to the cross-sectional area of the hole relative to the slot which creates a larger loss. Figure 5.3a shows the volumetric flow rate through the system for different holes sizes and pressure drops. The analytical result obtained before, appears to be an overestimation of the flow rate. A hole of 0.5 mm comes with a pressure drop of 0.21 bar to reach the required flow rate. When the pressure drop is kept at 0.1 bar, the hole size should be at least 0.65 mm in diameter, which will be used for this design. As the suction slot is significantly longer and no leakage occurs here, the same sizes are used to be able to use the same production method.

5.2. Internal Leakage Path Optimization

The internal leakage comes from two sources within the compressor. Firstly, the compression chamber loses pressure via the gaps between the components which is especially the case during the exhaust phase while the pressure is at its maximum value. This is about 12 percent of the time for each compression chamber. Secondly, the exhaust slot in the wall continuously loses pressure.

The top cross-sectional view of the compressor is drawn schematically in Figure 5.4 for both the original and adjusted design. The paths from both sources towards the low pressure compartments are almost similar and are given by some of the bearing surfaces and can be split in four paths:

1. Between the piston and cylinder walls, $\dot{m}_{L1}$
2. Between the piston and the cylinder top and bottom surfaces, $\dot{m}_{L2}$
3. Between the cylinder and cylinder sleeve, radial $\dot{m}_{L3}$
4. Between the cylinder and cylinder sleeve, vertical $\dot{m}_{L4}$

The first path is significantly shorter for the adjusted design than for the original design as it is interrupted by the centre hole for the piston and, at equal compression chamber volume, the path is higher. The second path on the other hand is in favor of the adjusted design as the piston is narrower. The effect

of the height and width between $\dot{m}_{L1}$ and $\dot{m}_{L2}$ therefore cancels. This path is shown by a striped arrow as the flow is not part of this cross-section in reality but on top and below the piston. The third path is mostly applicable to the leakage from the exhaust slot and equal for both designs. Leakage from the compression chamber hole is assumed negligible during the time it's not connected to either one of the slots as the compression chamber pressure is lower during these times and the hole is covered by the cylinder sleeve wall. The flow from the exhaust slot moves towards the suction slot but can also move up and down the cylinder wall to end up in the centre hole. This is added as path four and is positively influenced by the height of the cylinder and therefore better in the adjusted design. To summarize, the only disadvantage of the adjusted design compared to the original design is the interruption of the piston-cylinder walls by the centre hole. The vertical leakage from the exhaust slot on the other hand is reduced.

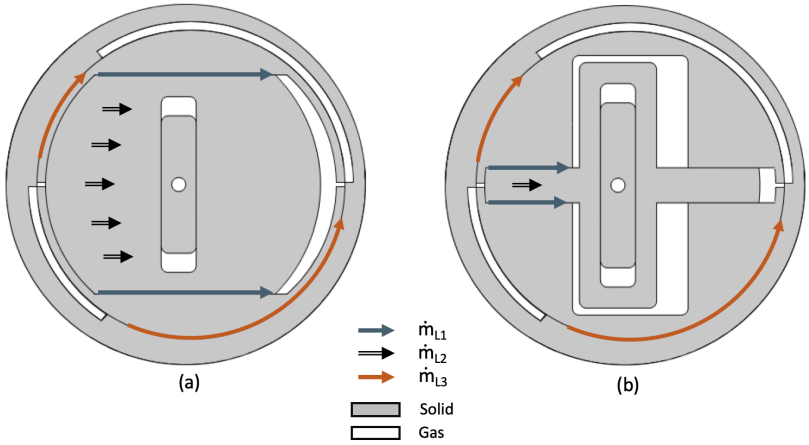

Figure 5.4: Schematic overview of the internal leakage paths of the original design and the adjusted design.

The leakage paths can be described by a set of geometric parameters as in Table 5.1 as the width-over-length-ratio of the paths have a large influence on the leakage rate, see equation 3.2 and 3.3. A minimum internal leakage exists for a specific set of parameters. Like the optimization process of the bearing load capacity, the parameters are related by the volumetric flow rate in equation 3.4. It can be concluded that the eccentricity, e, and the piston width, P_w, should be minimized to respectively values of 2 and 3 mm. For the piston width, an increase might be seen when this is required to increase the piston height due to the constraint that the height can't be larger than ten times the width of the piston as discussed in paragraph 4.1. The height of the piston, P_h, has an optimum and depends on the relative influence of each flow on the total leakage. This is also the case for the diameter of the cylinder, D. The frequency is not part of Table 5.1 and can theoretically be used to freely scale the other parameters and maintain the required volumetric flow rate. Due to the compressibility of gas, it is wise to do a check for dynamic effects when the frequency is varied.

	$W_{original}$	$L_{original}$	$W_{adjusted}$	$L_{adjusted}$
$\dot{m}_{L1}$	P_h	$0.5\sqrt{2}D - 2e - 4$	P_h	$(D - 4e - 15)/2$
$\dot{m}_{L2}$	$0.5\sqrt{2}D$	$(D - 2e - 7)/2$	P_w	$(D - 4e - 15)/2$
$\dot{m}_{L3}$	$0.12\pi D$	$0.32\pi D$	$0.12\pi D$	$0.32\pi D$
$\dot{m}_{L4}$	$0.12\pi D$	$P_h/2$	$0.12\pi D$	$P_h/2$

Table 5.1: Dependencies of the length and width of the leakage gaps to the compressor geometric parameters.

3D Leakage Model

To be able to accurately determine the bearing gap heights, a 3D leakage model is build using COMSOL Multiphysics. The model including a cross-sectional view is presented in Figure 5.5. A thin-film

flow analysis is applied on the outer radial surface of the cylinder that would be in contact with the cylinder-sleeve and on all four sides of the extrusion where the piston is positioned inside the cylinder. The outside top and bottom of the cylinder as well as the hole in the centre are connected by a thick layer of gas, in such a way that no pressure drop occurs.

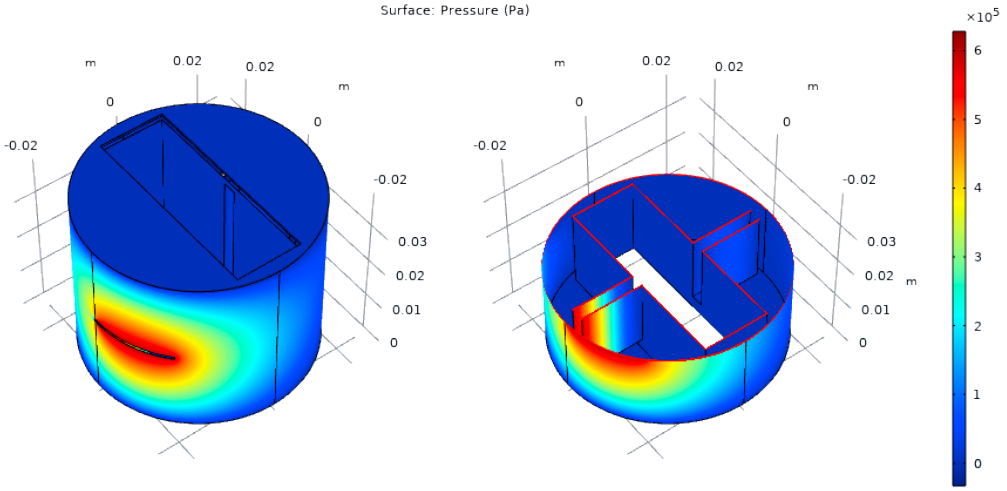

Figure 5.5: 3D COMSOL model to analyse the internal leakage inside the compressor.

The gas can enter and leave the model in multiple ways. One source is created by the exhaust slot and another one is created inside the compression chamber where the head of the piston would be. Equally a drain is created by the suction slot, the opposing compression chamber and the top edges of the centre hole. All drains are kept at a pressure of 0.75 bar. The compression chamber is not connected via the exhaust hole to the exhaust slot. The model is correct as long as the exhaust hole is in contact with the slot. When the hole is past the slot, all the pressure left in the compression chamber is part of the dead volume and irrelevant for the leakage analysis. Before the hole comes into contact with the slot, the pressure is below the exhaust pressure and covered by the cylinder wall which reduces the leakage rate significantly. Furthermore, the circumference of the hole is only just below three percent of the circumference of the piston for the parameters of Table 4.4. For these reasons, the system is modelled in a fixed position. A quick calculation also shows that in the given frequency range, the leakage rate due to the pressure difference is a few orders of magnitude larger than the leakage rate due to the sliding velocity. This means that only the pressure term is included in these results.

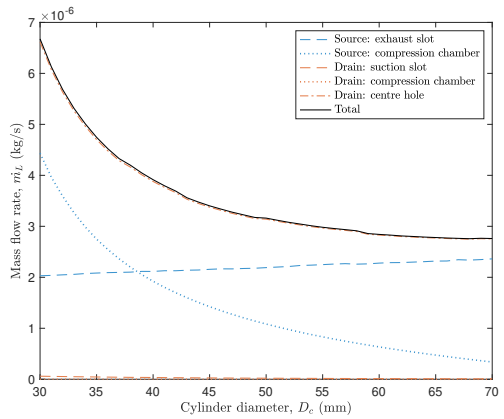

(a) Several cylinder diameters with $P_h = 39mm$, $P_w = 3mm$, $f = 39.7hz$, $e = 2mm$, $h = 2.9\mu m$.

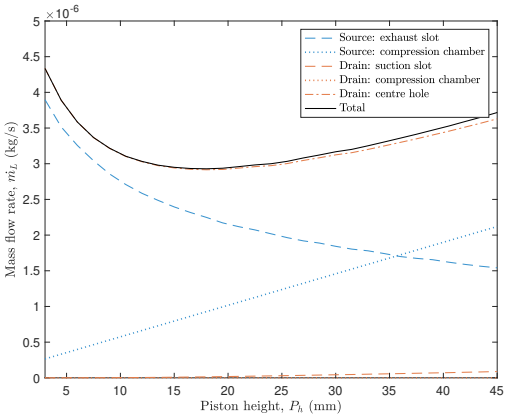

(b) Several piston height with $D = 50mm$, $e = 2mm$, $h = 2.9\mu m$.

Figure 5.6: Distribution of the mass flow rates in the compressor with a constant compression chamber pressure.

In Figures 5.6a and 5.6b both sources are kept at a constant pressure of 6.7 bar. In practise, the compression chamber pressure will vary over time and the average leakage rate over a cycle yields the effective leakage rate as mentioned in Table 3.1 column b. A constant pressure therefore results in a worst case analysis.

As concluded from Table 5.1, the diameter of the cylinder has an optimum value. For the range shown, the largest diameter of 70 mm gives the least amount of leakage. A smaller diameter comes with shorter piston walls and a shorter distance from the exhaust slot to the suction slot. A larger diameter increases the length of the exhaust slot and would eventually increase the flow again. Equal to Chapter 4 a constraint is put on the maximum diameter at 50 mm which is therefore the optimum value. Almost all internal leakage finds it way to the low pressure compartment via the centre hole. The piston height has an optimum around 18 mm. The height of the outer surface of the cylinder decreases with the piston which makes that the exhaust slot leakage becomes large for a small piston height. At large piston heights, the leakage along the piston wall dominates.

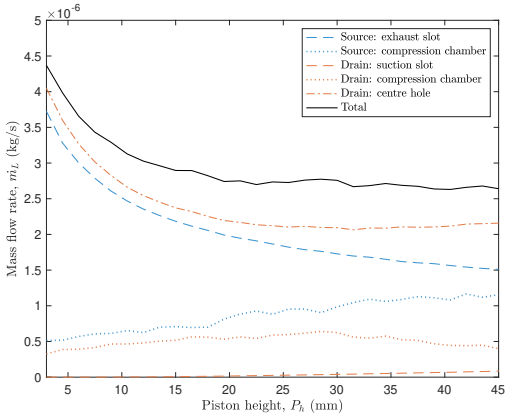

(a) Several piston height with $D = 50mm$, $e = 2mm$, $h = 2.9\mu m$.

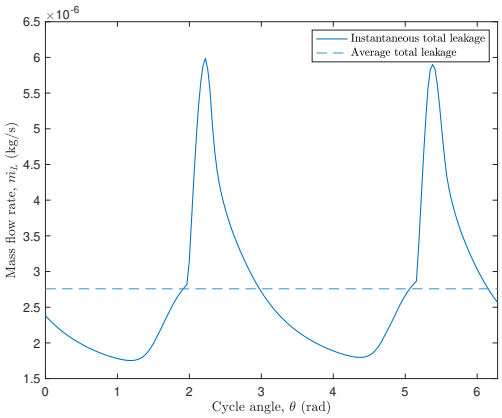

(b) Leakage over a compression cycle with $D = 50mm$, $P_h = 39mm$, $P_w = 3.9mm$, $f = 30Hz$, $e = 2mm$, , $h = 3\mu m$.

Figure 5.7: Distribution of the mass flow rates in the compressor with a time-dependent compression chamber pressure.

The effect of the frequency of the compressor on the internal leakage can only be analysed when the pressure has a time-dependent profile. Figure 5.7a is equal to Figure 5.6b except for the fact that each data points is given by the time average of a compression cycle instead of a steady-state result. A better result is expected as for part of the cycle a high pressure in the compression chamber is replaced with a lower pressure. At smaller piston heights and widths and with that higher frequencies the pressure in the compression chamber builds up so fast, that the pressure in the leakage gap lacks in time. The effective length of the gap becomes shorter which results in an almost equal value in both figures. At larger piston heights and with that lower frequencies the leakage rate of the time-dependent model is significantly lower. Between values of 25 and 45 mm the leakage rate is almost constant. This makes it convenient to equalize it to the value of 39 mm determined in Chapter 4. This makes the optimal leakage behaviour equal to Figure 5.7b which shows the mass flow rate throughout a cycle. The average value stays easily below 2.9e-6 kg/s as required in Table 3.1.

It could still be analysed to reduce the shaft width and with that the size of the centre hole, which would positively influence most leakage paths but have a major impact on the bearing load capacity. Another option is to make the gap height of the cylinder outer surface and the piston walls not equal. For example, a smaller gap at the piston would shift the optimum towards a larger piston height. This is mostly decided by the manufacturer when a specific surface is easier or cheaper to produce. These solutions won't be covered in this report.

6

Conceptual Design

An exploded view of the conceptual compressor design based on gas bearings is presented in Figure 6.1. The shaft-axis driving the piston is not visible as it's located inside the shaft bearing.

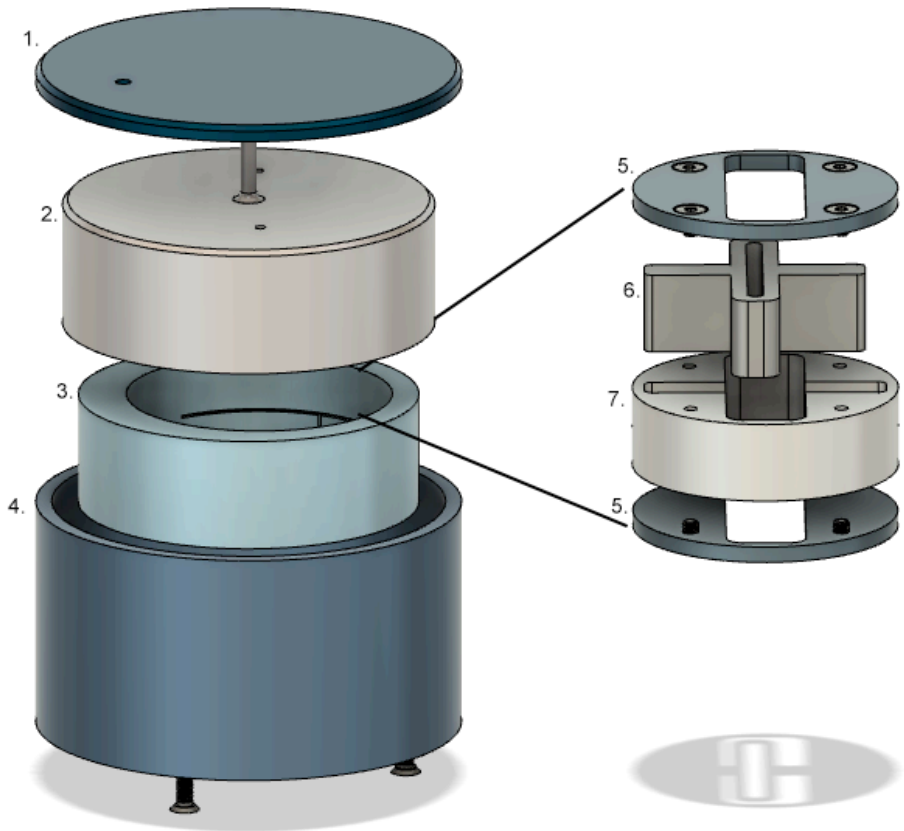

1. Casing lid
2. Shaft
3. Cylinder sleeve
4. Casing
5. Cylinder lid
6. Piston
7. Cylinder

Figure 6.1: Exploded view of the conceptual compressor design

The casing lid is welded to the casing to create a hermetic barrier. The cylinder sleeve is bolted to the casing floor with sealing bolts to prevent gas from escaping out of the casing. The cylinder sleeve is not welded to the casing as the high welding temperature may deform the components slightly and affect the bearing surfaces. The cylinder lids are bolted to the cylinder. It might be useful to add a sealing material between both bolted connections to make the system more airtight.

6.1. Manufacturability

Table 6.1 shows an overview of the function of the interfaces between all moving components in the compressor and the corresponding requirements for the nominal and minimum film thickness. Components A are in order of appearance of Chapter 4.

Component A	Component B	Function	h_{nom}	h_{min}
Piston	Shaft	Bearing	30 μm	2.9 μm
Piston	Cylinder	Bearing and seal	2.9 μm	2.1 μm
Cylinder	Cylinder sleeve	Bearing and seal	2.9 μm	1.7 μm
Cylinder sleeve	Shaft	Bearing	10 μm	3.4 μm
Piston	Cylinder lid	Seal	2.9 μm	N/A
Cylinder lid	Casing floor	None	N/A	N/A
Cylinder lid	Shaft	None	N/A	N/A

Table 6.1: Functions and requirements for the interfaces between all components

The minimum film thickness is directly related to the surface roughness of the components. As a guideline the surface roughness should stay below half the minimum film thickness. A lathing or milling process often results in a surface roughness larger than required between 0.2 up to 3.2 μm [9] [10]. This asks for an additional surface polish which can be done mechanically of by an electrochemical process. Naturally, this comes with additional manufacturing costs. The surface roughness is not the only manufacturing requirement related to the minimum film thickness. It also asks for a specific flatness or cylindricity of the components. Concerning both, it is an advantage that the components are relatively small sized.

For all parts that have a required surface roughness and required flatness, it is recommended to analyse to possibility of splitting components into multiple flat parts and create an assembly process without losing accuracy. A detailed analysis has not been performed but an overview of several options is given. The shaft-axis and piston e.g. could be constructed out of multiple rectangular parts of about 40x30mm that are significantly easier to manufacture with given specifications. The shaft-axis has to be connected to the cylindrical part of the shaft and the inaccuracy in this process in the direction of the compression chambers leads to an increased dead volume in one compression chamber and an equally decreased dead volume in the opposing compression chamber. In the direction orthogonal to the compression chambers, there is no negative consequence. For the piston, both ends that move in and out of the cylinder and form the compression chambers, should be manufactured out of one part. As they work together as a squeeze bearing, it would be practically impossible to assemble them inline within the minimum film thickness value. The piston parts that make contact with the shaft-axis are able to handle inaccuracy in the direction orthogonal to the compression chambers without any negative consequences. The required cylindricity can't be improved by an assembly process and should be manufactured as such with the associated costs.

From the table it is clear to see that the nominal film thickness is significantly lower for all the components that have a sealing function. This adds another tight tolerance to the inner and outer diameter of respectively the cylinder sleeve and cylinder. This is also required for the height and width of the piston and equally for the opposing surfaces inside the cylinder. In this case, it would also be beneficial to construct the piston out of multiple parts.

6.2. Second Compression Stage

Chapter 4 gives an overview of all the forces and torques that are applied on each bearing surface and the behaviour of the thin gas film in between. Chapter 5 determines the internal leakage rate from the high pressure to the low pressure compartments through this gas film. Both chapters are build with the goal to compress the gas from a suction pressure of 0.75 bar to an exhaust pressure of 6.7 bar. The goal for ZEF was to develop a compression process that could compress the gas up to a pressure of 60 bar. As shown in Table 3.1, a second stage is required for this and the volumetric flow rate of the compressor decreases by the pressure ratio to the power one over the polytropic index. This has several consequences for the bearing and leakage design:

- A lower volumetric flow rate asks for a smaller compression chamber volume or a lower frequency which shifts the optimum design parameters.
- As the leakage requirement is given as a percentage of the volumetric flow rate of each individual stage, the absolute allowed volumetric leakage rate is reduced by the same factor.
- The absolute pressure difference between the suction and exhausts pressure is almost nine times higher for the second than for the first stage:
  - The internal leakage rate is directly related to the pressure difference and therefore also nine times higher.
  - The compression chamber force that needs to be handled by several bearing surface increases up to nine times dependent on the adjustments of the piston area.

All of these have a negative impact and reduce the nominal and minimum film thicknesses. The absolute pressure difference could be kept constant by adding more stages with sequentially decreasing pressure ratios. This would however defy the purpose of building a compressor based on gas bearing technology as hydrodynamic bearings function properly for lower pressure ratios. This results in the fact that this report is limited to only the first stage of the compression process.

7

Conclusions

In this thesis, a thorough analysis of the rotary cylinder compressor has been performed. The lay-out of the compressor has been altered fundamentally to make the concept ready for gas bearing implementation. For this novel concept, an optimisation process is completed to improve both the bearing load capacity and the internal leakage of the system. This has been done to fulfill the following thesis objective:

"The conceptual design of an efficient two-stage compression process with a high pressure ratio based on gas bearing technology."

This conceptual design can be evaluated based on two sub-questions which have been answered throughout the report:

1. *"Is the design able to generate sufficient load capacity to handle the loads throughout the process without making any contact between the bearing surfaces?"*

Each bearing surface comes with its own loads and needs to have at least an equivalent load capacity. This is done by dynamically building up sufficient pressure between the two approaching surfaces before mechanical contact occurs. The induced pressure is mostly owed to the squeeze effect for gasses with a low viscosity at low frequencies. For the first stage of the ZEF process, each surface within the conceptual design is able to maintain a gas film thickness of at least 1.7 μm at steady-state.

2. *"Is the design able to achieve a predetermined efficiency considering the leakage flow through gas bearings?"*

As gas bearing have little to no friction, the power loss in the system due to this is negligible. The losses present itself as part of the volumetric efficiency which consists of the dead volume of the compressor and the internal leakage. The internal leakage is caused by flows from the high pressure to the low pressure compartments through some of the bearing gaps between the moving components that have a sealing function. A maximum allowed internal leakage rate is defined as ten percent of the effective mass flow rate of the compressor. This value is reached for the sum of all leakage flows when a film thickness of maximum 2.9 μm is applied for these specific bearings within the first stage of the ZEF compression process.

Both sub-questions can be answered positively under a few conditions. Both come with a specific thickness of the film that is in the range of the surface roughness of the material for general production processes. An additional surface treatment is required to obtain such a thin film without creating mechanical contact between the materials. Most components also have to meet tight tolerances regarding multiple dimensions and the flatness and cylindricity of some surfaces. All this makes the manufacturing process rather expensive which brings us to the conclusion that even in mass production it is unlikely to implement this compressor as part of the ZEF methanol micro-plant. Next to that, this evaluation is only done for the first stage of the compression process and the second stage is assumed to

have a worse performance due to a smaller size and higher absolute pressure difference.

A result that should be taken away from this report is that the squeeze effect of gas bearings comes with a large load capacity at relatively low frequencies. For applications with symmetric oscillating loads that operate at high temperatures or require a long lifetime, this lubrication method should be considered.

8

Recommendations

Based on this design process, a set of recommendations is presented to improve the results with respect to this conceptual compressor design. Some recommendations are applicable to general gas bearing technology.

- *Thermal expansion*
  The compressor is designed to handle a high pressure ratio. Due to the adiabatic compression process, a high gas temperature will be reached. A thermal analysis of the system should be performed to calculate the steady-state temperature of the components and corresponding thermal expansion of the system. Stainless steel has a thermal expansion coefficient between 10e-6 and 16e-6 m/mK [9] which means that a component of 10 mm will expand 1 μm when the temperature is increased by 100 degrees. As this is in the range of the bearing film thicknesses and seals, this should be taken into account in the manufacturing requirements.

- *Mechanical deformation*
  The loads on the system are relatively small but for most components proportional to their size. Equal to the thermal expansion, it is likely that the deformation due to bending of especially the shaft-axis and pistons in width direction is in the range of the bearing film thicknesses and seals. The domain of the piston height is already constraint to ten times the width. This could for example be altered to an equation related to the moment of inertia of the width.

- *Corrosion*
  In an oil lubricated compressor, the oil protects the bearing surface from corrosion by creating a barrier against oxygen and water. It can't be guaranteed that the CO_2 from the ZEF methanol micro-plant doesn't contain water and therefore the material should be chosen with care.

- *Start-up sequence*
  The bearings are analysed on its lubrication ability at steady-state. When the compressor is started from standstill, the gas inside the compressor won't reach its exhaust pressure of 6.7 bar which reduces the loads on the system. At low speeds an electric motor exerts a higher torque to speed up the system. It is shown in Appendix A.4 that the gas film recovers from this over time, but the impact on the wear of the system should be taken into account to obtain a sufficient lifetime.

- *Inertia*
  The change in film thickness of a bearing is created by the motion of one of the components with respect to the other. For the models in this report, the inertia of the components during these motions have been neglected. This means that film thickness and with that the pressure in the bearing changes quicker than in reality. This could be implemented in a more advanced model.

- *Additional internal leakage due to the bearing motion*
  The squeeze effect translates and rotates the components within the bearing gaps. For the internal leakage analysis a constant gap size has been assumed. As the leakage rate is related to

the third power of the gap height, the motion of the squeeze effect should be implemented in the leakage model.

- *In-plane bearing surfaces*
  All in-plane bearing are constructed as such that no loads are applied on these surfaces. It is therefore unnecessary to build up a dynamic pressure to handle these loads. This makes that the components also won't be forced to the centre with respect to their opposing surfaces. For example, the piston won't be centered between both cylinder lids. Vibrations of the system may push the components in a particular direction. This adds internal leakage for surfaces with a sealing function and, even without loads, may cause wear. Research could be done into adding grooves in the surfaces to create a small dynamic pressure that pushes the component to the centre or a surface treatment that hardens it against wear.

Appendices

A

Additional Results

A.1. Original RCC Cycle

Figure A.1 shows the rotary cylinder compression cycle as designed by Hu et al. The low pressure gas enters the compression chamber through the tube at the top of the figures. The high pressure gas leaves at the bottom via the exhaust valve. It is assumed that no dead volume exists between the piston and the casing wall. This means that the compression chamber has to make an instant switch from the exhaust to the suction phase. This is done by making the piston surface and the suction slot a quarter of the circumference of the casing. When the piston surface is decreased, the length of the suction and exhaust slot should be increased to maintain this function.

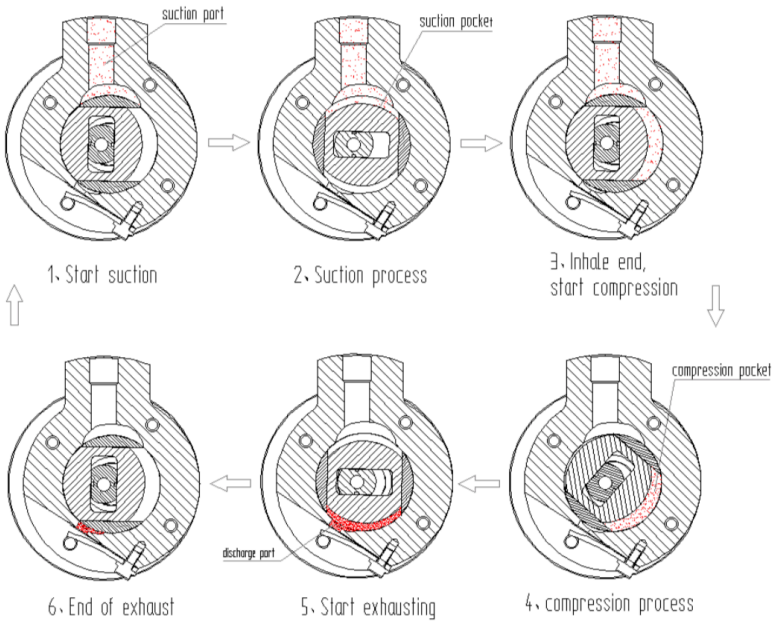

Figure A.1: Rotary cylinder compressor cycle [11].

A.2. Alternative Shaft Concepts

Figure A.2 shows two additional shaft concept that don't induce a moment in the shaft rotary bearing. The left concept does this by adding a second bearing which makes that the gas pressure pushes effectively in the centre of the bearings. Production and assembly is challenging as either the piston and cylinder of the shaft has to be produced out of two parts. The right concept adds a second compression chamber which places the bearing in the centre of both forces. This asks for the production of both an extra piston and cylinder which would increase the costs of the compressor.

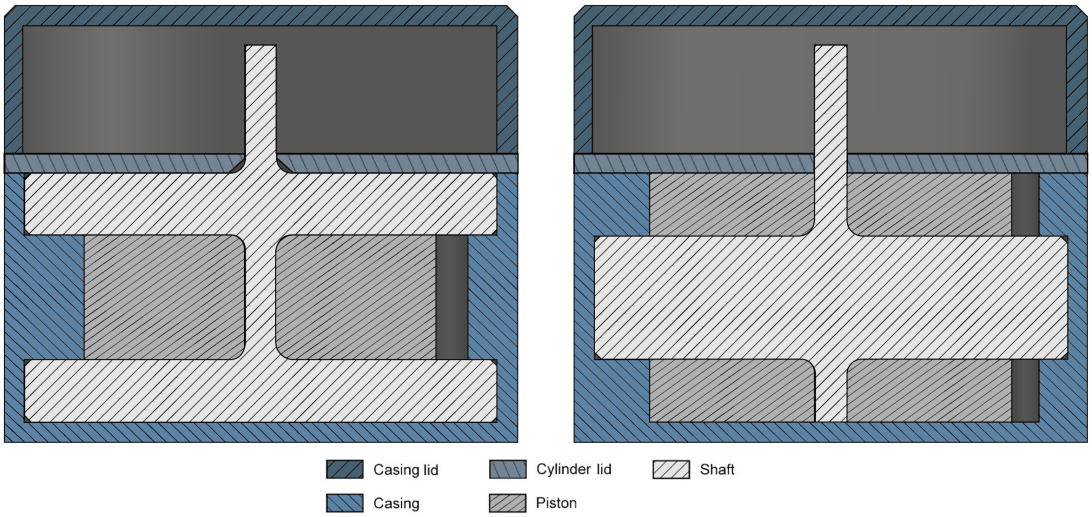

Figure A.2: Conceptual designs to prevent a moment on the shaft rotary bearing by implementing a split bearing or split compression chamber.

A.3. Speed-Torque Behaviour

The differential equation for the speed-torque behaviour of the system can be derived by the following equations. The motor torque has a maximum value that decreases with the rotational speed by a factor delta which is given by the motor specifications. It is visible that the piston mass and centrifugal force differ by a factor related to the angular acceleration which drops out of the equation for a controlled system.

$$T_{cc}(\theta) + T_{motor}(\dot{\theta}) + T_{inertia}(\ddot{\theta}) + T_{p-mass}(\theta, \dot{\theta}, \ddot{\theta}) + T_{p-cf}(\theta, \dot{\theta}) = 0 \tag{A.1}$$

$$F_{cc} e sin(\theta) + T_{stall} - delta\,\dot{\theta} + I_{tot}\ddot{\theta} + m_p a_p e cos(\theta) + m_p \dot{\theta}^2 e^2 sin(\theta) cos(\theta) = 0 \tag{A.2}$$

$$F_{cc} e sin(\theta) + T_{stall} - delta\,\dot{\theta} + I_{tot}\ddot{\theta} + m_p \frac{d(e sin(\theta))^2}{dt^2} e cos(\theta) + m_p \dot{\theta}^2 e^2 sin(\theta) cos(\theta) = 0 \tag{A.3}$$

$$F_{cc} e sin(\theta) + T_{stall} - delta\,\dot{\theta} + I_{tot}\ddot{\theta} + m_p e^2 (\ddot{\theta} cos(\theta)^2 - \dot{\theta}^2 sin(\theta) cos(\theta)) - m_p e^2 \dot{\theta}^2 sin(\theta) cos(\theta) = 0 \tag{A.4}$$

For constant RPM with voltage control variable, VR:

$$F_{cc} e sin(\theta) + V R T_{stall} - delta\,\dot{\theta} - 2 m_p e^2 \dot{\theta}^2 sin(\theta) cos(\theta)) = 0 \tag{A.5}$$

The value of VR is controlled to maintain a constant rotational speed and should be supported by either a current or speed sensor.

A.4. Initial Conditions of the Thin-film Model

Figure A.3 shows the behaviour of the film when the initial film thickness is varied between two, four and eight micrometer. It is clear to see that within three compression cycles the film restores itself to the same steady-state value.

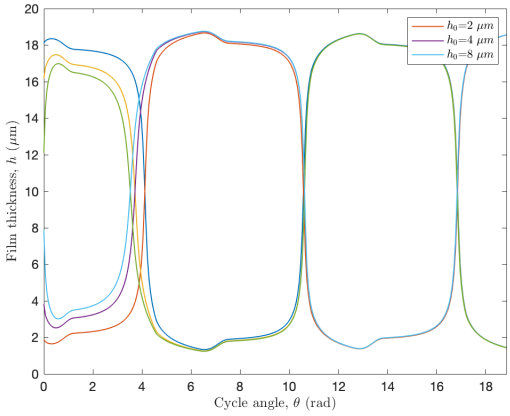

Figure A.3: Film thickness behaviour for different initial thickness values.

A.5. Torque Load Cases for Varying Eccentricities

The change in torque by deviations from the minimum eccentricity is analysed. It is visible in Figure A.4a that a decrease in frequency as a result of an increased eccentricity comes with a significant higher minimum and maximum torque. A lower frequency shows that the torque due to the compression chamber force becomes dominant. Figure A.4 shows the same result for a decreased piston height or width. Here a sinusoidal shape appears which comes from the piston mass and centrifugal torque.

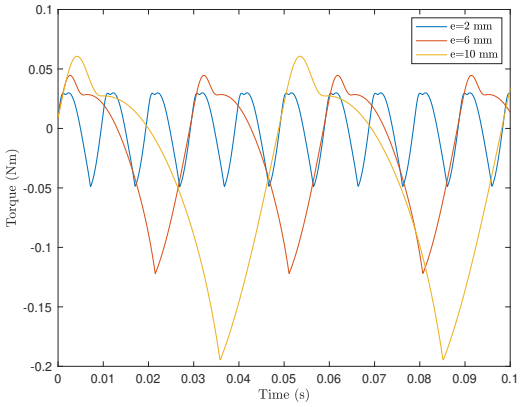

(a) Varying frequency and constant piston area.

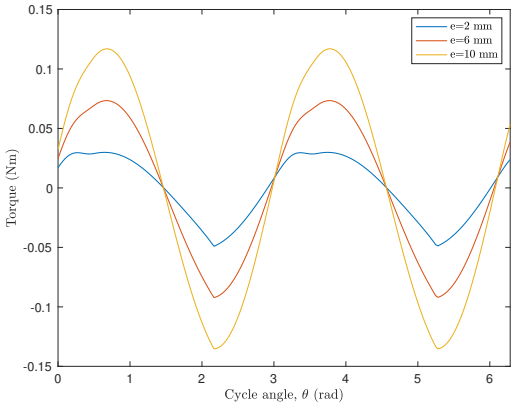

(b) Varying piston area and constant frequency.

Figure A.4: Bearing torque loads for different eccentricities.

A.6. Schematic Overview of Different Component Lay-outs

Figure A.5 shows nine different component lay-out. The design above the centre line are shaft-actuated and the ones below are cylinder-actuated. The top left lay-out is the original design solution which is equal to Figure 3.6. The adjustments on the original design are added in blue to the other lay-outs. For the cylinder-actuated case, there is one solution less as the shaft-enclosure is physically impossible to construct. The working principle for the shaft- and cylinder-actuated configurations are equal and therefore only five short descriptions will be given.

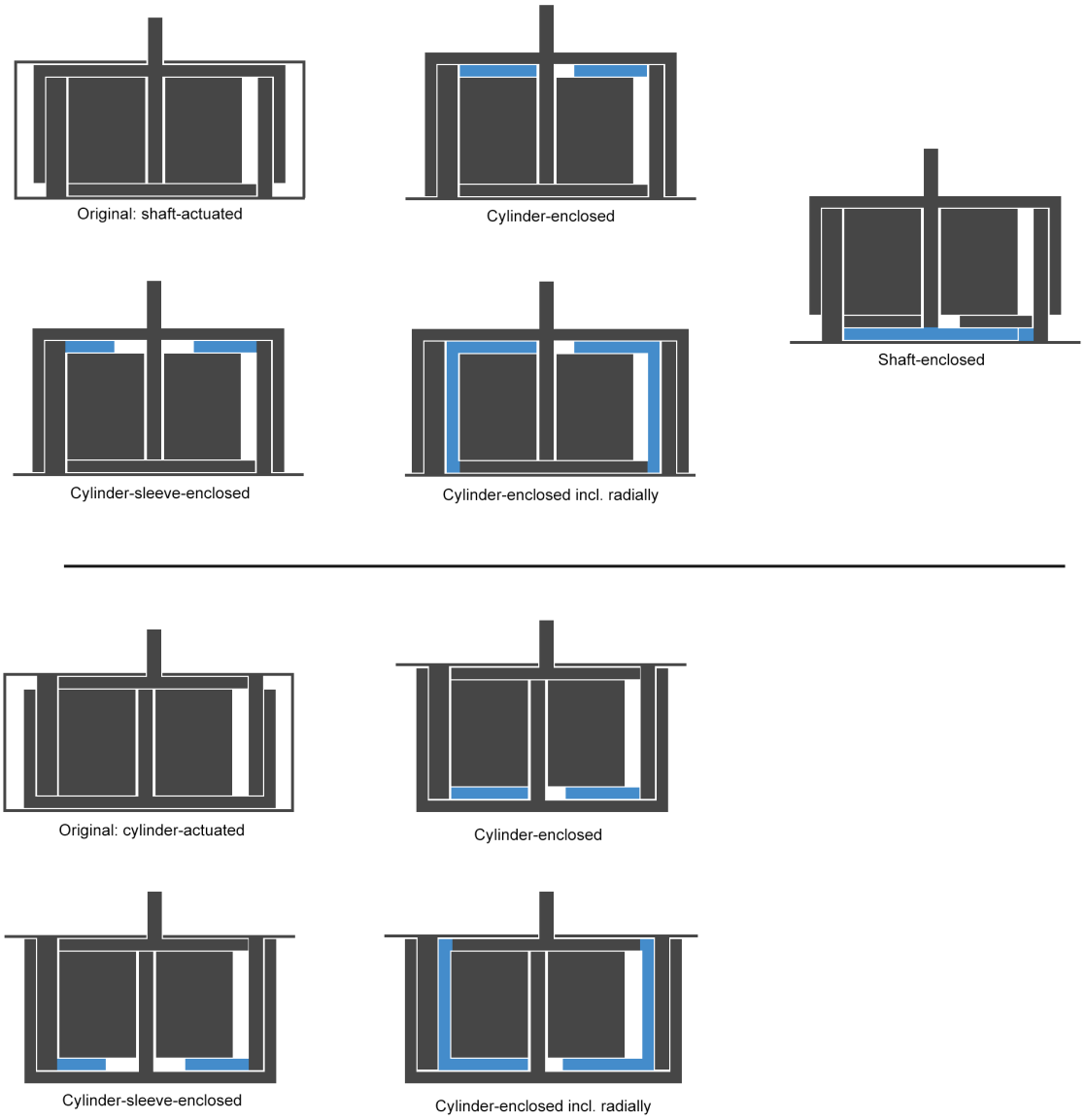

Figure A.5: Schematic overview of different component lay-outs.

1. *Original*
   The original design has a casing floor and lid build around all components. This is done as the differences in pressure (gradients) between the components separate some of them and actually create mechanical contact for others. Without the floor and lid, the shaft would definitely part from the other components and cause a huge leakage rate.

2. *Cylinder-sleeve enclosed*
   The cylinder-sleeve can enclose the piston and cylinder from the top side. In this way the shaft is unloaded. A large hole is required in the cylinder-sleeve to enable the shaft to rotate. This reduced area will either cause mechanical contact between the top surfaces or an equal reduction in area at the bottom which increases the leakage rate unnecessarily.

3. *Cylinder-enclosed*
   The cylinder-enclosed lay-out is a symmetric design which reduces most of the problems. As only the piston is enclosed by the cylinder, the vertical production tolerances are reduced to a minimum amount. The pressure between the top of the cylinder and the shaft should be negligible to function without a lid. This can be done by creating a very large pressure drop over the radial surface between the cylinder-sleeve and the thickness of the cylinder which seems unfeasible.

4. *Cylinder-enclosed incl. radially*
   When the cylinder is also enclosed radially, the flow from the compression chamber won't flow over the surface between the cylinder top and the shaft. This solves the problem from the previous solution while maintaining its advantages. A different exhaust method has to be designed.

5. *Shaft-enclosed*
   The shaft can enclose both the piston and the cylinder by adding a bottom plate. As the shaft rotates around a different centre, the floor of the casing should be adjusted. The assembly of the bottom plate on the shaft-axis requires high precision.

A.7. COMSOL Multiphysics Model Tutorial

The following figures give an overview of the modelling steps taken in COMSOL Multiphyics to analyse the gas bearing behaviour of the piston-shaft bearing. For other bearing surfaces, the method is similar.

1. The first step is to define a set of parameters that are required for the next steps of the model.

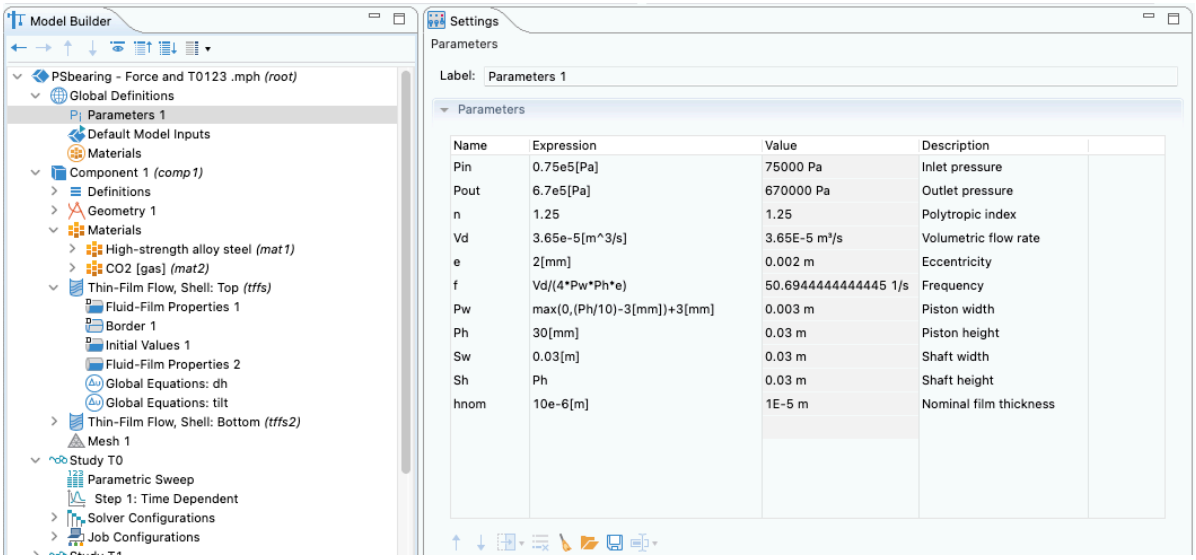

Figure A.6: Model parameters.

2. A pressure curve is constructed using the equations for adiabatic compression and minimum and maximum constraints. From that the force on the shaft over time can be found and after that the moment curve. This method can be executed for the loads from for example the piston mass and centrifugal terms as well.

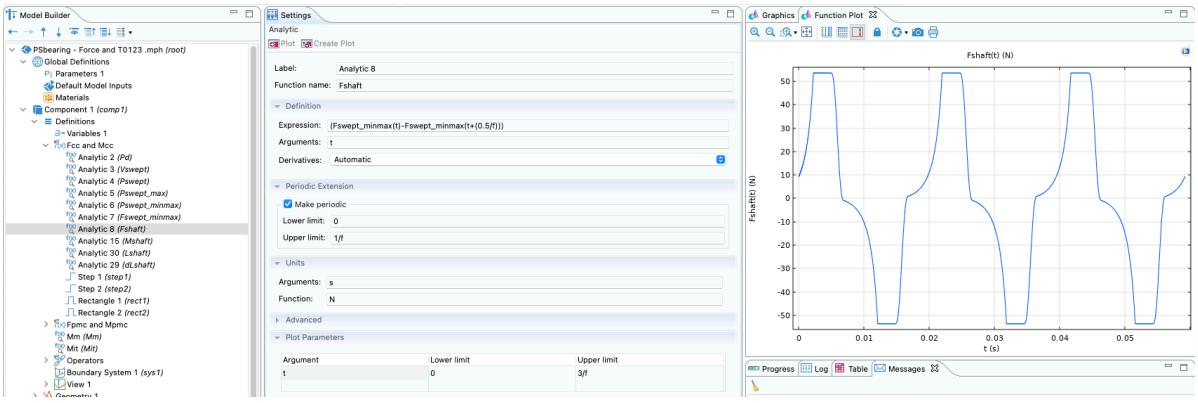

Figure A.7: Piston-shaft force graph.

3. It is sufficient to build only the shaft-axis geometry which is a block with dimensions P_w times P_h.

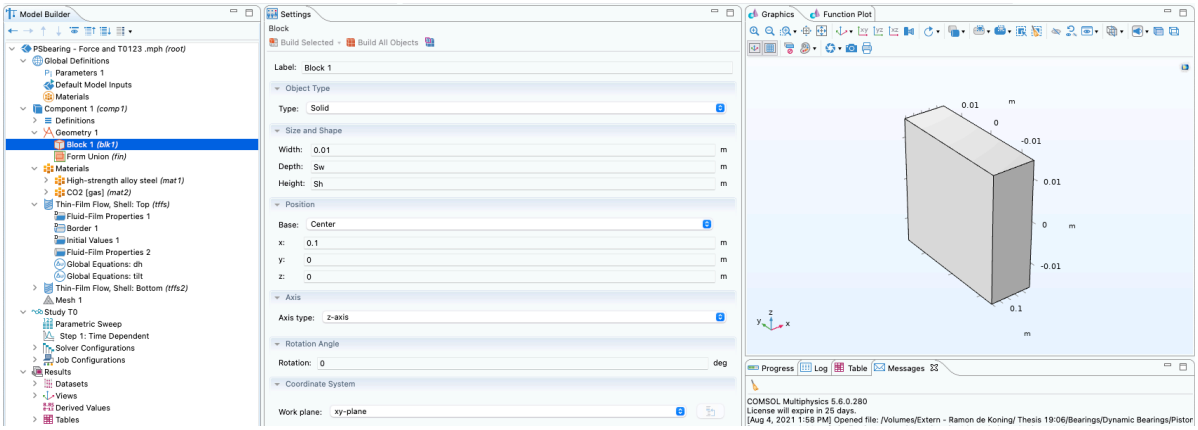

Figure A.8: Shaft geometry.

4. The forces and moments of both surfaces are defined as variables and will be used to set up the global equations, see Figure A.11. The film thicknesses are used to analyse the results.

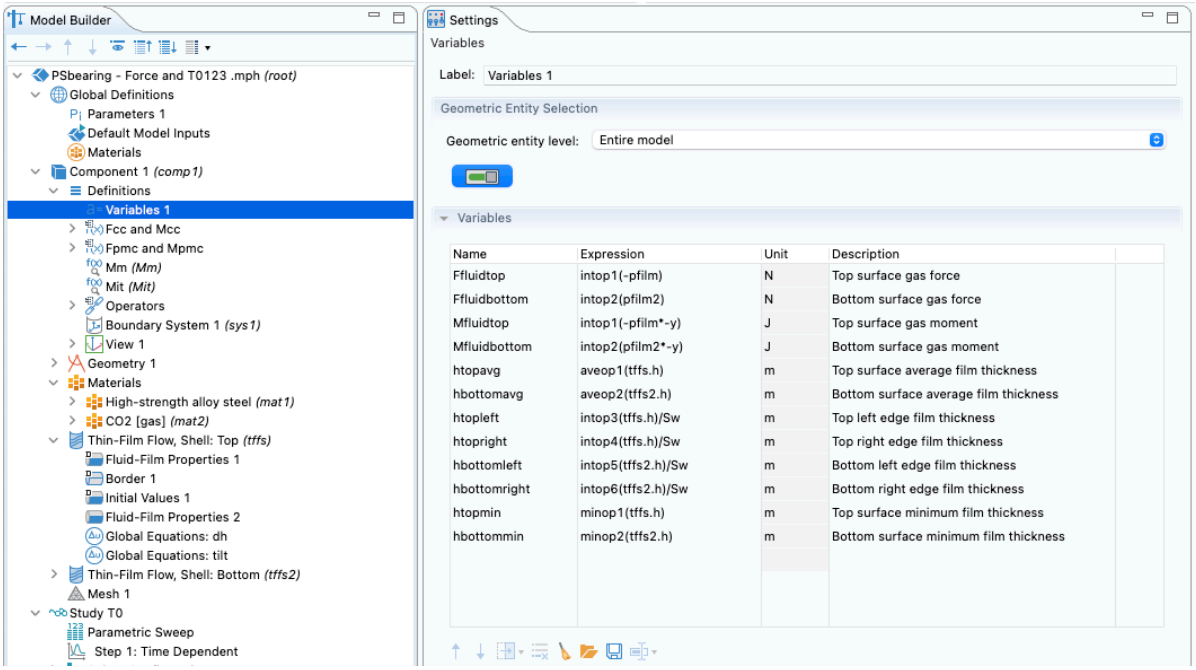

Figure A.9: Model variables.

5. Both the top and bottom surface have their own thin-film model. They operate using the modified Reynolds equation and the reference pressure is set to the inlet pressure, P_{in}. All borders of each surface are given a zero film pressure. The fluid film properties are shown in Figure A.10. The initial film thickness is set to the nominal film thickness. The wall displaces dynamically in x-direction by a value dh and rotates by a value $tilt * -y$, from the global equations in the next Figure. The wall velocity corresponds to this displacement. The base velocity is defined in y-direction as the relative sliding velocity of both surfaces, which is the derivative of the moment arm.

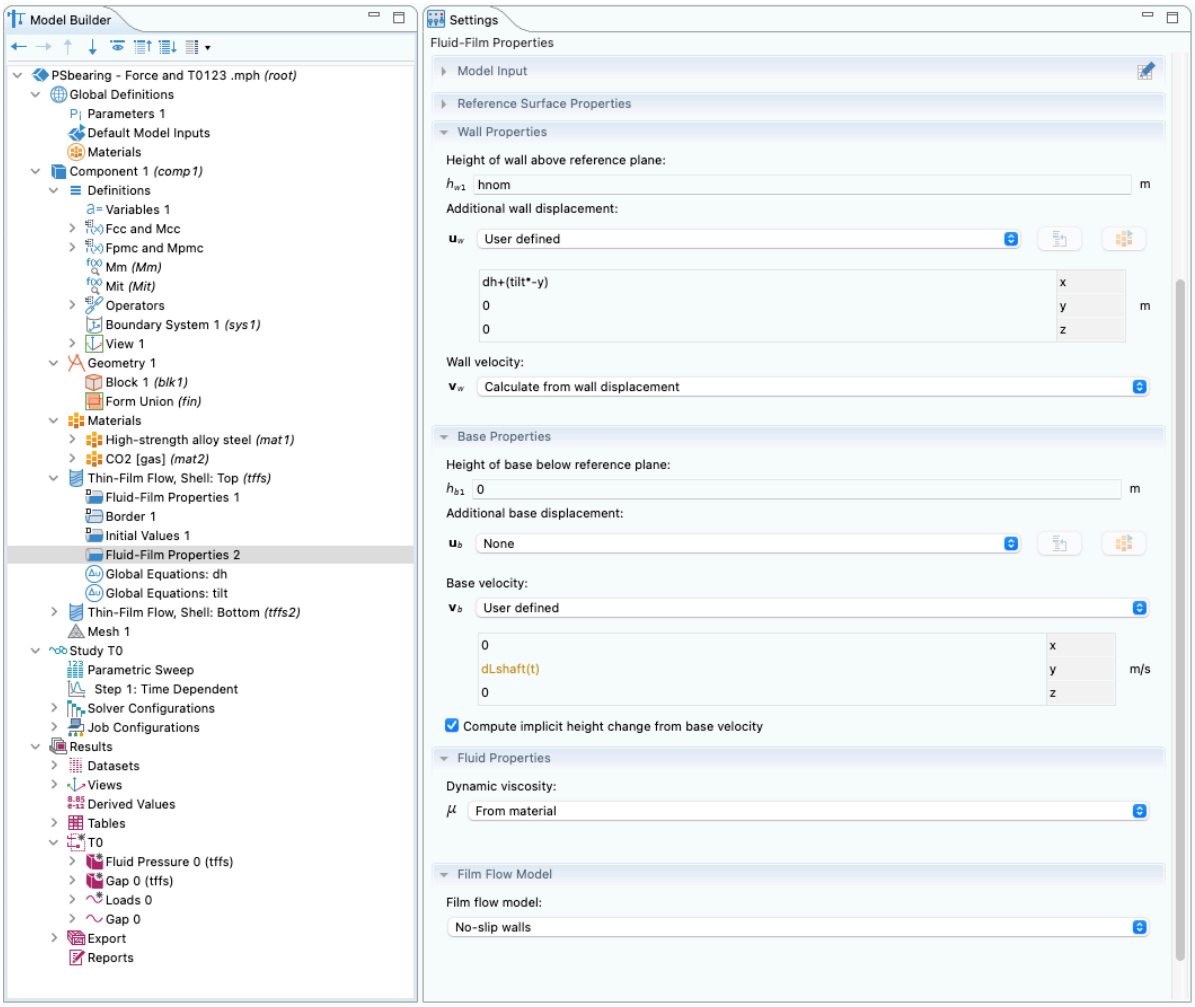

Figure A.10: Thin-film flow - Fluid film properties.

6. In this global equation, the force exerted on the shaft by the compression chamber is balanced with the gas bearing forces of both surfaces defined in the variables. The parameter dh adjusts accordingly to satisfy this requirement and therefore changes the film thickness of both gas films. A similar global equation is used for the moments that yields a parameter $tilt$, which influences the relative rotation of the surface and creates a wedge.

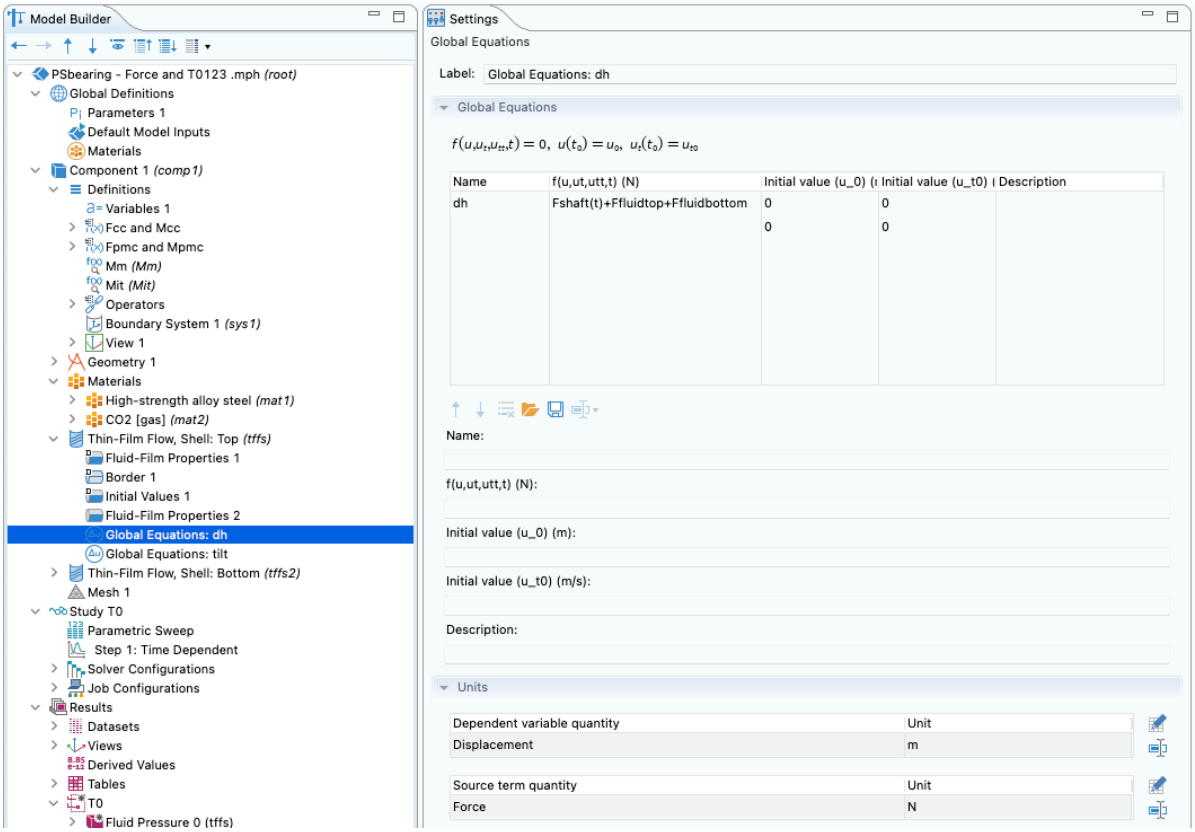

Figure A.11: Thin-film flow - Global equations.

7. The model is executed for three full cycles in 100 steps to be able to carefully analyse its behaviour. It is possible to do a parametric sweep for one or multiple components. This has been done extensively for the piston height and nominal film thickness.

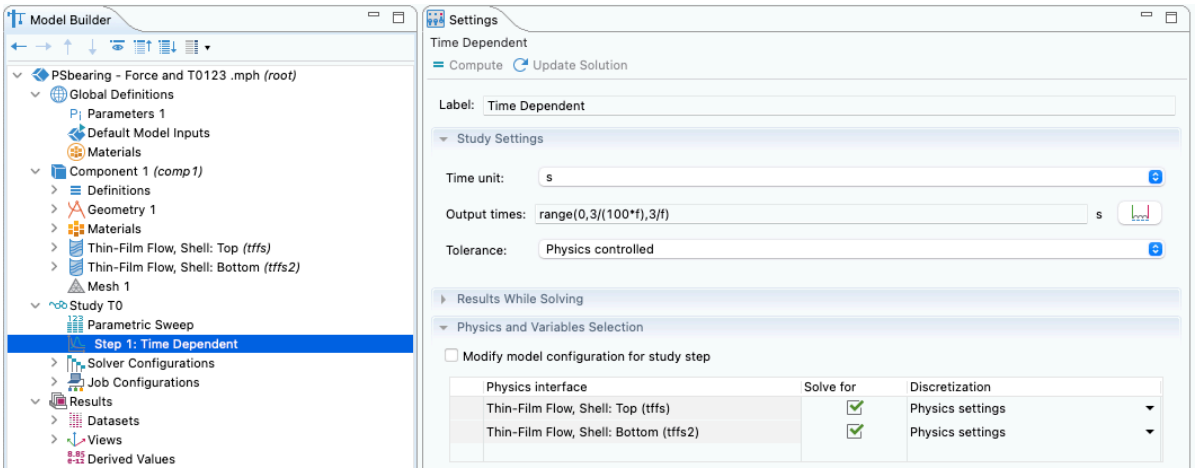

Figure A.12: Study.

A.8. Compliant Piston-Shaft Bearing

As the piston-shaft bearing is a reciprocating bearing that has no sealing function, a short analysis has been made of the possibility to replace the bearing with flexures. Within such a small compressor, the leaf springs have a a limited length of an estimated 15 mm each that need to handle a deflection of 4 mm. On top of that, the springs are loaded in axial direction by the compression chamber force which is the buckling direction. For these reasons, this bearing concept has not been applied.

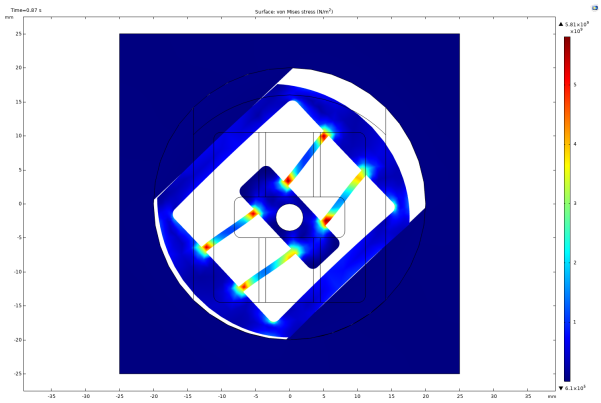

Figure A.13: Compliant shaft-piston bearing.

A.9. Contact Analysis

Both the shaft- and cylinder-actuated designs are modelled in COMSOL Multiphysics to compare the effects on the internal stresses and contact pressures between the components before a full gas bearing analysis has been done. Figure A.14 shows the results of these simulations. All results are drawn in the orientation at 2.1 radians in Figure 3.7. This is the point where the pressure reaches its exhaust value and the moment arm is largest which combined gives the highest loads. This analysis is performed using a penalty contact method which implements a finite stiffness between the components and inertial forces are neglected. Next to that, a zero coefficient of friction is applied as fully functioning gas bearings would operate close to this assumption. All components are made of high-strength alloy steel. The Poisson's ratio is set to zero as this would cause an expansion of the piston in the nanometer range. This would add significant stresses in the bearings in a perfect fit contact model, but would be negligible expansion compared to the thickness of an air film. The system is controlled by a prescribed rotation around either the centre of the shaft or the cylinder combined with a rigid connection against translation of the shaft centre in both cases.

The most visible difference between Figures A.14a and A.14b is the symmetry of the stress pattern in the material around the shaft centre. A closer look at the lower piston-shaft bearing shows that that stress pattern naturally reoccurs in the contact pressure distribution. Both are caused by the interaction of the gas pressure pushing on the bearing at an eccentric location with respect to the shaft centre and the reaction moment from the actuator. However, in the case where the cylinder is actuated, this reaction moment is first guided through both the cylinder-piston and piston-shaft bearing. A zero net torque is induced in the piston-shaft bearing and the pattern becomes symmetric. Figures A.14c and A.14d show a larger view of the system where the complete cylinder-piston bearings are visible. These bearings will naturally not bear any load from the gas pressure as they are parallel to this force. When the actuation torque is applied on the cylinder, the associated forces will pass through these bearings which makes that the contact pressures in Figure A.14d are 50 times higher. The maximum contact pressures of the piston-shaft bearing only differ by 5 percent. The values and distribution of the contact pressures on both bearing surfaces depend mostly on the stiffness of the penalty method used in the contact model and reliable results should be obtained using a thin film flow model.

The maximum stress in the material in Figure A.14a is located around the connection of the shaft to the

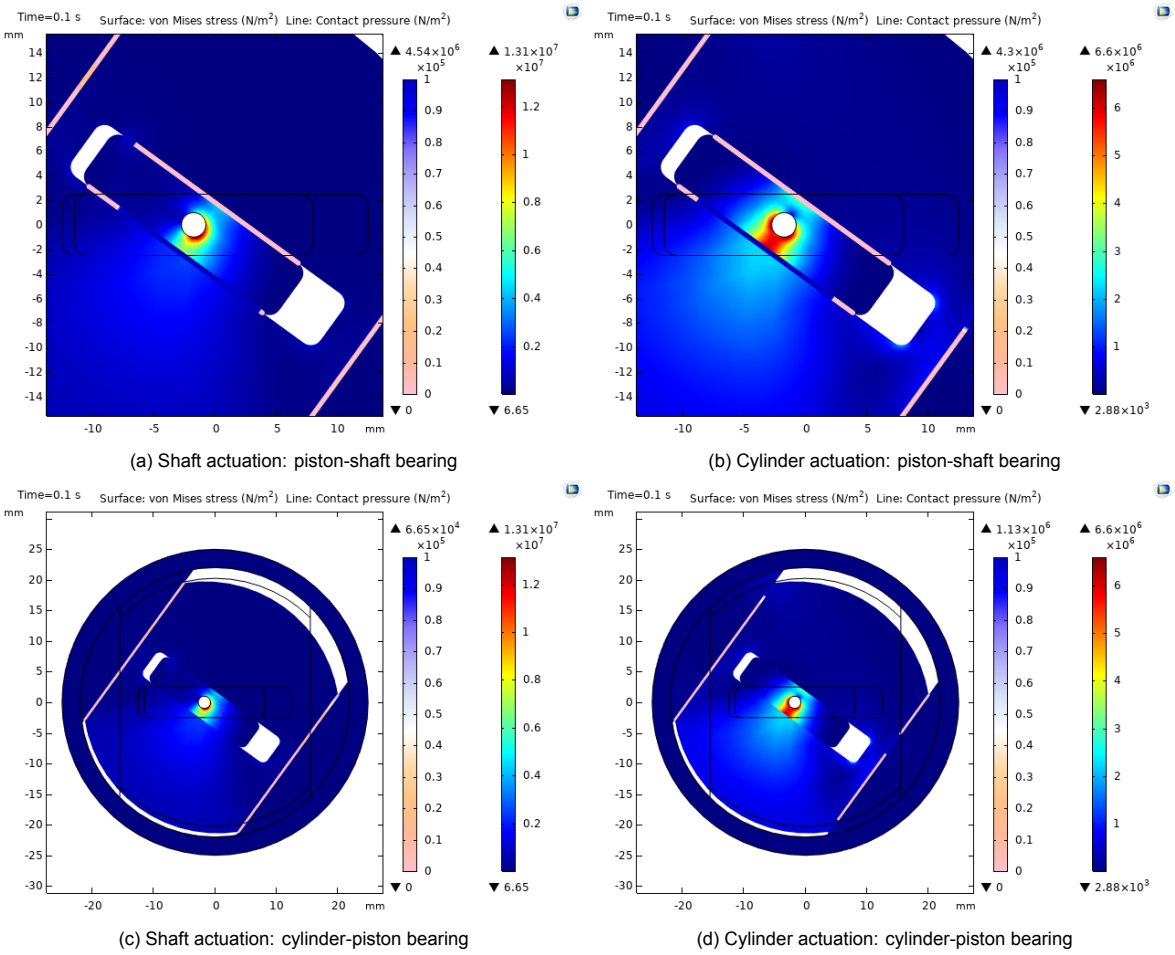

(a) Shaft actuation: piston-shaft bearing

(b) Cylinder actuation: piston-shaft bearing

(c) Shaft actuation: cylinder-piston bearing

(d) Cylinder actuation: cylinder-piston bearing

Figure A.14: Overview of material stresses and contact pressures from a contact analysis for different actuation methods.

rotor and is exactly twice the value in Figure A.14b. This value in the range of 10 MPa is rather low for a static load for steel which usually has a yield strength in the range of 1 GPa. The effects of a dynamic load over 20 years of operation would need more elaborate calculations. Due to the rigid connection of the shaft centre these stresses are a vast overestimation. The material stresses will therefore not be considered of relevance in the choice of actuation method.

Bibliography

[1] F. M. White. *Fluid Mechanics*. 7th. New York: McGraw Hill, 2011, pp. 275–277. ISBN: 978-007-131121-2.

[2] Werner Soedel. *Sound and Vibrations of Positive Displacement Compressors*. CRC Press, Oct. 2006. DOI: 10.1201/9781420006445.

[3] A B Tramschek and K T Ooi. *Purdue e-Pubs Effects of Port Geometry, Dimensions and Position on the Performance of a Rotary Compressor*. Tech. rep. URL: https://docs.lib.purdue.edu/icec.

[4] Craig Bradshaw et al. *Purdue e-Pubs A Comprehensive Model of a Novel Rotating Spool Compressor A Comprehensive Model of a Novel Rotating Spool Compressor*. Tech. rep. URL: https://docs.lib.purdue.edu/icec.

[5] Kim Tiow Ooi and Pradeep Shakya. *Purdue e-Pubs A New Compact Rotary Compressor: Coupled Vane compressor A New Compact Rotary Compressor: Coupled Vane Compressor*. Tech. rep. URL: https://docs.lib.purdue.edu/icec.

[6] Y. L. Teh and K. T. Ooi. "Theoretical study of a novel refrigeration compressor - Part I: Design of the revolving vane (RV) compressor and its frictional losses". In: *International Journal of Refrigeration* 32.5 (Aug. 2009), pp. 1092–1102. ISSN: 01407007. DOI: 10.1016/j.ijrefrig.2008.09.006.

[7] Myeong Su Shin et al. *A Novel Structure of Rolling Piston Type Rotary Compressor*. Tech. rep. 2018. URL: https://docs.lib.purdue.edu/icec.

[8] R. Gohar and M. M.A. Safa. "Fluid film lubrication". In: *Tribology and Dynamics of Engine and Powertrain: Fundamentals, Applications and Future Trends*. Elsevier Ltd., Jan. 2010, pp. 132–170. ISBN: 9781845693619. DOI: 10.1533/9781845699932.1.132.

[9] A Beek. *Advanced engineering design : lifetime performance and reliability*. 5th ed. [Delft]: TU Delft, 2012. ISBN: 9789081040617.

[10] "EML 2322L-MAE Design and Manufacturing Laboratory". In: ().

[11] Yusheng Hu et al. *Study of Novel Rotary Cylinder Compressor*. Tech. rep. 2018. URL: https://docs.lib.purdue.edu/icec.